Impact strength of dissimilar joints for the automotive industry

Submitted by:

Paulo David Pereira Nunes

MSc THESIS

Supervised by: Lucas F. M. da Silva

Co-supervised by: Eduardo A. S. Marques

José J. M. Machado

U.PORTO

FEUP **FACULDADE DE ENGENHARIA**
UNIVERSIDADE DO PORTO

Master Integrated in Mechanical Engineering

(January of 2018)

Acknowledgements

First of all, I would like to express my gratitude to Professor Lucas da Silva, my supervisor, for the opportunity to collaborate with him in this work.

I would like to thank Eduardo Marques and José Machado, my co-supervisors, for the time spent, and the complete availability during the development and execution of this dissertation.

To the adhesive group for all the tips given, and for helping me when it´s been necessary.

I wish to express thanks to Nagase ChemteX® (Osaka, Japan) for providing the adhesive for this work.

Lastly and the most important, I would like to express my gratitude to my family and friends, especially my parents and sister, for the support, encouragement and patience given during this long journey.

Abstract

The automotive industry is currently facing challenges in the reduction of emissions and fuel consumption. These targets can only be achieved with the use of lightweight materials for the vehicle structures, such as carbon fibre composites and aluminium alloys. The construction techniques for vehicle bodies with these materials differ greatly from the techniques used for the most commonly used steel bodies, with adhesive bonding being used extensively due to its capability to bond dissimilar materials. However, the use of adhesive bonding poses several challenges to the automotive engineers, as the dissimilar bonded joints must be designed to perform well under impact and extreme temperature conditions.

The aim of this work is to understand and predict the behaviour of dissimilar adhesive joints, using composite and aluminium adherends, under quasi-static and impact loads. A variety of testing temperatures (ranging from -30 to 80ºC) was considered, taking into account the requirements for the automotive industry. A numerical simulation procedure was also performed in parallel and produced numerical models which where validated against the experimentally obtained data in both quasi-static and impact conditions. It was possible to conclude that dissimilar adhesive joints, if used in conjunction with modern crash resistant adhesives, can effectively be used for the construction of automotive structures, without significant sacrifices in joint performance, with good energy absorption capabilities under impact. Moreover, their performance can also be simulated using advanced cohesive zone models minimizing the need to perform extensive experimental impact testing.

Resumo

Atualmente, a indústria automóvel enfrenta desafios significativos na redução de emissões e consumo de combustível. Esses objetivos só poderão ser alcançados pelo uso de materiais leves nas estruturas do veículo, tais como compósitos de fibra de carbono e ligas de alumínio. As técnicas de construção de estruturas de veículos com recurso a estes materiais diferem muito das técnicas utilizadas em estruturas de aço, sendo adotado o uso de ligações adesivas devido à sua capacidade de unir materiais dissimilares. No entanto, o uso de adesivos estruturais coloca novos desafios aos engenheiros de projeto, já que as juntas adesivas de substratos dissimilares devem ser projetadas para suportar condições de impacto e de temperatura extrema.

Com este estudo pretendeu-se determinar e compreender o comportamento de juntas adesivas com materiais similares, usando aderentes de material compósito e de alumínio, sujeitos a carregamentos quase-estáticos e de impacto. Os ensaios foram realizados numa ampla gama de temperaturas (variando de -30 a 80ºC), levando em consideração os requisitos da indústria automóvel. Um procedimento de simulação numérico foi realizado em paralelo ao trabalho laboratorial, gerando modelos numéricos que, após validação experimental, permitiram prever o comportamento mecânico das juntas em condições quase-estáticas e de impacto. Modelos de dano coesivas foram utilizados para simular a falha do adesivo e a delaminação dos compósitos, enquanto modelos de dano foram usados para simular deformação plástica e falha nos substratos de alumínio. Concluiu-se que é possível utilizar juntas adesivas dissimilares na construção de estruturas de veículos, sem ser necessário sacrificar o comportamento mecânico da ligação e com boas capacidades de absorção de energia ao impacto. Foi também possível concluir que a aplicação de modelos de dano coesivo permite simular com sucesso a performance deste tipo de juntas dissimilares, reduzindo assim a necessidade de efetuar ensaios de impacto.

Contents

List of acronyms

CBBM   Compliance based beam method

CBT   Corrected beam theory

CCM   Compliance calibration method

CFRP   Carbon fibre reinforced polymer

CZM   Cohesive zone model

DCB   Double cantilever beam

DLJ   Double lap joint

ENF   End notched flexure

FEA   Finite element analysis

FPZ   Fracture plastic zone

RT   Room temperature

LT   Low temperature

HT   High temperature

SLJ   Single lap joint

Notation

a	Crack length
a_{eq}	Equivalent crack's length
C	Compliance
E	Young's modulus
E_x	Longitudinal normal modulus
G_{xy}	Longitudinal shear modulus
E_f	Corrected bending modulus
G	Shear modulus
G_{Ic}	Critical strain energy release rate or fracture toughness in mode I
G_{IIc}	Critical strain energy release rate or fracture toughness in mode II
k	Shear stress distribution constant
K	Elastic constitutive matrix
P	Applied force
T_g	Glass transition temperature
t	Thickness
t_n	Cohesive strength in tension
t_s	Cohesive strength in shear
w	Width of the specimen
σ	Tensile strength
$\delta_{o,i}$	Cohesive strength critical relative displacement
$\delta_{max,i}$	Maximum relative displacement

δ Displacement

Δ Correction factor of crack's length

v Poisson's ratio

List of figures

List of tables

1 Introduction

This dissertation presents a study on the mechanical behaviour of adhesive joints with dissimilar adherends under static and impact conditions, tested under a range of temperatures suitable for the automotive industry. To accomplish this aim, several experimental and numerical studies were made.

In this introductory chapter, a brief description of the research problem is made, the intended objectives are listed as well as the necessary steps undertaken for successful accomplishment of the research work. The methodology followed in this work is also described.

1.1 Background and motivation

With the increasing restrictions in emissions that automotive industry is currently being subjected, coupled with the drive for manufacturing higher performing cars, a light-weight approach for vehicle design is now essential. In order to tackle such objective, the automotive industry has significantly increased the application of light-weight materials such as aluminium and composite materials instead of more common materials like steel. It is within this context that adhesive bonding has gained importance, as this is the optimal method for joining dissimilar materials. However, the design of structural bonded joints for the automotive industry, especially those with dissimilar substrates, still poses significant challenges for the design engineers, especially when considering the necessity of performing well under impact loads (ensuring passenger safety) and the large temperature ranges involved. This is a relatively new field which requires further experimentation as well as the development of innovative and advanced numerical models.

1.2 Objectives

The objectives of this thesis are twofold. The first objective is to fully understand the mechanical behaviour of dissimilar adhesive joints, using composite and aluminium substrates, tested under quasi-static and impact loads, performing a comparison with the behaviour of joints

with similar substrates. A variety of testing temperatures (ranging from -30 to 80ºC) was also considered, taking into account the requirements for the automotive industry.

The second objective consists in the development of a numerical simulation procedure, developing experimentally validated numerical models able to predict adhesive joint behaviour under both quasi-static and impact conditions.

1.3 Research methodology

The main goals of this thesis were achieved through the performance of step by step research procedures, which can be divided in the following chronological order:

1. A detailed literature review, considering some of the most recently published works, was performed focusing on themes such as: adhesive bonding, composite materials, aluminium alloys and impact tests, as well under the influence of temperature;

2. Single lap joints (SLJs) made with carbon fibre reinforced polymer (CFRP) and aluminium substrates (in both similar and dissimilar configurations) were manufactured to perform quasi-static and impact tests, under different testing temperatures (from low to high);

3. Double cantilever beam (DCB) tests were performed to characterize the crash-resistant adhesive under three different strain rates from the range of low to high temperatures;

4. Numerical simulations were developed using Cohesive Zone Models (CZM) to evaluate the obtained experimental results under quasi-static and impact conditions and tested at room temperature (RT).

1.4 Dissertation outline

This dissertation is divided in seven chapters, which include an introduction and the main conclusions. In the introductory chapter, a brief description of the study is described, as well as background, motivations and objectives of the thesis.

The chapter regarding the literature review comprehends a brief description of adhesive bonding, and considerations regarding the mechanical properties of different types of adhesives. Once a structural adhesive was used in this work, a detailed description was performed on its mechanical properties under the influence of strain rates and temperature. The mechanical properties of the CFRP used were analysed under different strain rates and testing temperatures. The quasi-static and impact behaviour of SLJs was considered.

The experimental details chapter clarifies in detail the manufacturing process of the SLJs tested, the specimens' geometry and testing procedures.

The numerical details chapter reports the 2D finite element models built, both under quasi-static and impact simulations.

The experimental results chapter presents the results of the adhesive characterization regarding the fracture energy in mode I as a function of strain rate and testing temperature, as well the quasi-static and impact tests of SLJs as a function of temperature. Failure loads and energy absorbed, fracture modes and the corresponding simulations are also presented.

The last two sections of this document are the conclusions and future works. Here, conclusions are drawn regarding the main topics of research, complemented by a discussion of the most relevant suggestions for further work.

2 Literature Review

2.1 Survey of adhesive joints

An adhesive joint is a bonded connection between two similar or different materials using non-metallic fillers (adhesives). The materials which are joined together by the adhesive are commonly designated as substrate or substrates [1].

According to Adams and Wake [2] an adhesive can be defined as a material which, when applied to surfaces, can join them together and resist separation. Adhesive is the general term and includes cement, glue, paste, etc. It´s known that adhesives are used for centuries, since biblical times. For example early hunters used beeswax to join feathers to arrows to improve their aim, this can be considered as a primitive adhesive [3].

In the last century, or so, with the appearance of the first synthetic polymers, namely epoxy resins, engineers started to look to adhesives as a meaningful alternative to bolting, riveting, brazing and welding in structural bonding, thus leading to creation of the structural adhesive [4]. Structural adhesives can be defined as an adhesive used when the load requirement to cause separation is substantial such that the adhesive provides for the major strength and stiffness of the structure [2].

When compared with more traditional techniques for joining materials, adhesives can offer some advantages such as [5]:

- Possibility to bond dissimilar materials;

- The ability to bond thin sheets of-material;

- Good stress distribution (Figure 1), which consequently leads to a good resistance to dynamic-fatigue;

- Very convenient and often cost-effective technique, since can of be automated;

- Design flexibility, allowing the use of new concepts and materials;

- Regular contours, since it avoids holes (rivets and screws) and welding marks;
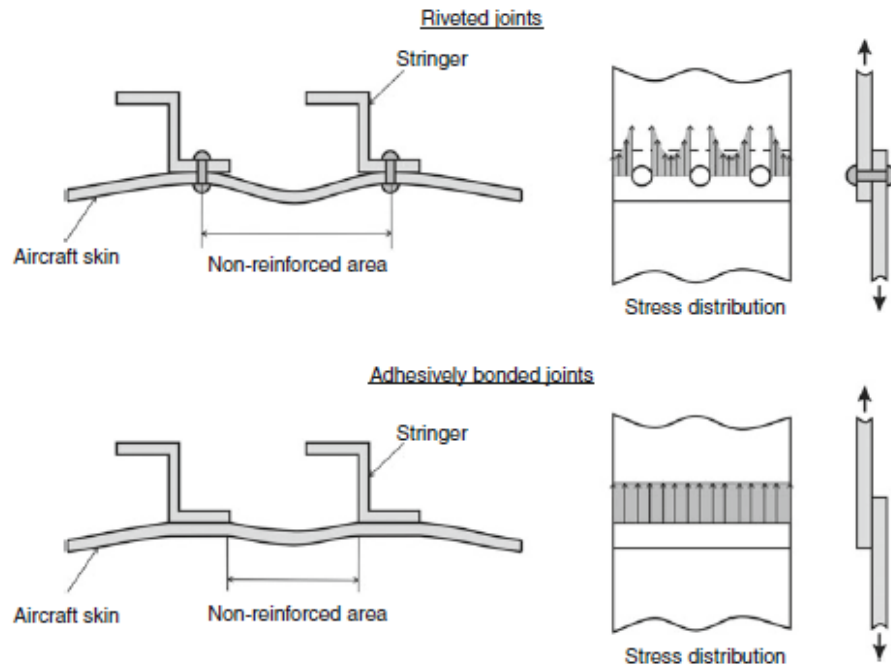
Figure 1 - Comparison between riveted and adhesive bonded joints [1].

There are some disadvantages when it comes to adhesive joints [6]:

- Need to avoid peel and cleavage stresses (the biggest enemy of adhesive joints);

- Limited resistance to extreme environmental conditions like as high temperature and humidity;

- Necessity of fastening tools to keep the parts in position since the bonding process is not instantaneous;

- Requirement of extremely careful surface preparation, to avoid bad adhesion;

- Often requires high temperatures for curing (applied with oven, press, heater pads etc.);

- Quality control is difficult to perform;

- Low maximum service temperature.

2.1.1 Failure modes and joint design

For bonded joints of metallic substrates, three different failure modes can occur in adhesive joints (Figure 2) [1]. The first, cohesive failure in the adhesive, can be due to a few reasons, like inadequate overlap length, thermal stresses or gross void defects. Sometimes, when ductile substrates are used, this kind of failure can be caused by the onset of plastic deformation on the substrates, introducing excessive peel stresses in the ends of the overlap leading to cohesive failure in the adhesive. The second one, adhesive (interfacial) failure appears in the interface between the adhesive and the adherend and is caused by poor surface preparation. This can be the case if the adherend is contaminated with grease, rust, loose particles or when the superficial energy of the adherend surface is much lower than that of the adhesive. The third failure mode, cohesive failure in the adherend, occurs when the adherend reaches its limit in terms of material strength. This is considered as an ideal case since it means that the bonded region did not fail.
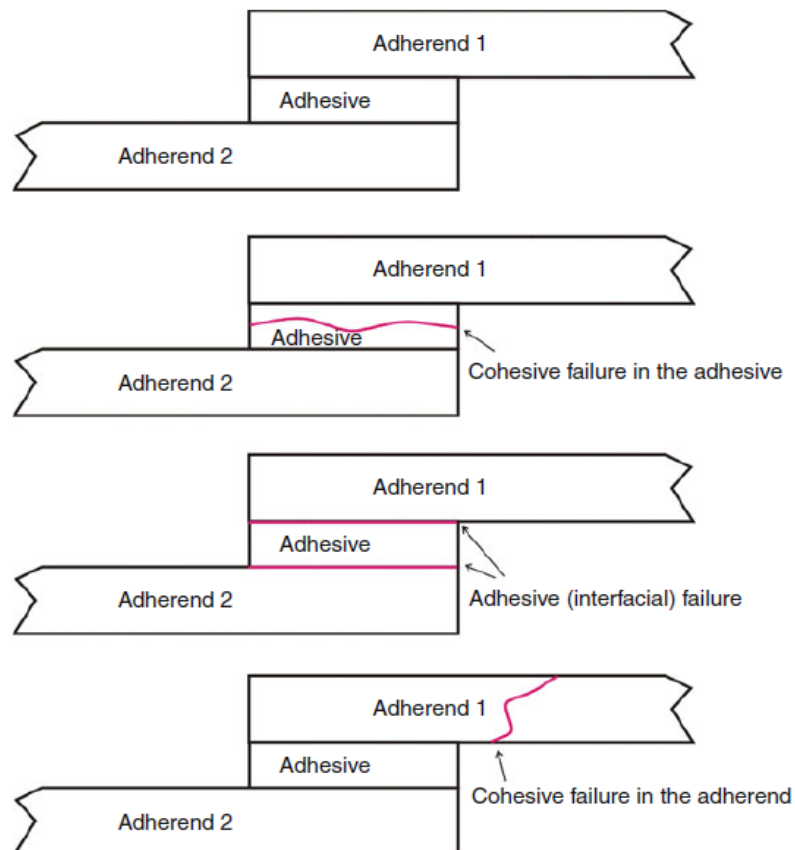
Figure 2 - Representation of failure modes: cohesion and adhesion [1].

Due to the anisotropic characteristics of composite materials, a more detailed analysis is needed when it comes to the failure mode of adhesive joints that employ these materials as substrates. In FRP (fibre reinforced polymer) composite joints, according to ASTM D5573 standard, there are seven typical characterized modes of failure. Six of them are illustrated in Figure 3 and the last one is a mixed failure, that is, typically a combination of two or more of those represented below.
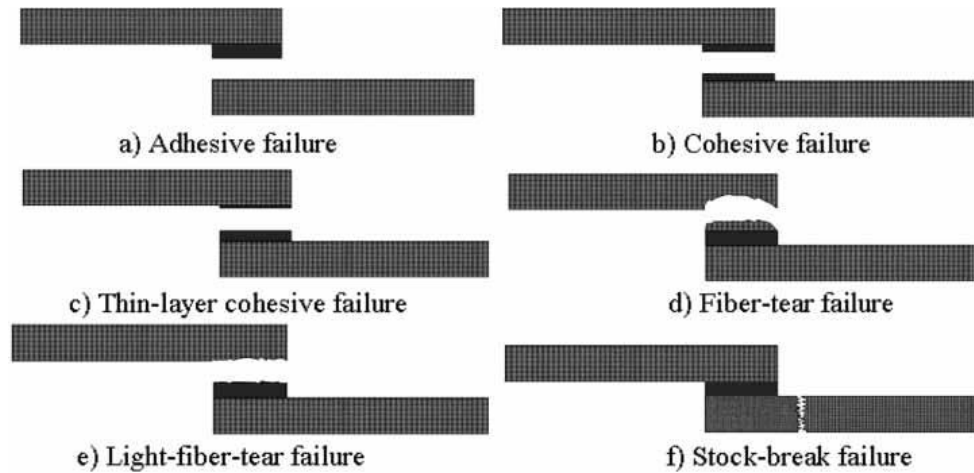
Figure 3 - Failure modes with composite substrates [7].

The big novelty when compared with the failure modes in metal joints is the addition of a new mechanism of failure, delamination of the composite materials, that in the image above is referred as fibre-tear failure. This additional failure mode is related with the inherent properties of composite materials, which will be addressed later in this review.

Bonded joints can be subjected to various types of stress (Figure 4) depending of the geometry of the joint, the way that the load is applied and the properties of the adhesives and substrates. While some of the load types are suitable for bonded joints (shear stress), others exist that must be avoided (cleavage and peel stresses) [6, 7]. The different types of stresses present in bonded joint are [1]:

- Normal stresses (stresses which occur on a perpendicular plane where they act and can be compressive or tensile);

- Shear stresses (stresses parallel to the plane where they act);

- Peel stresses (stresses that appear on the edges of adhesive layer due to eccentric loading);

- Cleavage (stresses originated from an offset tensile force or bending moment).
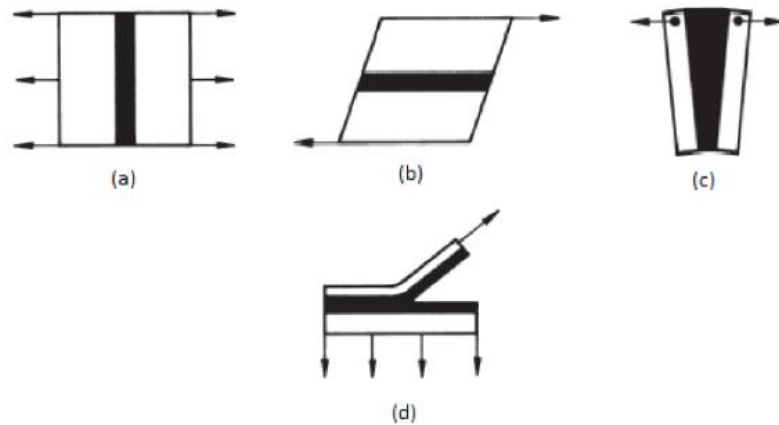
Figure 4 - Types of stresses in adhesive joints. (a) normal (or direct) stress, (b) shear stress, (c) cleavage, (d) peel stress (adapted from [5]).

As mentioned before, geometry is a major factor when it comes to the types of stresses present in a bonded joint, thus during the design stage, peel and cleavage stresses should be minimized. Design changes on the substrates, the use of double lap joints (DLJ) and even the use of local mechanical restraints are a few of the most common methods suggested to avoid the most problematic situations. The most studied joint configurations in the literature are [7]:

- SLJs);

- Double-lap joints (DLJs);

- Scarf joints;

- Stepped lap joints.

Figure 5 - Adhesive bonded joints configurations: (a) Single lap joint, (b) Double lap joint, (c) Double scarf joint, (d) double stepped-lap joint (adapted from [7]).

Single lap joints are the most commonly studied adhesive joints due to their simplicity and to the fact that this is the joint configuration that best represents the adhesive joints used industrially.

2.1.2 Types of adhesives

Due to the large variety of properties they exhibit and the different possible chemical compositions, adhesives can be classified according to a wide range or parameters. The most common classification parameter used are: source, chemical structure, function, reaction method and physical form.

The source can be synthetic or natural. Examples of synthetic adhesives are: acrylics, epoxies, silicones and polyesters. Examples of adhesives derived from natural sources are: natural rubber, animal glue and casein-based, and protein- based adhesives.

In terms of chemical structure as categorizing parameter, the major different types are: thermoplastics, thermosets, elastomers and hybrid. Thermoplastic adhesives are cured by cooling from a melted state or by loss of solvent. They can be melted after curing if subjected to temperatures above T_g (glass transition temperature). Due to this fact, they are usually unable to handle high temperature and their use is not recommended for service temperatures above 60°C. These materials are also characterized as having poor creep resistance and fair peel strength. Thermosetting adhesives, after the cure cycle, cannot be heated and melted again. These can be found as a one-part or two-part system (resin and hardener come separately). The

one-part system usually requires high temperature to cure, and its shelf life is reduced. On the other hand, the two-part systems cure at RT and have a longer shelf life, but the working temperature is lower than the one-part adhesives. Elastomeric adhesives are not especially strong but present a higher toughness, elongation and superior peel strength. Currently, many adhesives on the market are hybrid formulations, which mix more than one type of adhesives in one single product, offering a combination of the best properties from those adhesives. The combination of different adhesives provides tougher and more flexible adhesive, with better mechanical properties when subjected to impact [1].

Adhesives can also be classified regarding their function, and this is a very important division, as it separates the adhesives between structural and non-structural. While non-structural adhesives are most used as sealants, structural adhesives can withstand significant loads. Examples of non-structural adhesives are: synthetic rubbers and polyesters. Examples of structural adhesives are: epoxies, phenolics and polyurethanes.

The physical form of adhesives is another classification parameter. Adhesives are available as liquids, pastes, films and powder. This is a very useful classification method to the industry, mainly due to its implications in the joint manufacture process. For example, while liquid adhesives have good gap filling capabilities they can flow out from the joint during manufacture, something which does not occur with paste or film adhesives but the last struggle to properly wet the surfaces.

The reaction method is also an important classification parameter with practical importance, as it divides adhesives according to their cure method. Adhesives can cure by chemical reaction, by loss of solvent, by loss of water or by cooling from melted state.

2.2 Adhesive joints in the automotive industry

The automotive industry has significantly increased the use of adhesives for joining load-bearing components in an effort to reduce vehicle weight, improve fuel economy and reduce emissions. However, the design process of a bonded structure can be complex, as the properties of adhesives vary widely from brittle to highly deformable adhesives [1]. Adhesives are viscoelastic, and their properties greatly depend on several factors such temperature,

humidity and loading rate. While some design criteria consider these effects [5], there is still limited information regarding the impact behaviour of bonded joints [8], especially when used with composite substrates. Adhesive joints in the modern automotive industry can be found in three main areas of application: the body shop, the paint shop and the trim shop. In the body shop adhesives are used for hem flange bonding, anti-flutter bonding, and hybrid joining. The use of adhesives in the paint shop is limited to a few minor applications, but in the assembly lane/trim shop the use of adhesives is extensive, as most of the trim pieces are bonded to the vehicle.

2.2.1 Structural adhesives used in the automotive industry

Due to this wide range of application, the types of adhesives used in the automotive industry are varied (Figure 6). For many automotive components, the forces involved are small and non-structural adhesives can be used. However, for structural applications the loads can be considerably higher.
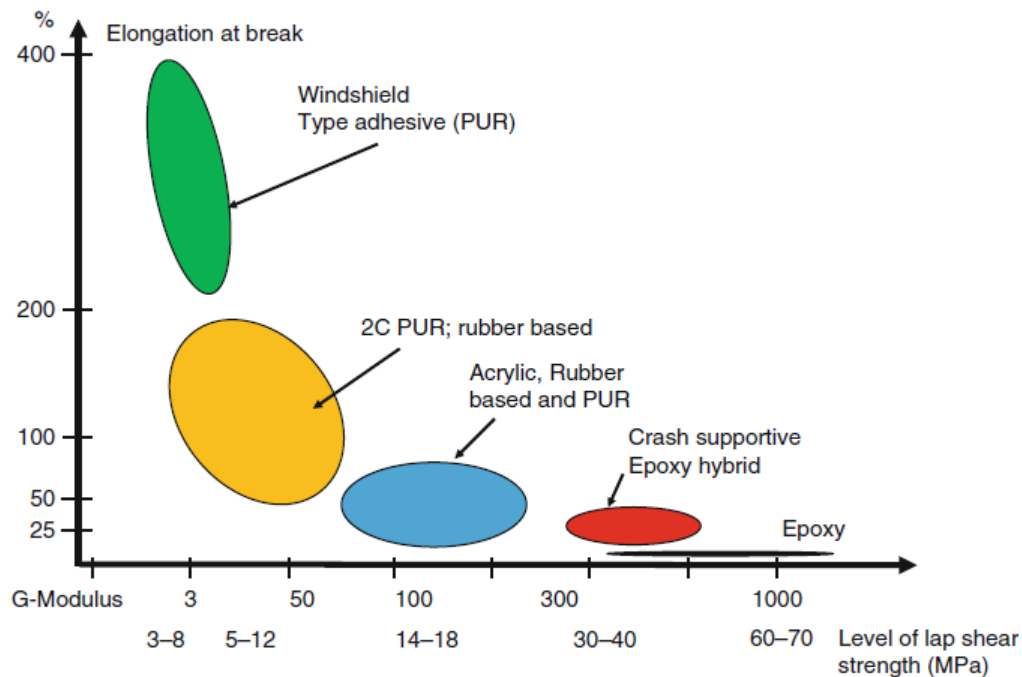
Figure 6 - Landscape of adhesives for structural automotive applications [1].

11

The range of strength of structural adhesives used in automotive production is marked at one end by windshield adhesives with rather low modulus and high elongation and at the other end by very high strength epoxy adhesives. The top end of adhesives for automotive bodies are crash-supportive epoxy-hybrid adhesives which have a somewhat lower shear modulus than very high strength epoxies, but significantly higher elongation. The most common adhesives used in this industry are epoxies, acrylics and polyurethanes. Table 1 indicates examples of the typical properties for some structural adhesives.

Table 1 - Example of the mechanical properties of some structural adhesives (adapted from [7]).

Adhesive	Type	Shear modulus G (MPa)	Shear strength (MPa)	Shear strain (%)
AV138	Epoxy	1559	30	7.8
DP805	Acrylic	159	8.4	180
SikaFlex 265	Polyurethane	0.7	4.5	450

Epoxy adhesives are very versatile type of adhesive since they can be applied in every type of substrates used in the industry except plastic. Modern modified epoxies have improved in terms of impact and peel strength when compared with older versions of brittle epoxy, making of them the best choice to crash resistant applications. Epoxies adhesives are available in one-part or two-part system. The service temperature ranges between -40 to 100°C with modified epoxies going up 180°C. This type of adhesive usually presents high strength and temperature resistance, relatively low cure temperatures, easy to use and low cost.

Acrylics adhesives are known as resin-based adhesives. It's a versatile adhesive because it has the capability of fast curing and tolerate dirtier and less prepared surfaces. It is also resistant to water and humid conditions. The service temperature ranges between -40 to 120°C and cure through a free radical mechanism.

Polyurethanes adhesives have high peel strength, toughness, durability and flexibility, but exhibit generally lower mechanical strength when compared to epoxies. Due to their low modulus and high ductility, a more uniform stress distribution takes place on the bonded joint, which leads to a good behaviour to fatigue. Their high failure strain makes it a good adhesive

for the absorption of impact. This type of adhesive is also available in one-part or two-part system. The service temperature ranges between -200 to 80°C and they cure at RT.

2.2.2   Substrates used in the automotive industry

Although the majority of structural pieces used in the automotive industry are still made from steel, it is also true that the aluminium and composite materials are gaining more and more space in the industry. Vehicle bodies, that before were mainly made of steel, now increasingly include assemblies made of aluminium. Additionally, the use of composite materials for bonnets and other body panels is becoming more frequent [1]. Since various types of loads are applied in different parts of a car, the use of different materials and geometries is necessary for optimize weight reduction and overall structural stiffness. These two parameters are the focus of the industry at the moment, in order to reduce emissions and increase performance. Figure 7 demonstrates the advantages of aluminium and CFRP in comparison with a steel construction.
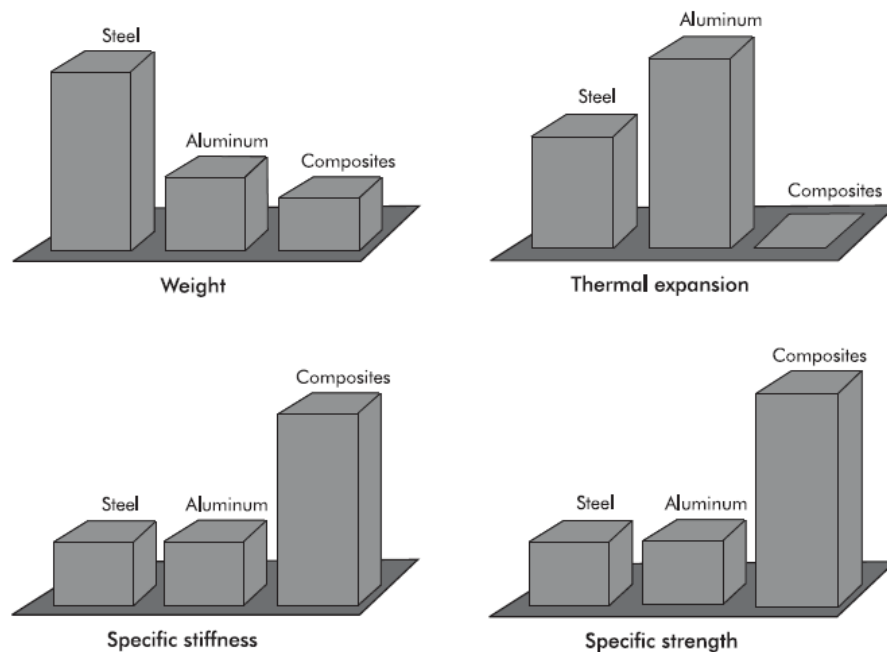
Figure 7 - Properties comparison [9].

2.2.2.1   Aluminium

The characteristic properties of aluminium, like high strength stiffness to weight ratio, good formability, good corrosion resistance, and recycling potential make it the ideal candidate to replace heavier materials (steel or copper) in the car to respond to the weight reduction demand within the automotive industry. Despite aluminium density (2700 kg/m^3) being about one third of the steel (7600 kg/m^3), the weight reduction when replacing steel by aluminium in car manufacturing is around 50% because, to ensure strength and stiffness equivalent to that of steel, the cross-sectional areas of aluminium elements need to be larger. The utilization of aluminium in structural parts of vehicles is continually increasing as new alloys and design solutions are developed. The use of aluminium alloys used in cars have increased more than 80% in total mass during the past 5 years. An increase from about 110 kg to approximately between 250 to 340 kg was though to occur from 1996 to 2015 [10].

The 5000 and 6000 alloy series are particularly interesting for the automotive industry since they allow the construction of the majority of the structure of a car body and because of the improved bare metal corrosion when compare to steel [11]. The current requirements for frontal impact can already be achieved using the AA6060 T6 alloy for construction of a space frame-based vehicle.

Aluminium is also a good material for application in structures aiming at the absorption of energy since it presents a mass-specific energy absorption capacity twice of that for mild steels and is comparable with the latest high-strength steels (HSS steels). However, it is important to mention that the behaviour of a given element during impact also strongly depends on shape, wall thickness or the use of filling material [12, 13].

Table 2 shows some of the most important aluminium alloys that are used in different parts of a vehicle in Europe and America.

Table 2 - Comparison between aluminium alloys used in different car components in Europe versus North America [11].

	Europe	North America
Outer panels		
Alloy	6016-T4	6111-T4
Surface texture	EDT or EBT	MF
Pre-treatment	pickling+Zr/Ti conversion	none
Lubrication	oil or dry-lubricant	Oil
Inner panels		
Alloy	5051/5182/6181A	6111/2008/5182
Surface texture	MF or EDT	MF
Pre-treatment	pickling+Zr/Ti conversion	none
Lubrication	oil or dry-lubricant	Oil
Structure/sheet		
Alloy	6xxx-T4	5754-O
Surface texture	EDT	MF
Pre-treatment	pickling+Zr/Ti conversion	conversion
Lubrication	oil or dry-lubricant	oil
Structure/extrusion		
Alloy	6xxx	6xxx

2.2.2.2 Composite materials

Composite materials, as the name indicates, are made of dissimilar constituents, combined in order to obtain better properties than each constituent would have by their own. The basic composite parameters provide the design flexibility enabling fibre architectural design, adjustment of the fibre content, and the fibre packing ability. These types of materials are increasingly used in automotive, aeronautical and aerospace industries because their high specific strength. Composite materials also performed well under fatigue conditions. Other good properties of these materials are: high specific stiffness, corrosion resistance and low thermal expansion coefficient [14-16]

The basic constituents of a composite material are the load-carrying fibres, also known as reinforcement, and the matrix, which in general is called the resin system during processing phase and matrix in the consolidated phase, that is needed to keep the fibres together, in the appropriate direction and protected from environment and abrasion. Matthews and Rawlings [17] did a schematic classification of the most common composite types (Figure 8).
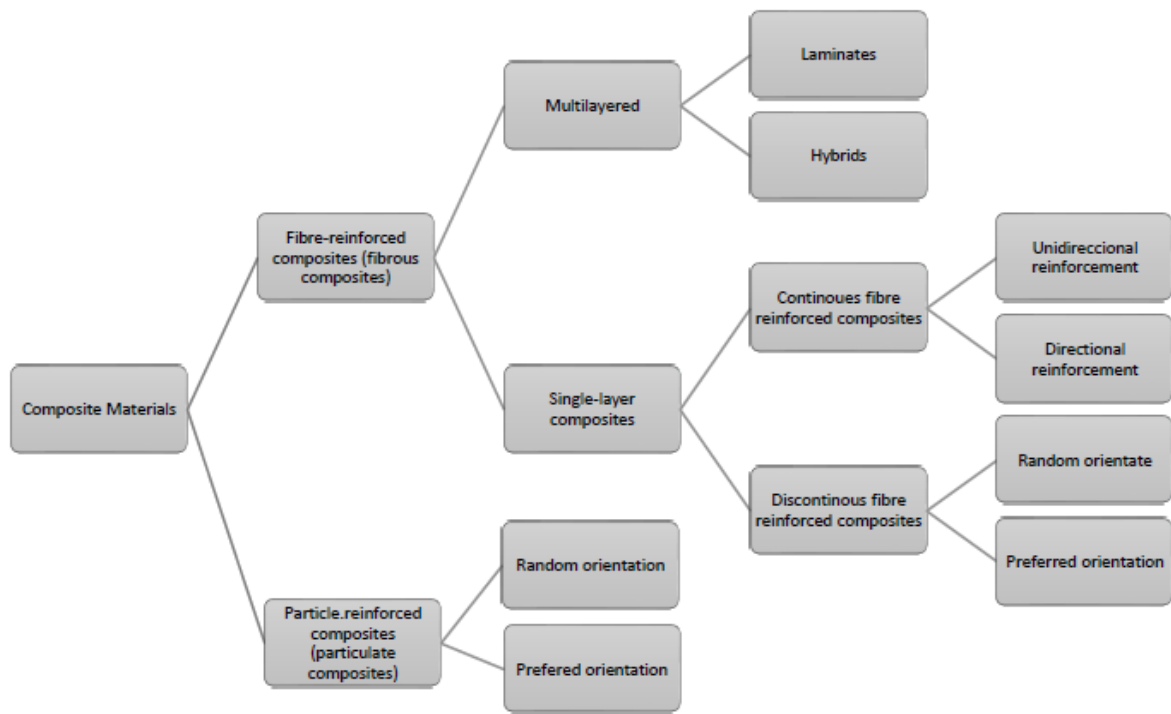
Figure 8 - Types of composite materials [17].

The most common composite type used in the automotive industry is the carbon fibre reinforced polymer (CFRP), that consists in a polymer matrix reinforced with carbon fibres [18]. Considering that the strength is provided mainly by the fibres, composites materials are considered an anisotropic material, being stronger in the direction of the fibres and weaker in the perpendicular direction.

These types of materials present some disadvantages as well, like high cost when compared with most common materials (steel and aluminium) and possibility of failure delamination between plies, specially under impact conditions [14-16].

Since fibre direction is fundamental to define mechanical properties is possible during design to have that in consideration. The composite plies can be stacked in different directions providing a more isotropic finished product when loads are applied in different directions (Figure 9).
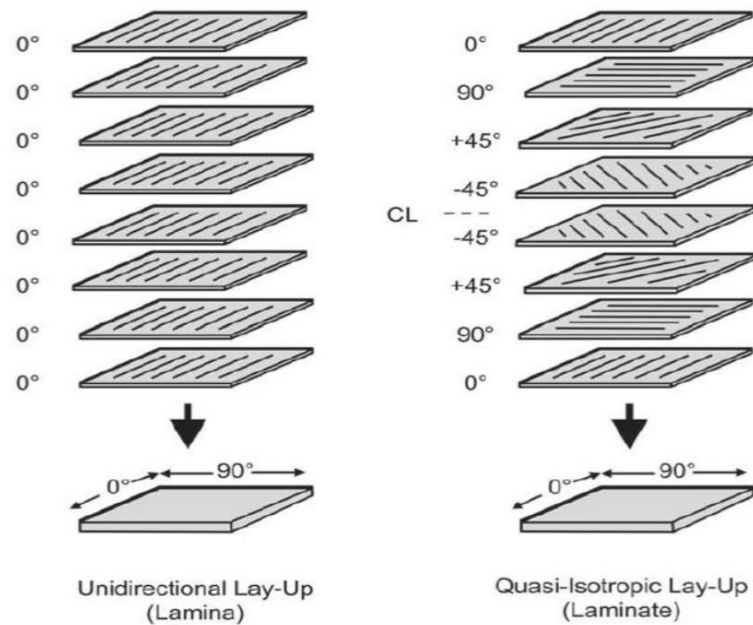
Figure 9 - Examples of configurations for plies orientation [19].

As composite materials are a combination of materials the failure analysis is a complex subject due to the interactions between fibres and matrix. Completely different failure modes are observed when composites are compared to metallic materials. In composites it is typical to observe a damaged area, where different mechanisms of failure can be presented (Figure 10): fibre breakage, fibre micro buckling, fibre pull-out, matrix cracking, delamination and debonding [20]. Three different failure modes should be taken in account when composites are associated with adhesive joints: tensile failure in the fibre direction, tensile failure perpendicular to the fibre direction and interlaminar shear failure. Although a few failure modes are presented, due to the high strength in the fibre direction and the direction of load under tests, the real concern is the interlaminar shear failure, also referred as delamination.
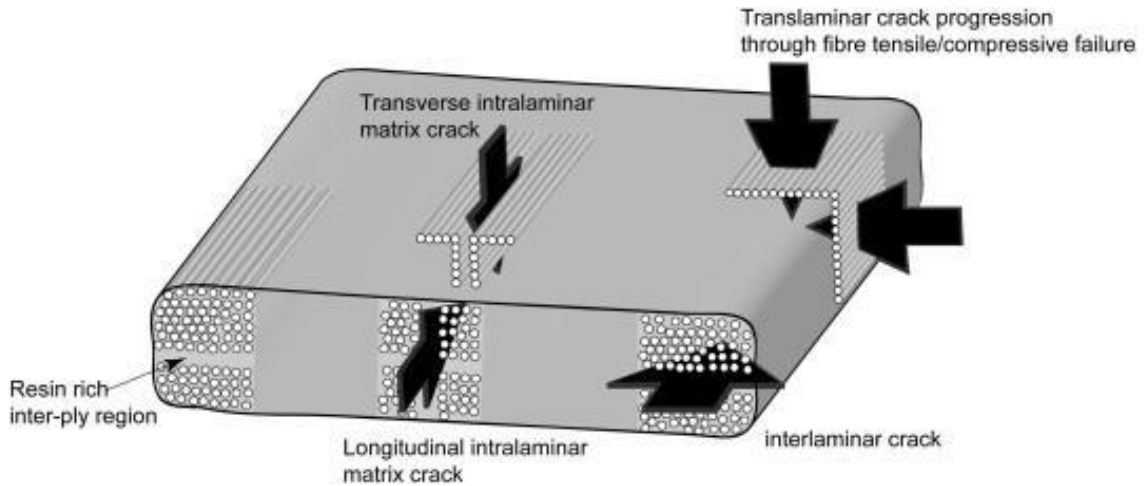
Figure 10 - Overview of ply-level failure modes [21].

2.3 Effect of temperature and impact loads

As mentioned before, cars are subject to all type of loadings and conditions and the industry takes to serious the safety of the car´s users, thus an understanding of the behaviour of adhesive joints in such conditions, and all the materials that are involved in this kind of connections, is needed. A revision of the influence of impact loads and temperature are made regarding the properties of adhesives, aluminium and CFRP materials, as well as the overall behaviour of adhesive joints Especially when taking into account the effect of temperature a few more concepts, like T_g and thermal expansion needed to be enlightened.

The T_g is the most critical value referring to temperature in polymers. It is a property of the amorphous part and marks the transition from a glass-like to a rubber-like structure. In amorphous polymers, when they go above the T_g, the long coiled molecular chains can rearrange and extend, causing fast stress relaxation due to the viscoelastic nature of the polymer, lowering its modulus and strength. This is mostly unwanted in rigid structures so structural adhesives should normally work below their T_g [1, 2].

The thermal expansion coefficient can be defined as the amount of expansion (or contraction) per unit of length of a material resulting from one-degree change in temperature. If the thermal expansion coefficient of the adhesive is not close to the one of the substrates, additional interfacial stresses are created which can lead to a premature failure of the joint [22,

23]. Since this coefficient is generally higher for the adhesive when compared to the most commonly used materials for the substrates, this is an important factor to consider when creating an adhesively bonded structure. This expansion can be reduced by the addition of mineral fillers [1].

Regarding impact loads analysis, the energy that adhesive joints are capable of absorbing is an important factor, since, in case of accident it is important to guarantee the structural integrity of the car structure, but, at the same time it is necessary that the structure absorbs the energy of the collision, otherwise this energy will be transferred to the passengers [24].

Harris and Adams in 1985 [25] tested SLJs with various substrates and adhesives types for both quasi-static and impact conditions. They conclude that, regardless the strain rate, the energy absorption was not directly provided by the adhesive, but is derived instead from the plastic deformation of the substrate. As a ductile and strong adhesive was being used, the plastic deformation of the substrate is what determined the failure load and absorbed energy. High strength substrates produced high failure loads but very low absorbed energy while the opposite occurred for more ductile substrates.

From Figure 11 it is possible to notice that SLJs with ductile adhesives performs better. The ductile adhesives allowed better stress distribution along the overlap leading to failure in the substrate.
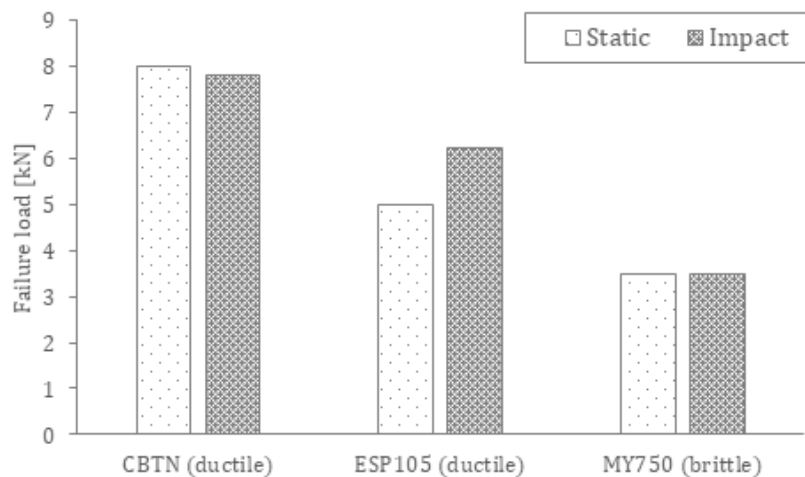
Figure 11 - Effect of strain rate in failure load of joints with aluminium substrates and three different adhesives. (Adapted from Harris and Adams, 1985) [25].

From Figure 12 is possible to observe that brittle adhesive break very easily and are unable to plastically deform the metal substrates, leading to very small absorbed energy. In contrast, ductile adhesives can hold the joint together during the impact and enable large energy absorption, especially when used in conjunction with, low strength, ductile substrates.
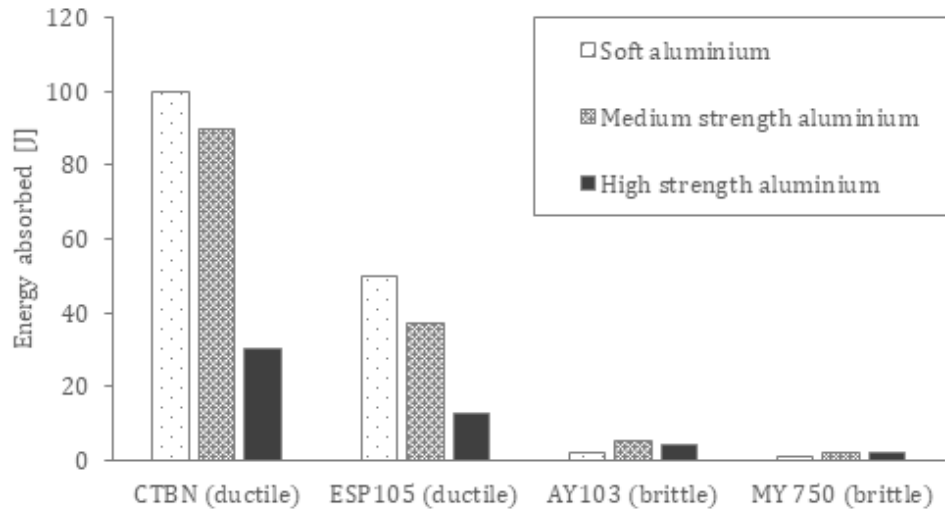
Figure 12 - Absorbed energy at impact conditions for three types of substrates and two adhesives. (Adapted from Harris and Adams, 1985) [25].

2.3.1 Adhesives under impact loads and temperature influence

Adhesives, owing to their polymeric nature, are highly sensitive to strain rate and temperature. A few studies have concerned on the effect of temperature and strain rate on adhesive behaviour.

Sharon et al. [26] studied the effects of loading rate and temperature on the viscoelastic related properties of four structural adhesives. They conclude that the yield stress and modulus decreased with temperature while the loading rate presented a pronounced effect on the yield stress which increased with increasing loading rate and had a negligible influence on the modulus.

A similar study was done by Banea et al. [27] to find the tensile properties of a high temperature epoxy with a T_g of 155°C (Figure 13). It is easy to perceive the effect of temperature and loading rate on tensile stress-strain curve of the adhesive. They found that the ultimate tensile stress decreased linearly with temperature while increased logarithmically with the loading rate. The Young´s modulus presents a similar behaviour than ultimate tensile stress, as function of loading rate while the decrease as function of temperature as nonlinear. It's also worth mentioning that the effect of temperature on the properties was more significant than that of the strain rate.
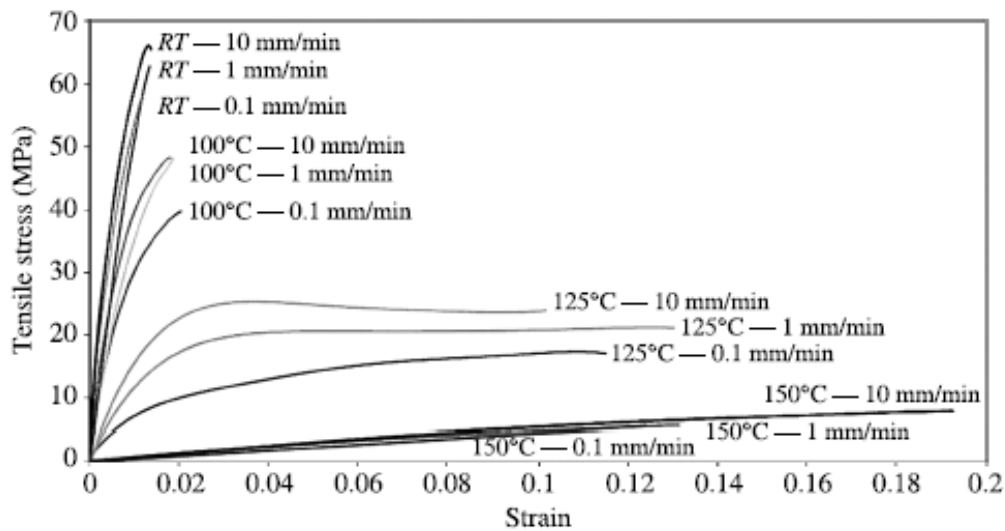
Figure 13 - Representative XN1244 adhesive tensile stress–strain curves as a function of temperature and test speed (the curves for 150◦C — 0.1 mm/min and 150◦C — 1 mm/min are nearly coincident) [27].

2.3.2 Aluminium substrates under impact loads and temperature

Aluminium has traditionally been considered to have low strain rate sensitivity, however this strongly depends of the alloy. Holt [28] found that pure aluminium reveals moderate sensitive to strain rate. The flow stress of pure aluminium increases linearly with the logarithm of strain rate at RT, and the strain rate sensitivity increases at rates above $1x10^3 s^{-1}$ [29]. However, with increasing alloy content or processing, such as heat treating or cold working, the strain rate sensitivity for aluminium alloys decreases [28-30]. Negative strain-rate sensitivity, cause by dynamic strain aging, was found by some authors for some alloys in the AA5xxx series [31-33].

Oosterkamp et al. [34] did compression tests on AA6082 and AA7108 in tempers T6 and T79 at strain rates ranging from 0.1 to approximately 2000 s^{-1}. At RT, they found a very low, yet slightly positive, increase in flow stress with strain rate.

Smerd et al. [35] studied the stress-strain behaviour in tension of two non-tempered aluminium alloys for a four strain rates from 3.3x10^{-3} s^{-1} to 1500 s^{-1} and for four temperatures (23, 50, 150 and 300°C). The results show that strain rate sensitivity to was low for both alloys at al temperatures tested.

Chen et al. [36] studied the stress-strain behaviour of four aluminium alloys for a wide range of strain rates (Figure 14). They found that while AA6060 T6 and AA6082 T6 exhibit only slight sensitivity to the strain rate, and could probably be modelled as rate-insensitive with good accuracy, AA7003 T6 and AA7108 T6 show a marked sensitivity to strain rate, which should be included in simulations.
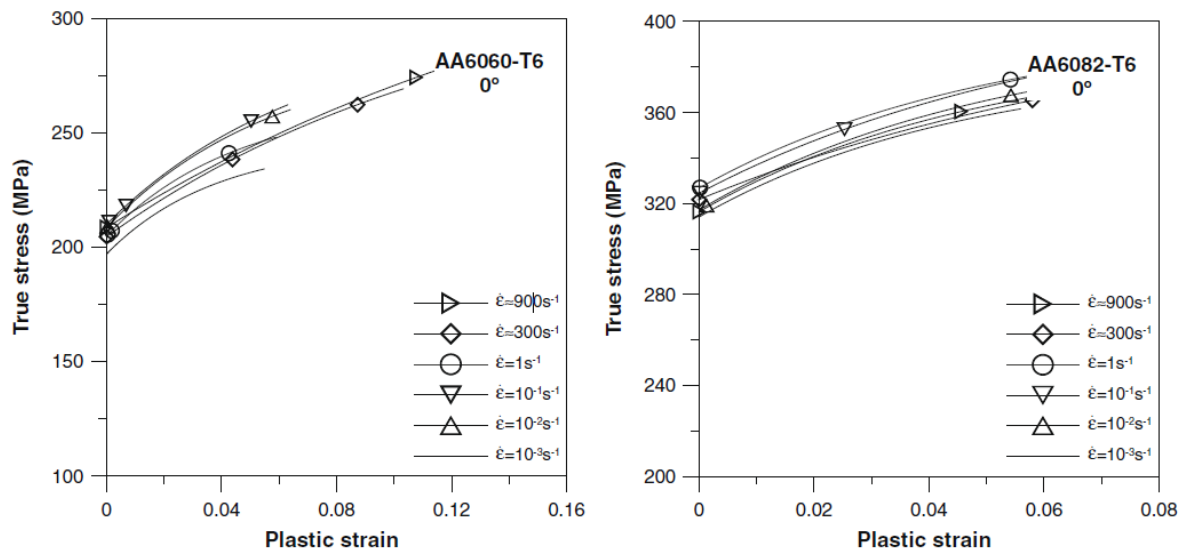
Figure 14 - Representative true stress versus true plastic strain curves at wide range of strain rates for AA6060 T6 and AA6082 T6 alloys0 [36].

It can be concluded that the bulk mechanical behaviour of aluminium alloys does not appear to present significant sensitivity to the range of temperatures and strain rates typical of automotive industry construction.

2.3.3 CFRP substrates under impact loads and temperature

Considering that composite materials are anisotropic and composed by two constituents, the behaviour analysis as a function of temperature and strain rate isn´t straight forward. While the carbon reinforcements are highly insensitive to temperature variation and loading rate, the matrix is made of a polymer material, the same family material that adhesives are made of.

From what was mentioned a above regarding adhesives, it is expected that temperature and strain rate have influence in the CFRP properties. This topic was investigated by several authors.

Harding and Welsh [14] studied the effect of strain rate in the longitudinal tensile properties of unidirectional CFRP and found no significant effects of strain rate. Taniguchi et al. [37] performed a more detailed study of the effect of strain rate also for unidirectional CFRP, since transversal tensile properties and shear properties were also determined as function of strain rate (Figure 15).
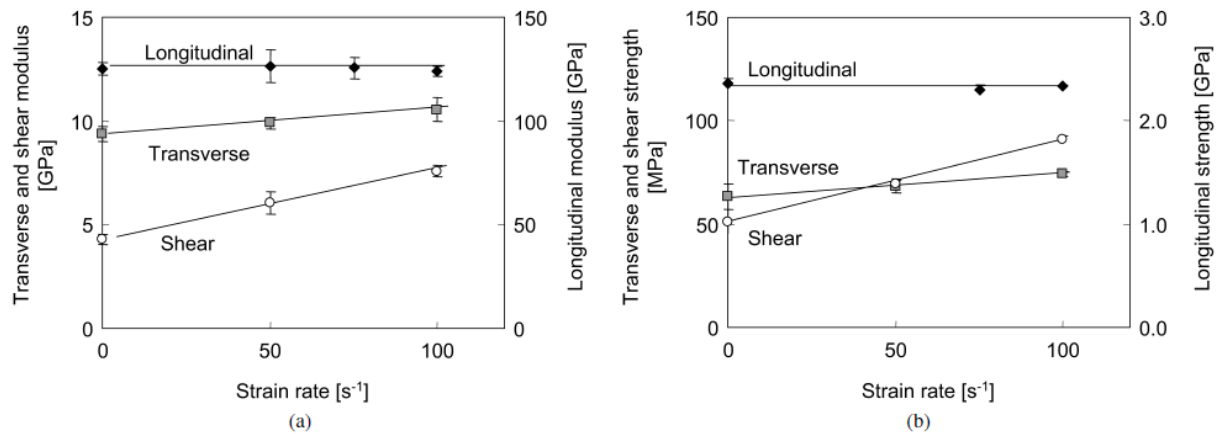
Figure 15 - (a) Dependence of the strain rate on modulus, (b) Dependence of the strain rate on tensile strength. [37].

From Figure 15, it is possible to confirm that the longitudinal tensile properties were unaffected by the strain rate but regarding the transversal tensile properties and shear properties the same conclusion cannot be made. While for transverse tensile modulus and transverse strength the increase with strain rate is slight, for shear modulus and shear strength this trend is more pronounced.

23

Hou and Ruiz [38] also concluded in their study that properties that are dominated by the matrix like compression strength, Poisson's ratio, in-plane shear modulus, shear modulus and shear strength are strain rate dependent. The properties dominated by the fibres like tensile modulus and strength are virtually rate independent.

Gómez-del Río et al. [39] studied the effect of low temperature on the dynamic tensile properties of unidirectional and quasi-isotropic CFRP. For unidirectional CFRP, they found that the effect of temperature was negligible in the longitudinal direction whereas in the transversal direction the strength increased appreciably (Figure 16).
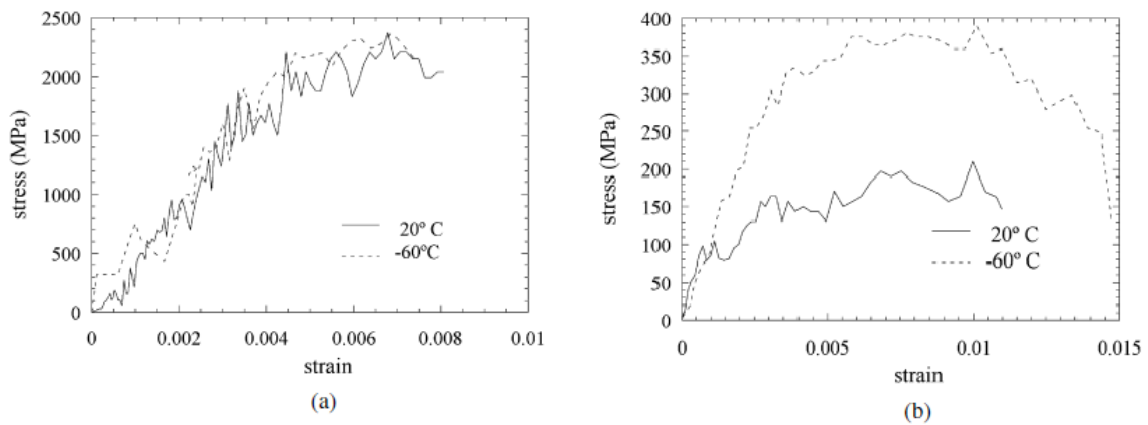
Figure 16 - Stress–strain curves for unidirectional laminate, (a)longitudinal direction, (b) transversal direction, at 20 and 60°C. Strain rate around 750 s-1 [39].

Machado et al. [40] studied the effect of both temperature and strain rate on fracture energy in mode I (G_{Ic}) [40] (Figure 17) and mode II (G_{IIc}) [41] (Figure 18) of CFRP plates. They tested double cantilever beam (DCB) specimens at -30, 20 and 80°C, with strain rates of 0.2 and 11 s^{-1}. With the use of a logarithmic trend function, they extrapolated the values for impact condition. This work has demonstrated a significant influence of the strain rate and temperature on fracture energy of both modes of the composite materials, with higher strain rates and lower temperatures causing a decrease in the G_{Ic} and G_{IIc} values.
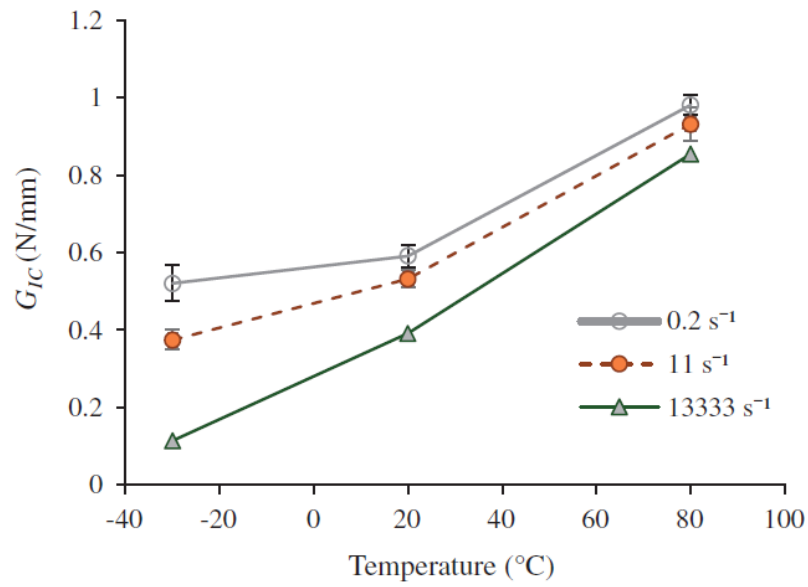
Figure 17 - G_{Ic} of unidirectional CFRP as function of strain rate and temperature [40].
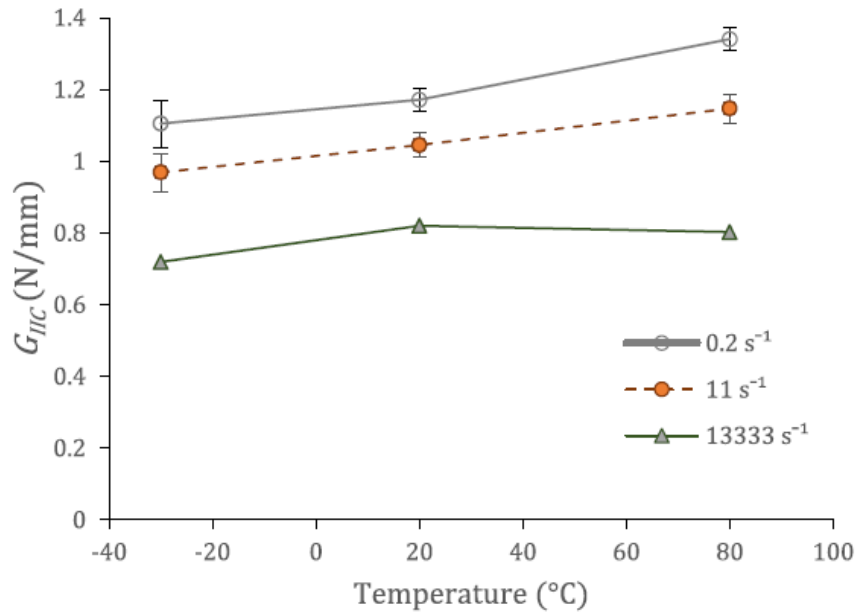
Figure 18 - G_{IIc} of unidirectional CFRP as function of strain rate and temperature [41].

Understanding the capability of a composite structure to absorb energy through-controlled failure mechanisms is critical to improve safety of a vehicle under impact conditions. The energy absorption of composite materials depends on several parameters such as: type of

fibre and matrix, fibre architecture, specimen geometry, fibre volume and processing conditions, and testing speed. The rate at which the structure is loaded has an important effect on both the material´s behaviour and the structure response of the target [42]. The energy absorbed response of composite materials has been assessed by several authors with diverse results. While some authors [43-47] have found a decrease of the energy absorption of composite structures with the increase of strain rate, other authors such as Thornton [48] and Farley [49] found a significant increase of the energy absorption of composites with the increase of strain rate. These works suggest that that the configuration and the materials comprising the composite has significant influence on the energy absorption process.

2.4 Strength prediction of single lap joints

Strength prediction of SLJs can be made by analytical and numerical approaches. There are several useful analytical methods available to predict strength joints but despite their simplicity, they are very restricted to well defined geometries and loading conditions. For more complex geometries and more powerful material models, the use of finite element analysis (FEA) is preferred, due to the improved flexibility of this type of approach.

2.4.1 Numerical methods

The first authors that used FEA for adhesive joints were Wooley and Carver [50] in 1971, followed by Adams and Peppiatt [51] in 1974. Despite the work of Wooley and Carver [50] being considered as a significant evolution in the prediction of the failure load in SLJs, these models do not consider fracture mechanics. Linear elastic finite models have been recently combined with fracture mechanics to create cohesive damage models, which offer the possibility of predicting the crack propagation as a result of simulated degradation of the material. To explain how the cohesive zone model works it is necessary to understand a few concepts of fracture mechanics.

2.4.1.1 - Fracture critical energy

In fracture mechanics it is assumed that materials in a structure are not necessarily a continuum medium, this means that defects can occur in the manufacturing process, for example, and it is essential to understand how these defects can evolve during the life time of the structure, if it leads to a catastrophic failure or if can safely being used despite a possible stable propagation.

The basic principles of fracture mechanics, mainly due to Griffith [52], state that all bodies have a defect distribution and fracture occurs from the critical one. There are two different criteria that allow to develop the principle above, a stress concentration factor-based criterion and energetic criterion. Griffith established that an internal defect will propagate when the available energy at the tip of the defect (G - release rate energy), due to the loading, equals the energy needed for crack propagation (G_c - critical release rate energy), that is a material property. Kinloch [5] refers that is advantageous to use the energy criterion instead of the factor criterion, in what concerns adhesive joints.

Mode I: Mode II: Mode III:
Opening   In-plane shear   Out-of-plane shear
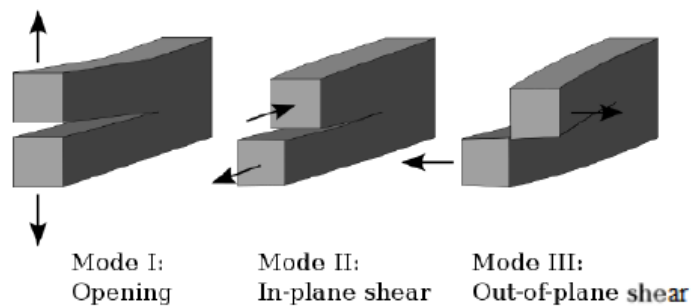
Figure 19 - The three modes of loading [1].

Regarding fracture mechanics, there are three fracture modes that depend mainly how the load is applied: Mode I, II and III (Figure 19). Mode I loading occurs when the load is applied perpendicularly to the plane of the crack, conducting to the tensile mode, Mode II, where a shear load is applied parallel to the plane of the crack and perpendicular to its front, in-plane shear mode and Mode III, where a shear load is applied on a parallel plane to the crack and also parallel to the crack's front, out-of-plane shear mode. In homogenous and isotropic materials crack tend to propagate in mode I. However, in bonded joints the direction of crack propagation

is restricted by the substrates causing, in most of the cases, a mixed-mode propagation in mode I+II.

For each loading mode there are a few tests to determine the fracture energy. For mode I, Double Cantilever Beam (DCB) and Tapered Double Cantilever Beam (TDCB), while End-Notched Flexure (ENF), End Loaded Split (ELS) and Four-Point Notched Flexure (4ENF) are used for mode II [1].

2.4.1.2 - Cohesive damage model

The necessity to make a bridge between stress analysis criteria and classical fracture mechanics led to the creation of a computational tool called the Cohesive Zone Model (CZM). The combination of the stress criteria with the fracture mechanics data made possible to determine the crack initiation and growth. The CZM was first introduced by Barenblatt [53] based on the Griffith´s theory of fracture, however the first researcher that applied it to the computational frameworks of FE modelling was Hillerborg et al. [54], who established the relation between traction and the crack opening displacement, and consequently the law of traction-separation (Figure 20).
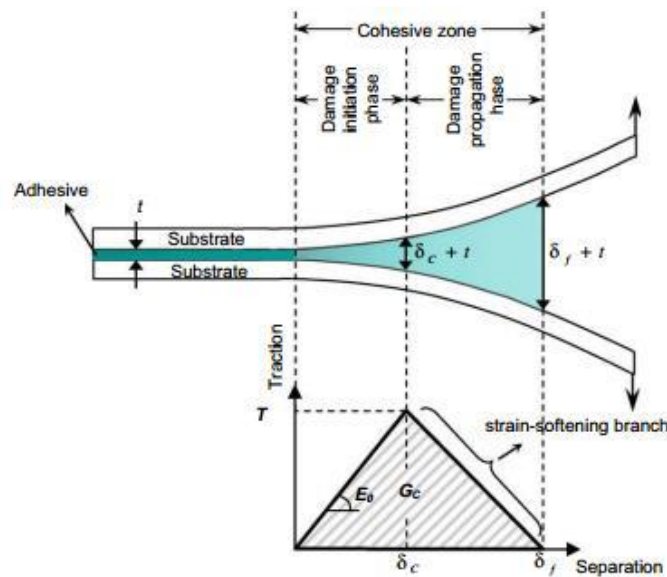
Figure 20 - Representation of the damage zone and corresponding bi-linear traction-separation law in an adhesively bonded joint [55].

The traction-separation law (Figure 21) describes the material behaviour in two distinct phases, the first related to the damage initiation phase, that can be delimited by the elastic behaviour and its limit and another related to the damage propagation phase. Traction-separation laws can present various shapes like triangular, the most common, trapezoidal and exponential, these shapes are related with the plastic behaviour of the material. Although trapezoidal law is mainly used on ductile materials, and the triangular law is used on brittle and composite materials, some authors use triangular law for ductile materials as it is the most common.
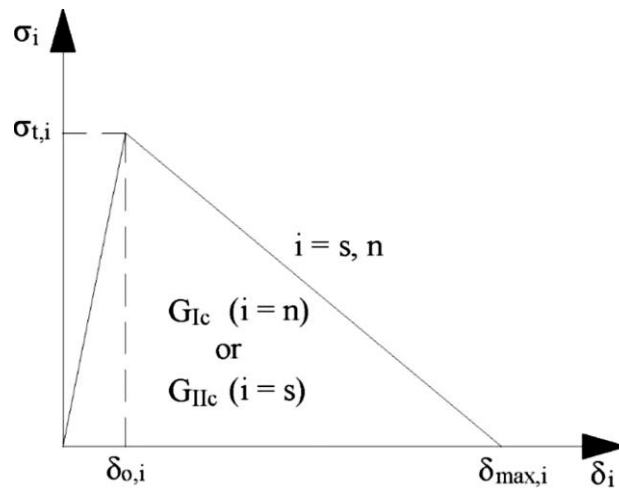
Figure 21 - Example of the triangular traction-separation law [56].

Figure 21 presents a triangular traction-separation law that can be divided in two triangles. The first one is defined by the elasticity modulus (the slope) and limited by the cohesive strengths ($\sigma_{t,i}$) that correspond to the peak on the graphic and defines the critical relative displacement ($\delta_{o,i}$), once it is exceeded the failure starts, defining the second triangle, the sum of both areas corresponds to the critical failure energy. So, knowing the elastic modulus, the cohesive strength and the critical failure energy, it is possible to find the maximum relative displacement ($\delta_{max,i}$) [56, 57].

The traction separation law can be made for the three modes (I, II and III) referred earlier. Also mentioned earlier was that in bonded joints the direction of crack propagation is described by a mix-mode propagation in mode I+II. Figure 22 shows a pure-mode (tension and shear) law, and the mixed mode law.
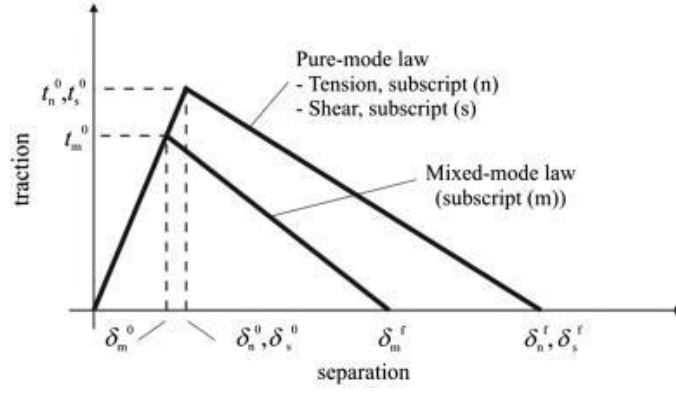
Figure 22 - Traction-separation law with pure and mixed laws [58].

Regarding to the mathematical approach, as the initial behaviour of the law is elastic it can be modelled by the elastic constitutive matrix, *K* (Equation 1) [59].

$$t = \begin{Bmatrix} t_n \\ t_s \end{Bmatrix} = \begin{bmatrix} K_{nn} & K_{ns} \\ K_{ns} & K_{ss} \end{bmatrix} \begin{Bmatrix} \varepsilon_n \\ \varepsilon_s \end{Bmatrix} = K\varepsilon$$

(Eq. 1)

For thin adhesive layers, several considerations can be made: $K_{nn}=E$, $K_{ss}=G$ and $K_{ns}=0$, where *E* and *G* are the Young's modulus and shear modulus, respectively.

The complete separation and mixed-mode failure displacement are predicted by the following linear power law form equation of the required energies for failure in the pure modes (Equation 2) [59].

$$\frac{G_n}{G_n^c} + \frac{G_{s1}}{G_{s1}^c} = 1$$

(Eq. 2)

To implement this method, varied property data of the substrates and the adhesives is required, such as the Young´s modulus (E) and shear modulus (G), cohesive strength in tension and shear (t_n and t_s, respectively), the tensile (G_{Ic}) and shear toughness (G_{IIc}), that can be obtained experimentally.

3 Experimental details

3.1 Material selection

One adhesive was selected for this study, a ductile, one-component, epoxy based adhesive, Nagase-ChemteX XNR6852 E-3, supplied by Nagase ChemteX® (Osaka, Japan) (Table 3). This adhesive was selected because is a crash resistant adhesive and has been study by the adhesive group in previous works. The CFRP selected for this specific lay-up and fibre orientation was due the existence of data from previous works performed by the adhesive group.

Table 3 - General properties of the crash-resistant adhesive used (Nagase-ChemteX XNR6852 E-3).

Adhesive	XNR6852E-3
Type of adhesive	Epoxy
Physical forms	One-part system
Cure cycle	4h at 165°C
T_g (° C)	132 ± 4.51°C (experimentally)
Comments	Crash resistant

Three different materials for the substrates were used in this study, two aluminium alloys (AA5754 H22 and AA6060 T6) and a composite material (CFRP). The aluminium alloys were selected as a request from Aston Martin Lagonda®, aiming to evaluate the behaviour of adhesive joints with these alloys as substrates, as well with CFRP, under conditions typical of the automotive industry (Table 4), that is, under quasi-static and impact conditions for a range of temperature between -30 to 80°C. These types of materials are currently being used in the latest models commercialized, as well as prototypes being developed by this car manufacturer.

Table 4 - Designation of substrates tested.

Substrates
Unidirectional CFRP with 2.1 mm thickness (made of 14 plies of carbon/epoxy pre-preg SEAL® Texipreg HS 160 RM)
Aluminium alloy AL5754 H22 with 1.5 mm thickness (in the graphics below will be designated as *Al 1.5*)
Aluminium alloy AL6060 T6 with 2.0 mm thickness (in the graphics below will be designated as *Al 2.0*)

Elastic and plastic aluminium properties were provided by Aston Martin Lagonda®, and are presented in the Table 5 and the Figure 23. The substrates thicknesses previously indicated are representative of the average value for each material being used in the vehicles manufactured by Aston Martin Lagonda®.

Table 5 - Elastic properties of the aluminium alloys used (AA5754 H22 and AA6060 T6).

	Elastic modulus (GPa)	Poisson´s ratios
Al 5754 H22	69	0.33
Al 6060 T6	69	0.33
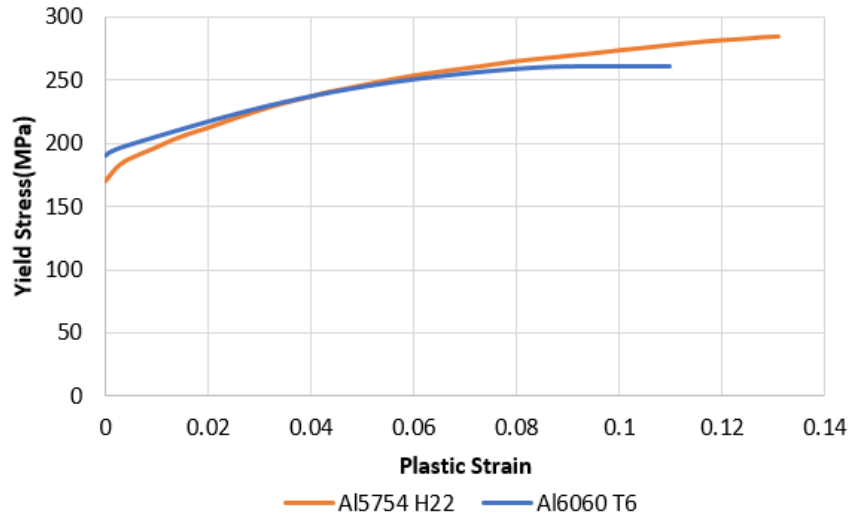
Figure 23 - Yield stress versus plastic strain of the aluminium alloys used (AA5754 H22 and AA6060 T6).

3.2 Adhesive characterization

Because the adhesive used in this work is still in the development stage, the properties could change from batch to batch. To verify the properties of the adhesive and understand the effect of temperate on the adhesive, tensile tests were performed under different displacements rates, and three temperatures, -30, 24 and 80°C. DCB tests were also performed to determine the fracture energy tests in mode I.

3.2.1 Tensile test

Bulk tests were performed to obtain the Young's modulus and the tensile stress of the adhesive since they are the properties needed to introduce into the Finite Element Analysis (FEA) model. Specimens were manufacture according to EN ISO 527-2 standard using the geometry represented in Figure 24.
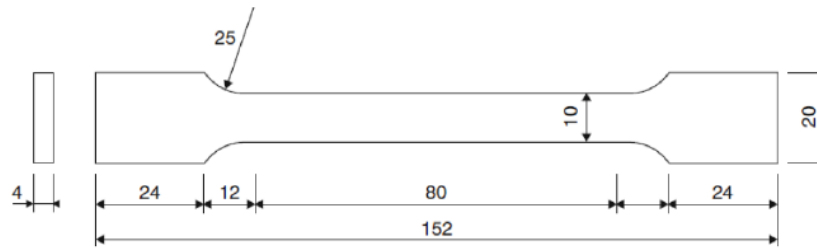
Figure 24 - Geometry of bulk specimens according to EN ISO 527-2 (dimensions in mm) [60].

3.2.1.1 Manufacture

To produce the adhesive bulk specimens, bulk sheet plates were manufactured. To do so, a steel mould was used, with the help of a silicon rubber frame to ensure that the adhesive does not flow out, following a design based on French standard NF T76-142 (Figure 25). To ensure that the bulk sheet plate is free from contamination, the mould was first abraded with sandpaper and then degreased with acetone. To finish the mould preparation, three layers of mould release agent (Loctite® Frekote 770-NC) were applied to promote easier removal of the cured bulk sheet plate from the mould.
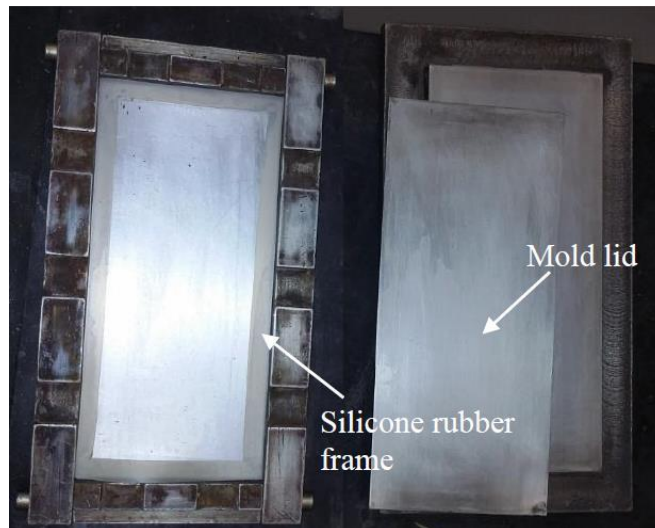
Figure 25 - Mould for producing the bulk specimens with steel plates and silicone rubber frame.

Decreasing the viscosity of the adhesive was achieved using a high speed centrifugal mixing machine (SpeedMixer® DAC 150.1 FVZ-K). Mixing the adhesive raises its temperature and thus lowers its viscosity. To apply the adhesive into the cavity mould, a spatula was used, applying an excessive amount of material to guarantee that voids are avoided. After the conclusion of adhesive application, the mould was closed and inserted into a hot press at curing temperature and under pressure, according to the specific cure cycle (Figure 26).
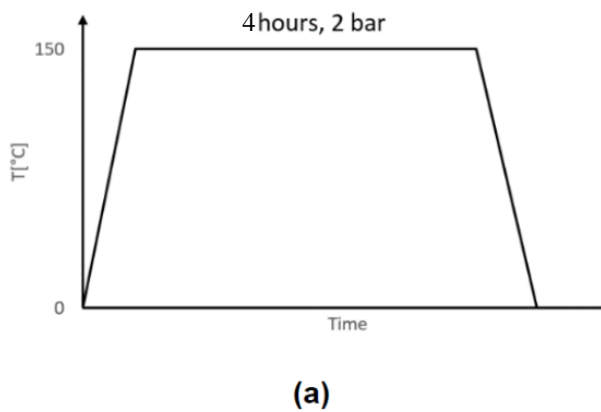
Figure 26 - Cure cycle of Nagase-ChemteX adhesive XNR6852 E-3.

As soon as the cure cycle was completed, the bulk sheet plates were removed from the mould and machined with the dogbone shape geometry described in Figure 24. To allow displacement measurement and recording using an extensometer video system, two dark lines were drawn on the specimens perpendicular to the longitudinal direction.

3.2.1.2 Testing procedure

The tests were carried out in an INSTRON® universal test machine (Norwood, Massachusetts, USA) (Figure 27), equipped with a load cell with a capacity of 30 kN. A tensile test consists in imposing a displacement rate in the longitudinal direction of the specimen until failure. During the test an increasing load is applied by the machine and recorded by the load cell. An optical method was used to record the displacement of the specimen, with a digital camera taking pictures of the gauge length between the two lines during the test, allowing to

record all the stages until failure. An image processing and analysing software was used to obtain the strain for each specimen. The width and thickness of each specimen were measured in order to calculate the stress of each strain stage.

Figure 27 - INSTRON® universal test machine.

At least four specimens of each adhesive for each condition were tested. The strain rate conditions were, 0.004 s⁻¹, equivalent to a displacement rate of 1 mm/min, and 0.42 s⁻¹, which is equivalent to a displacement rate of 100 mm/min. For each strain rate tests were performed at three different temperatures (-30, 24 and 80°C).

The conversion of machine cross-head displacement to strain rate was conducted, resorting to Equation 3 to correctly estimate the effect of the testing speed, since it is more accurate to use the actual strain rate of the tested material.

$$\dot{\varepsilon}(t) = \left(\frac{L(t) - L_0}{L_0}\right) = \frac{v(t)}{L_0} \qquad \text{(Eq. 3)}$$

Where, L_0 is the original length, $L(t)$ corresponds to the length at each time t, and $v(t)$ corresponds to the speed at which the ends are moving away from each other. For bulk tests 80 mm was used for the value of L_0 as corresponds to the gauge length.

With the tensile test, the Young's modulus and the tensile strength were obtained. Young's modulus was determined considering the slope of stress-strain curve whereas tensile strength is obtained directly from the stress-strain curve.

3.2.1.3 Bulk tensile tests results

From the bulk tensile tests, only two adhesive properties were obtained: Young's modulus (E) (Figure 28) and tensile strength (σ) (Figure 29). These properties were selected since those were the only properties required in the FE simulation.

Figure 28 presents the measured Young´s modulus and respective standard deviations. It is possible to notice that Young´s modulus decreases linearly with the increase of temperature and increases with strain rate. As the temperature approaches T_g, the adhesive becomes more ductile.
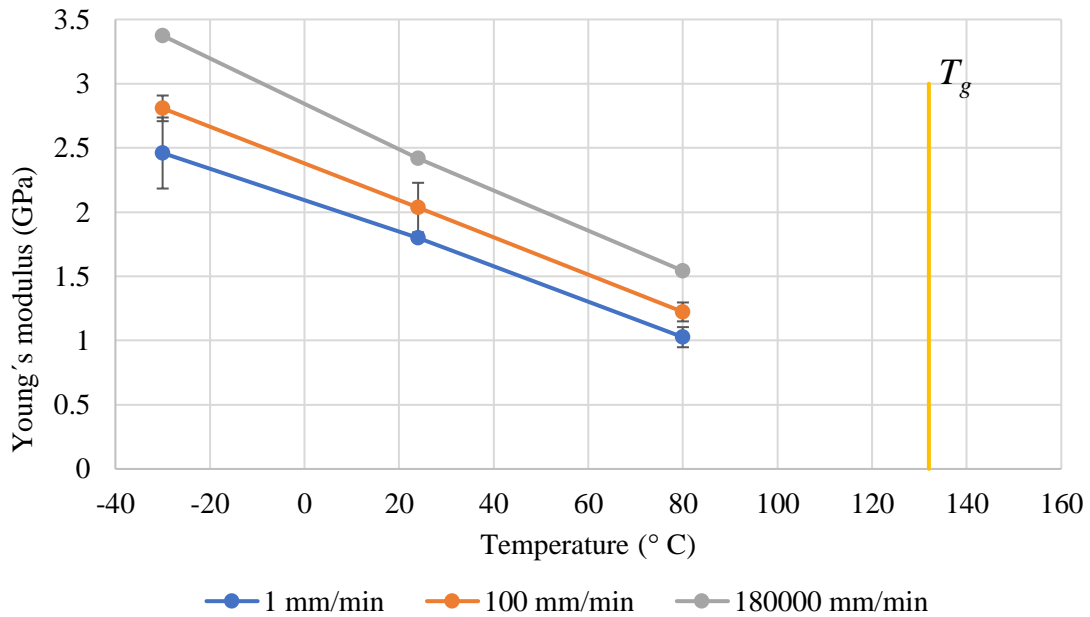
Figure 28 - Young´s modulus of adhesive XNR6822E-3 as a function of strain rate.

Figure 29 presents the measured tensile strength and the respective standard deviation. The tensile strength decreases with increase of temperature and increases with strain rate. As the temperature approaches T_g, the adhesive presents a considerable reduction in the tensile strength.
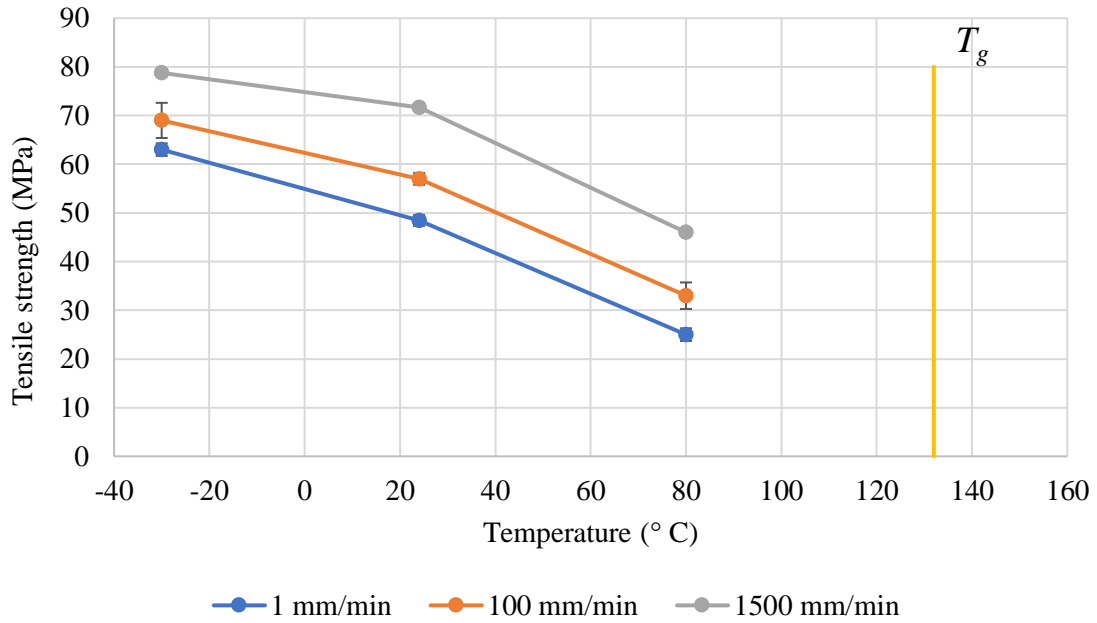
Figure 29 - Tensile strength of adhesive XNR6822E-3 as a function of strain rate.

For both properties, Young´s modulus and tensile strength, it is possible to notice that the effect of temperature is considerable more significant than that of the strain rate.

Young´s modulus (Figure 30) and tensile strength (Figure 31) were extrapolated using a logarithmic trendline to impact condition with a value of 180000 mm/min for the three different temperatures.
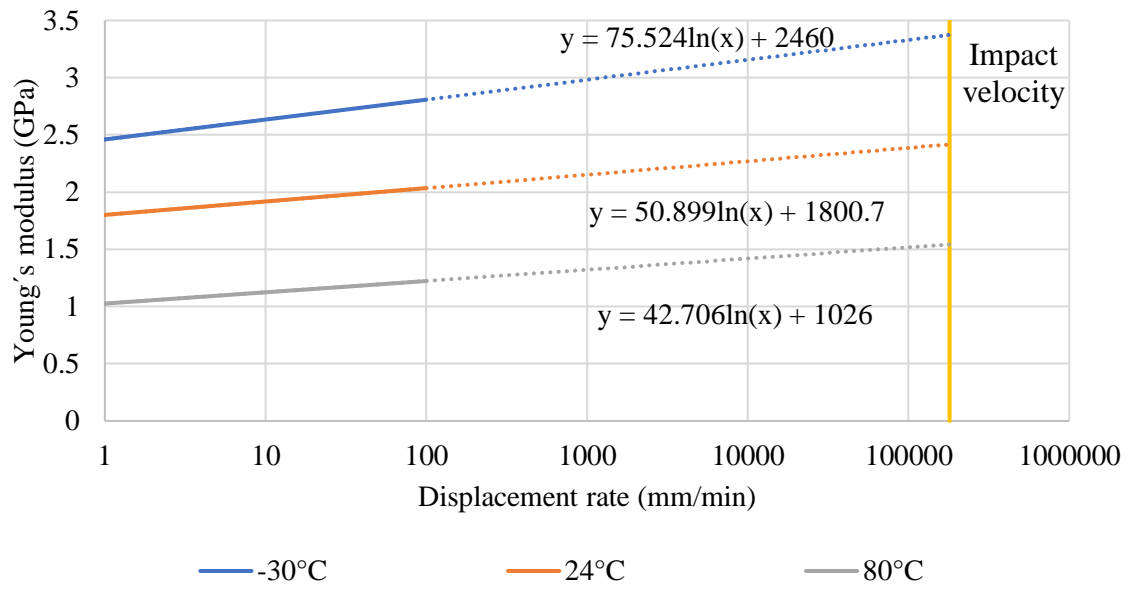
Figure 30 - Values of Young´s modulus of adhesive XNR6852 E-3 estimated for impact conditions.
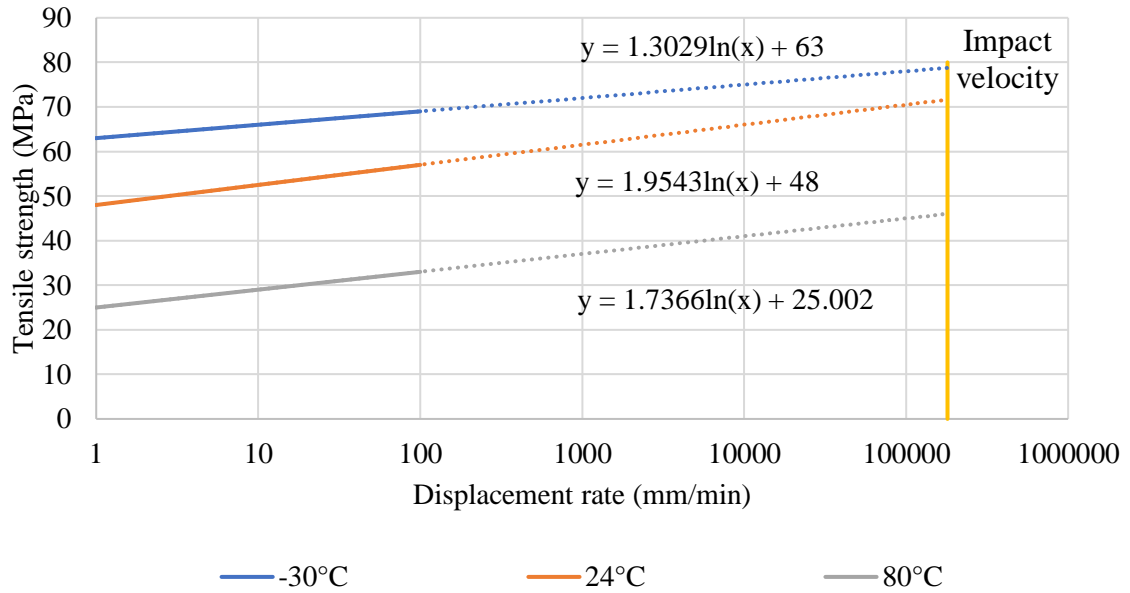
Figure 31 - Values of tensile strength of adhesive XNR6852 E-3 estimated for impact conditions.

3.2.2 Double cantilever beam

In this work DCB tests were selected to determine the fracture energy in mode I. Because the need to determine the fracture energies at different temperatures, and the relatively small size of the temperature chamber, an adaptation to the normalized specimens was made, making then slightly shorter, changing the total length from 290 to 190 mm (Figure 32).
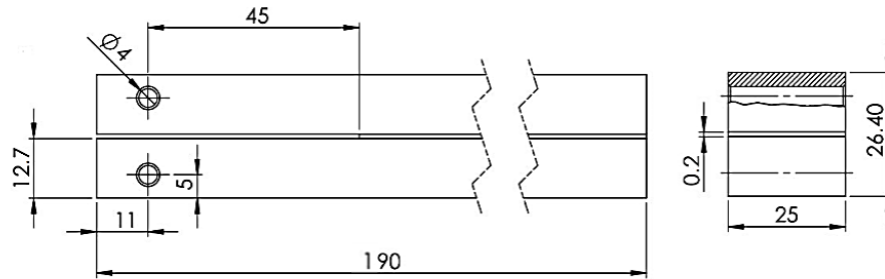
Figure 32 - DCB specimen geometry (dimensions in mm).

3.2.2.1 Manufacture

To obtain the fracture energies in mode I of the adhesive in study specimens were produced according to the geometry represented in Figure 32. The substrates used were made of steel (DIN 40 CrMnMo 8-6-4) to avoid plastic deformations (Figure 33).
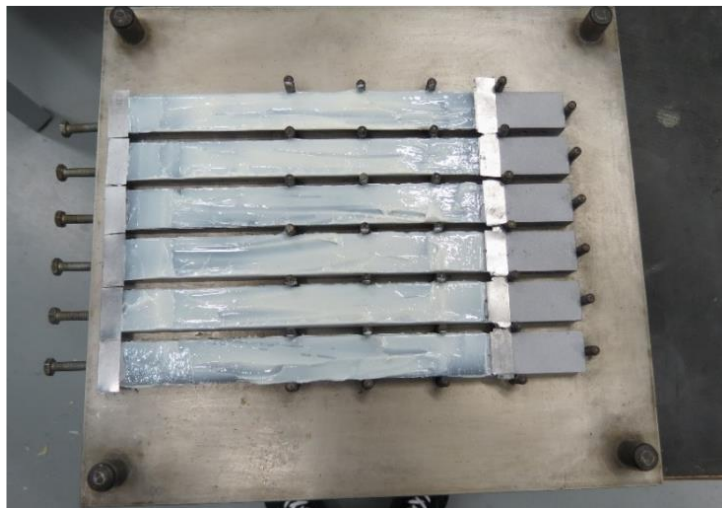
Figure 33 - Adhesive applied in the open substrates.

For surface preparation the steel substrates were sandblasted at a pressure of 6 bar with aluminium oxide particles and then cleaned with acetone to degrease the surfaces, since a proper adhesion is fundamental.

Figure 34 - Shot blasting machine.

To ensure the adhesive thickness, spacers and a razor blades were used. Calibrated tape of 0.2 mm was used in the opposite extreme of crack initiation and at the begin of the crack a 0.1 mm razor blade, with 0.05 mm tape glued on each side, was used. The razor blade serves other purpose as well, since it introduces a specific geometry at the beginning of the crack that controls the crack initiation in the middle of the adhesive layer and thus ensures a stable crack propagation through the test.

The adhesive was placed in the SpeedMixer® DAC 150.1 FVZ-K, a mixing machine, as used in the tensile test, and was then applied in both substrates using a spatula. The substrates were assembled in the mould, aligned by the mould pins.

Figure 35 - Mixing machine SpeedMixer® DAC 150.1 FVZ-K.

The mould was closed and inserted in the hot plates hydraulic press at the cure cycle referred above in the tensile test manufacturing procedure.

Once the cure cycle was finished, the mould was removed from the press, and then, the specimens were unmoulded. During the cure cycle excessive adhesive flowed out from the bond line. To enable clear measurement of the pre-crack length the excess of adhesive was removed from the sides of the specimens with sand paper and a milling machine.

3.2.2.2 Testing procedure

The tests were performed on INSTRON® universal testing machine, according to ASTM D3433 standard. The setup used to test the DCB specimens is shown on Figure 36.
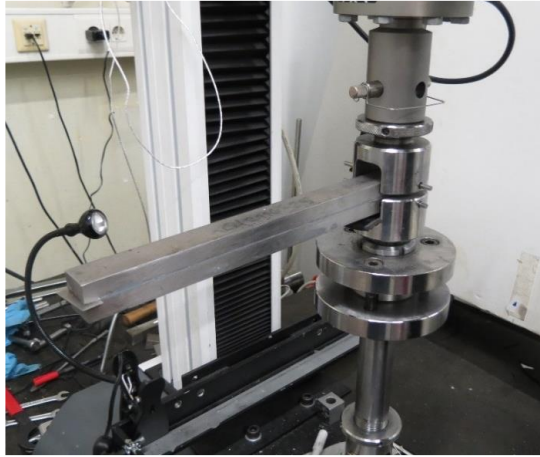
Figure 36 - DCB setup.

In this test, the loading was applied perpendicularly to the adhesive layer (Figure 37). For DCB tests, four specimens of XNR6852 E-3 were tested for three different displacement rates (1, 10 and 100 mm/min) that is equivalent to the following three strain rates (0.083, 0.83 and 8.33 s-1). For each strain rate, the tests were performed for three different temperatures (-30, 24 and 80°C). The conversion from displacement rate to strain rate was performed resorting to Equation 3. For DCB tests 0.2 mm was used for the value of L_0 as corresponds to the adhesive thickness.
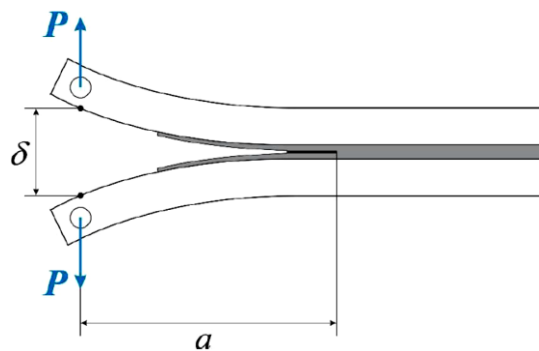
Figure 37 - Loading scheme of the DCB specimen.

3.2.2.3 Data reduction schemes for fracture energy determination

Compliance Calibration Method

This method is based on Irwin-Kies equation and it also uses the load displacement data and the real crack's length [61, 62]. Equation 4 gives the failure energy based on Irwin-Kies theory,

$$G_{Ic} = \frac{P^2}{2b}\frac{dC}{da} \qquad \text{(Eq. 4)}$$

Where G_{IC}, is the energy available for an increment of the crack propagation, P is the applied load, b is the width of the specimen, C is the compliance (Equation 5) and, a is the crack length.

$$C = \frac{\delta}{P} \qquad \text{(Eq. 5)}$$

The partial derivative of compliance is calculated using the displacement (δ) and the applied load (P). The compliance, based on the flexibility of the substrate, is given by a polynomial function of third degree (Equation 6) which is a function of the crack length

$$C = C_3 a^3 + C_2 a^2 + C_1 a + C_0 \qquad \text{(Eq. 6)}$$

Corrected Beam Theory

As in the previous method, this method requires load-displacement data and also the real crack's length, which it also derives from the Irwin-Kies theory [62]. The failure energy is given by the following equation:

$$G_{Ic} = \frac{3P\delta}{2b(a + |\Delta|)} \qquad \text{(Eq. 7)}$$

The crack tip rotation and deflection are considered in this method. In order to supress such effect, a correction factor of crack's length is used, Δ, which was proposed by Wang and Williams [63] in 1992 and is given by Equation 8:

$$\Delta = h\sqrt{\frac{1}{13k}\left(\frac{E_x}{G_{xy}}\right)\left(3 - 2\left(\frac{\Gamma}{1+\Gamma}\right)^2\right)} \qquad \text{(Eq. 8)}$$

Where E_x and G_{xy} correspond to the longitudinal normal and shear modulus of the substrate, h is the thickness of the substrate and k is the shear stress distribution constant for correcting the deflection caused by shear force, which is 0.85 for DCB specimens.

$$\Gamma = \frac{\sqrt{E_x E_y}}{k G_{xy}} \qquad \text{(Eq. 9)}$$

and, E_y is the Young's modulus of the substrates in the thickness direction [64].

The crack's length correction factor is set by a linear regression $C = f(a)$, which can be obtained experimentally, loading the specimen with three different loads, obtaining three different cracks' lengths (Figure 38) [65].
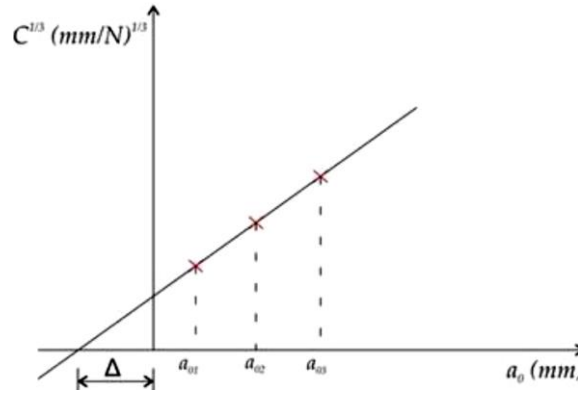
Figure 38 - Representation of linear regression of the correction crack length factor [66].

Compliance Based Beam Method

This method is based on beams' theory, which allows to define the compliance of substrates. Since this theory does not take in consideration the stress concentration and rotation of the substrates near the crack, a corrected bending modulus is used [67].

The failure energy is given by Equation 10.

$$G_{Ic} = \frac{6P^2}{b^2 h}\left(\frac{2a_{eq}^2}{h^2 E_f} + \frac{1}{5G_{13}}\right) \qquad \text{(Eq. 10)}$$

where, E_f and G_{13} are, respectively, the corrected bending modulus and shear modulus of the specimens and a_{eq} is the equivalent crack length.

Contrarily to the previous methods, as it can be seen in Equation 10, instead of the use of real crack's length, this method has its own definition of equivalent crack length. This measurement depends only of the specimen's compliance during the test. Equivalent crack's length is measured until half of the Fracture Process Zone (FPZ) (Figure 39), which is defined by the existence of multiple micro-cracks and plasticization's ahead the major crack that absorb some of the energy (Figure 44). For ductile adhesives, the energy dissipated in the FPZ is higher. This method is based on the beam theory of Timoshenko [67-69].
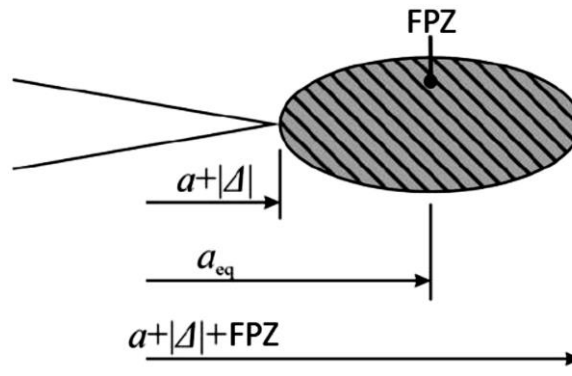
Figure 39 - Schematic representation of the FPZ (adapted from [67]).

3.2.2.4 Double cantilever beam tests results

The fracture toughness in mode I (G_{IC}) was obtained for the adhesive under different strain rates and temperatures (Figure 40).
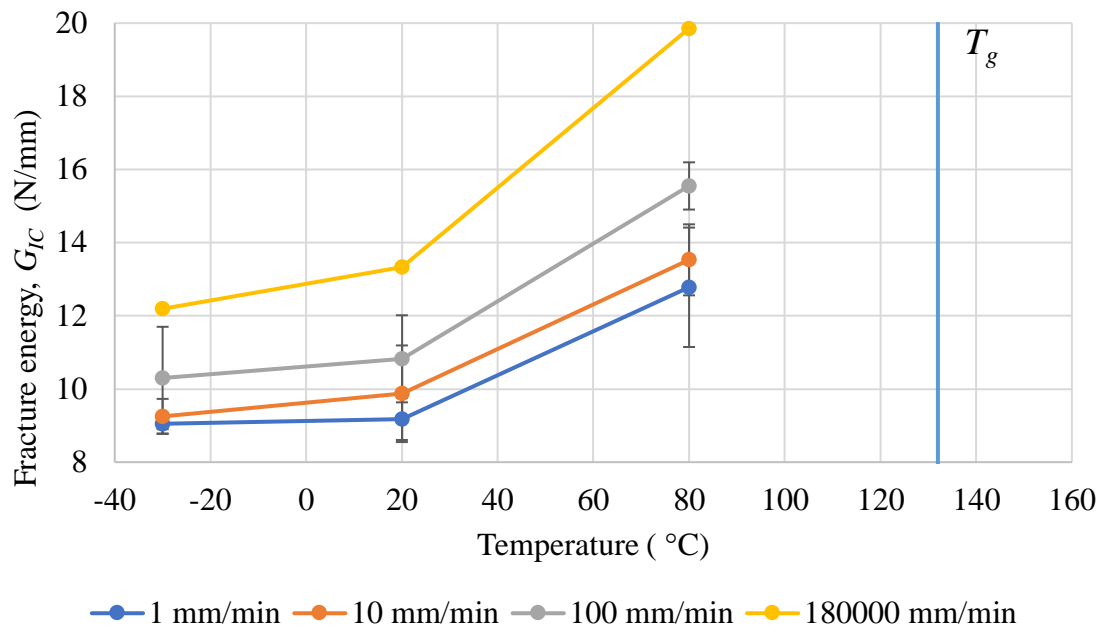
Figure 40 - Results of fracture toughness in mode I (G_{IC}) for adhesive XNR6852 E-3 as a function of strain rate and temperature.

The value of G_{IC} increases with the increase of both temperature and strain rate. As the temperature approaches T_g the adhesive becomes noticeably more ductile and tough. The values of G_{IC} in impact conditions (180000 mm/min) were extrapolated as explained in the end of the present sub-chapter.

The use of CBBM allowed to obtain the resistance curve (R-curve) of each experiment. The values were obtained from the plateau in the R-curve of each experiment, that occurred when the crack propagation stabilized. A representative R-curve is shown in Figure 41.
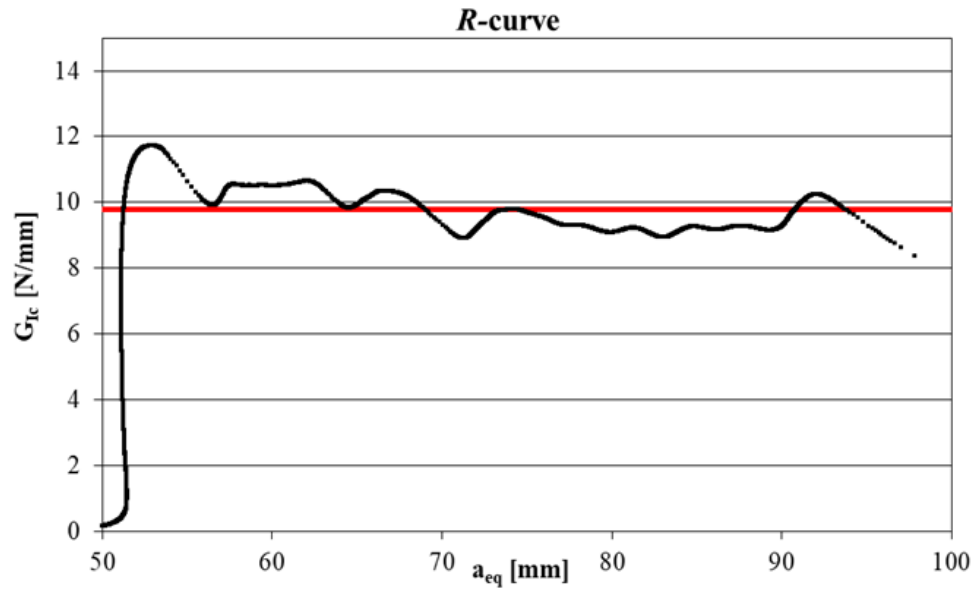
Figure 41 - Example of *R*-curve from the DCB test performed at 10 mm/min for a testing temperature of 24°C.

An inspection of the fracture surfaces allowed to conclude that mixed failure in the adhesive layer occurred, with a combination of adhesive and cohesive failure for all temperatures and strain rates. Further analysis of the fracture surface makes it evident that the adhesive suffered plastic deformation in all cases, since it presents a whitish colour, whereas its colour before the test was beige (Figure 42).
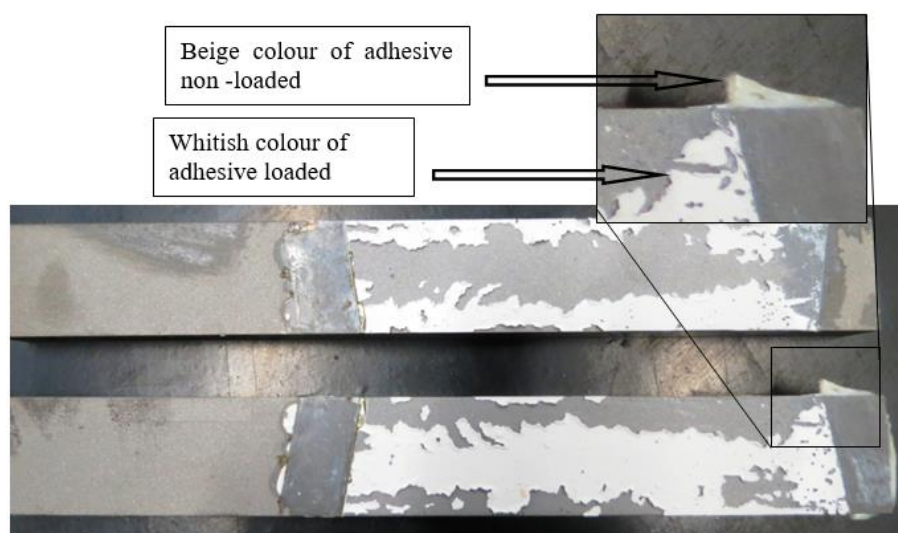
Figure 42 - Example of failure surface of a DCB.

Fracture toughness in mode I (G_{IC}) was extrapolated using a logarithmic trendline to impact condition with a value of 180000 mm/min for the three different temperatures (Figure 43).
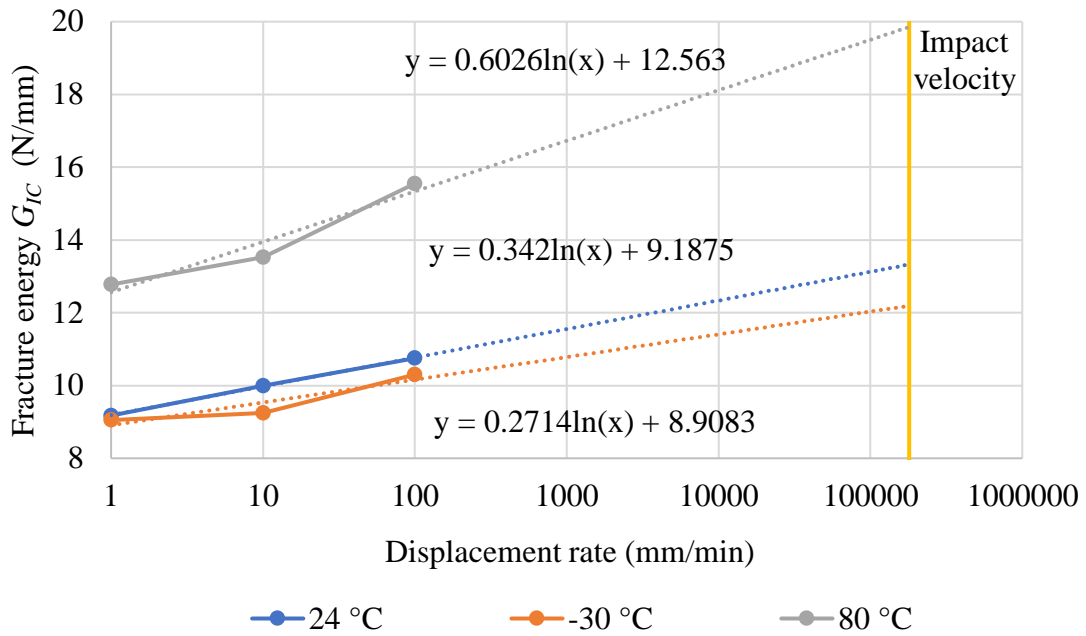
Figure 43 - Extrapolation of values of fracture toughness in mode I (G_{IC}) under impact conditions as a function of temperature.

Unlike the CFRP resin, the adhesive exhibits an increase in the fracture toughness with increase of strain rate. The positive influence of strain rate in the fracture energy was already observed by some authors [70, 71]. Such phenomena can be explained by the fact that the adhesive in this study is a modified epoxy, that demonstrates a combination of the best properties of epoxy and polyurethane adhesives. Kinloch et al. [72] tested both an unmodified and a rubber-modified epoxy and reached to the conclusion that while the unmodified adhesive did not exhibit great improvement of the fracture energy with the strain rate, the multiphase microstructure of the rubber-modified epoxy led to a significant increase of the fracture energy at higher strain rates.

3.3 Fabrication and testing of single lap joints

For a better understanding of the behaviour of dissimilar joints, both similar and dissimilar configurations of SLJs (aluminium and CRFP substrates) were manufactured. The adhesive used was the Nagase-ChemteX XNR6852 E-3.

3.3.1 CFRP plates manufacturing

The CFRP specimens tested in this work consisted on unidirectional laminates of CFRP cut from bulk laminates, which were produced by hand lay-up and cured in a hot plate press. The bulk laminates with dimensions of 300x300 mm2 were fabricated from stacking of unidirectional 0°lay-up (with the aim to obtain better properties in the loading direction) in a total of 14 plies of carbon/epoxy pre-preg (SEAL® Texipreg HS 160 RM) with 0.15 mm of ply thickness. The cure cycle applied was of 130°C for one hour.

Campilho [65] determined the mechanical properties of the pre-preg being used. Table 6 presents the Young´s modulus (E), the shear modulus (G), and the Poisson´s ratio (v) in the 3 axis direction (x,y,z), being E_1 the normal direction, E_2 the transverse direction and E_3 the out plane direction. As previously mentioned, the tensile properties of CFRP are known not to vary significantly with strain rate.

Table 6 - Properties of pre-preg SEAL® Texipreg HS 160 RM [65].

Elastic modulus (MPa)	Poisson´s ratios	Shear modulus (MPa)
E_1 = 1.09E5	v_{12} = 0.342	G_{12} = 4315
E_2 = 8819	v_{13} = 0.342	G_{13} = 4315
E_3 = 8819	v_{23} = 0.380	G_{23} = 3200

The manufacture process of CFRP substrates consisted on pilling manually one pre-preg composite layer above another until the desired thickness was obtained. The process can be divided in the following steps:

- The prepreg roll was removed from the freezer, being left to warm at RT;

- The pre-peg was cut in 300x300 mm squares using a metal cutter;

- The protecting Teflon layer was removed from each ply;

- The plies were positioned on top of each other, pressure was applied with one weight to avoid air bubbles and ensure correct position. The fibre direction (0º orientation) was ensured;

- For the last layer, the paper protection was kept, protecting the bulk plate during the curing cycle (Figure 44).

Figure 44 - Hot press pressure machine.

It was also necessary to prepare the mould used on the hot plates press. The process is therefore described.

- The first step consisted in sanding the aluminium plates surfaces and cleaning them with acetone;

- At least three layers of release agent were applied (Loctite® Frekote 770-NC).

The plates were then cured in a hot plate press (Figure 44) with an applied pressure of 137 bar and with a temperature of 150°C during one and half hour.

The last stage consisted in cutting the square with the necessary dimension for future use. In this case, a diamond disc cutting machine, model DV 25 Batisti Meccanica was used

(Figure 45). Edge finishing was carried out 40 manually by using a 120-grit sandpaper with the aim to remove the loose fibres and smoothen the sharp edge.

Figure 45 - Cutting machine used for to cut the squares of CFRP.

3.3.2 Joints manufacturing

The SLJs used in this work were produced using a mould (Figure 46). First the mould was cleaned with acetone and three layers of mould release agent were applied on the surface. Spacers and calibrated tape were used to ensure the correct position and adhesive thickness. The aluminium specimens were cleaned with isopropanol, followed by an hour on an oven at 190º C and then cleaned again with isopropanol to ensure that all the grease is removed. The CFRP specimens were sandblasted before being degreased with acetone to ensure good adhesion. The adhesive was spread manually, taking care to ensure that no air bubbles stay trapped in the adhesive. Once the setup was ready the mould was closed, and it was placed in

the hot plate press according to the adhesive cure cycle stated above. The pressure applied during curing was of 137 bar.
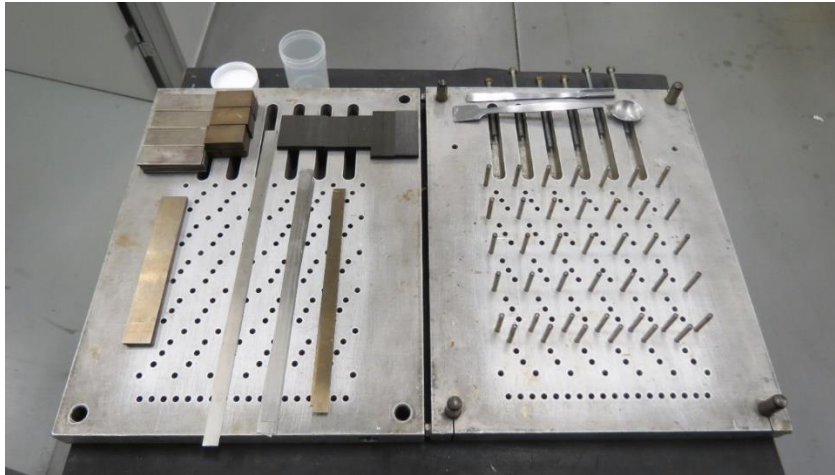
Figure 46 - Mould used to manufacture SLJs.

3.3.3 Joints configurations

The geometry used in both quasi-static and impact tests was chosen as its configuration is representative of the joints used in an automotive structure, with the thickness, overlap length of substrates and adhesive layer thickness being defined to be as close as possible to those used in the final application.

The CFRP substrates of the SLJs used have a thickness of 2.1 mm. The aluminium substrates used have a thickness of 1.5 and 2 mm for the alloys AA5754 H22 and AA6060 T6, respectively. The overlap length used was 25 mm for all ranges of temperature tested. The thickness of the adhesive layer used was 0.2 mm. The dimensions of the SLJ specimens used are shown in Figure 47.
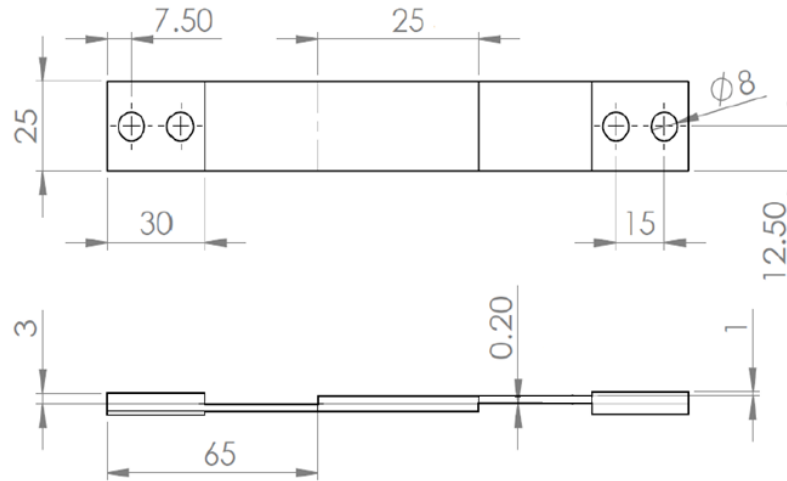
Figure 47 - Geometry of SLJ specimens (dimensions in mm).

All the combinations tested in this work are presented in Table 7.

Table 7 - Different combinations of similar and dissimilar SLJs.

	AA5754 H22 + AA5754 H22
Combinations with similar substrates	AA6060 T6 + AA6060 T6
	CFRP + CFRP
	AA5754 H22 + AA6060 T6
Combinations with dissimilar substrates	AA5754 H22 + CFRP
	AA6060 T6 + CFRP

3.3.4 Testing procedure

3.3.4.1 Quasi-static conditions

The quasi-static tests of SLJs were performed in a universal testing machine, model INSTRON® 3367 (Norwood, Massachusetts, USA) with a load cell capacity of 30 kN. All tests were performed at a constant cross-head rate of 1 mm/min, which corresponds to an average

strain rate of 0.08 s^{-1} in the adhesive layer. The conversion from displacement rate to strain rate was performed resorting to Equation 3. For SLJs tests 0.2 mm was used for the value of L_0 as corresponds to the adhesive thickness.

In tests performed under LT (low temperature) and HT (high temperature), a heated climatic chamber was integrated in the testing machine. In the case of LT, the same chamber was used, with nitrogen being injected in a controlled manner to achieve the lower temperature. With the use of a thermocouple positioned in contact with each SLJ the temperature was measured, ensuring a homogeneous temperature distribution. Each test was only performed after a period of 10 minutes at the intended temperature. While the tests were being performed the SLJs remained enclosed in the chamber under a constant temperature.

A total of four specimens were tested for each overlap and temperature condition, and force-displacement (P-δ) curves were obtained for all SLJs tested.

3.3.4.2 Impact conditions

The impact tests were performed in a Rosand$^{®}$ Instrumented Falling weight impact tester, type 5 H.V. (Stourbridge, West Midlands, U.K.) coupled with a load cell of 60 kN. This equipment consists of a mass being dropped from a certain height, until it impacts the specimen. The specimen is mounted and kept vertically with the use of a specially designed grip. The impactor strikes the lower section of the grip, accelerating the test assembly so that the specimen is loaded in tension-shear. A total impactor weight of 26 kg was used in the setup of the testing machine. An impact speed of 3 m/s was used, corresponding to an available impact energy of 117 J.

For tests performed at LT, gaseous nitrogen was applied directly in every SLJ. In the case of HT, a heat gun to heat-up the SLJs was used. In both stages of temperature, a thermocouple was attached in the beginning of the area of overlap length to measure and control the temperature of the specimen. Each test occurred when the adhesive layer temperature was found to be stabilized at the desired value.

A total of four specimens were tested for each overlap and temperature condition, and a P-δ curve was obtained for each SLJ tested.

4   Numerical simulation details

A numerical analysis was performed to predict the SLJ strength under quasi-static and impact conditions. For this purpose, Abaqus® (Dassault Systèmes, Suresnes, France) was FEA software used. Quasi-static and dynamical simulations were only developed for RT because there was no information available regarding cohesive properties for the adhesive and the substrates at low and high temperature.

P-δ curves were determined and the prediction of the failure load was recorded. The software also allows to extracted information regarding crack initiation and propagation and state of plasticity from cohesive elements.

4.1   Cohesive zone modelling

The triangular CZM was used due to its simplicity and common use in previous studies. This model is available in the Abaqus® and enables the use of mixed mode loading (Figure 22). The adhesive layer was modelled with 0.2 mm thick cohesive elements, the same thickness of the adhesive layer to control the zone of crack initiation.

4.2   Quasi-static model

For the numerical simulation, a few conditions were considered with the objective of making the models as reliable as possible. Since three distinct types of materials were used during this work, the elements used to simulate them need to be chosen according to their physical behaviour. Figure 48 shows the model of a dissimilar joint with aluminium and CFRP substrates, where all the different types of elements used in all the possible configurations are presented. As mentioned before, for the adhesive a 0.2 mm layer was modelled with cohesive elements. For CFRP substrates elastic orthotropic properties (engineering constants) were used but it was also necessary to resort to cohesive elements to predict a possible failure by delamination. To simulate this type of failure, a 0.15 mm layer was added at 0.15 mm from the interface between adhesive and CFRP. The thickness of 0.15 mm corresponds to one ply of the

prepreg used to manufacture the CFRF substrate, close to the close to the adhesive/substrate interface. Aluminium substrates were simulated with elastic isotropic and plastic properties. For aluminium damage initiation and evolution, ductile damage parameters were used. Due to the limited information available, this data was only used for modelling the AA6060 T6 alloy. Data from Chen et al. [73] was adapted as the alloy used in their work is quite similar to AA6060 T6.
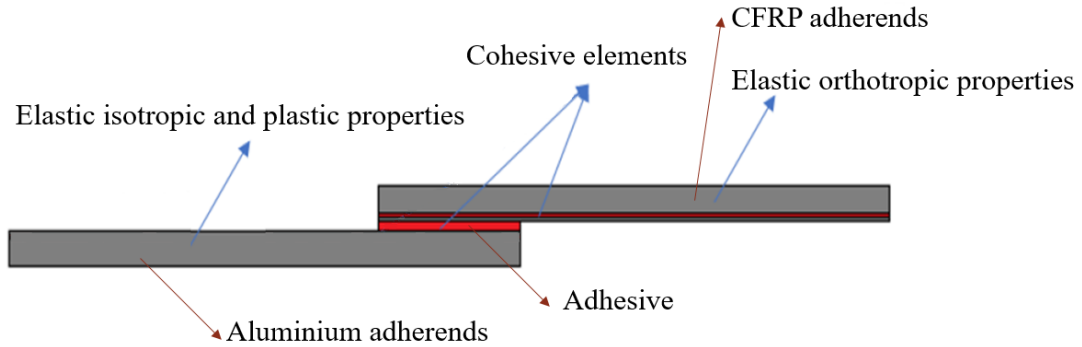

Figure 48 - Elements introduced in FE software for the static analysis.

The elastic properties used for aluminium alloys (Table 5 and Figure 23) and CFRP (Table 6) have already been introduced in Chapter 3. The curves of yield stress- plastic strain for the aluminium alloys are presented in the Figure 23. The data related with the aluminium alloys was provided by Aston Martin Lagonda®.

Triangular laws for adhesive (Figure 49) and for cohesive layer of CFRP (Figure 50) were performed for both loading modes. The adhesive tensile properties, Young's modulus (E) and normal cohesive stress (t_{n0}), were obtained from bulk tensile tests. Fracture toughness in pure mode I (G_{n0}) was obtained from DCB tests. The other properties, shear modulus (G), shear cohesive stress (t_{s0}) and fracture toughness in pure mode II (G_{s0}), needed to complete the triangular law was obtained from a previous works [40, 41, 74], as well the cohesive and elastic properties for the CFRP.
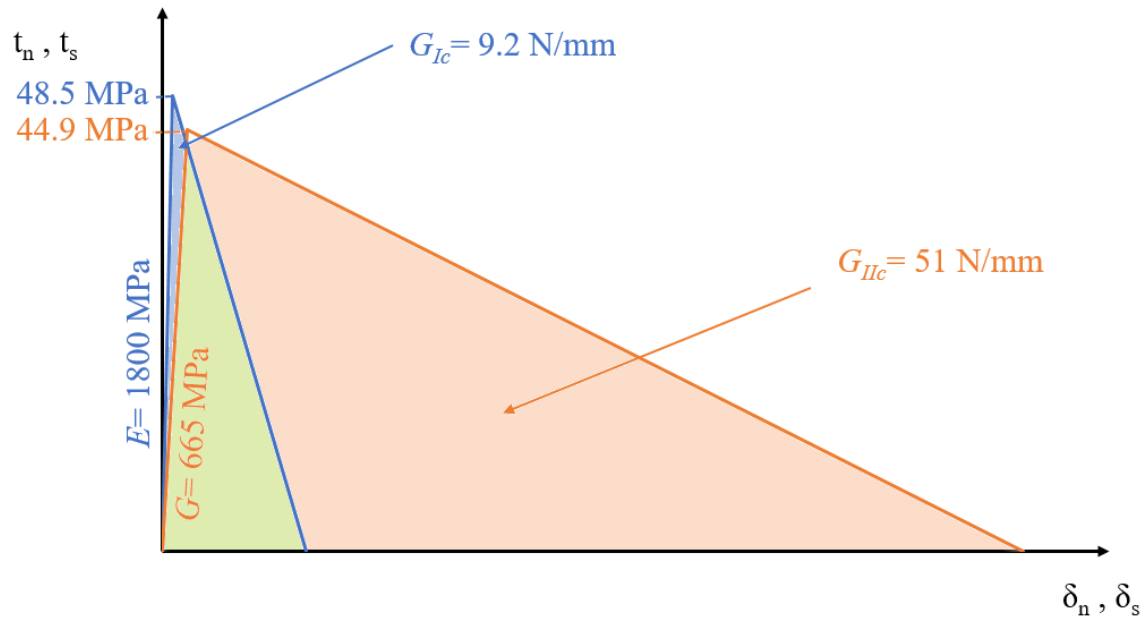
Figure 49 - Triangular law for adhesive XNR6852 E-3 in quasi-static conditions.
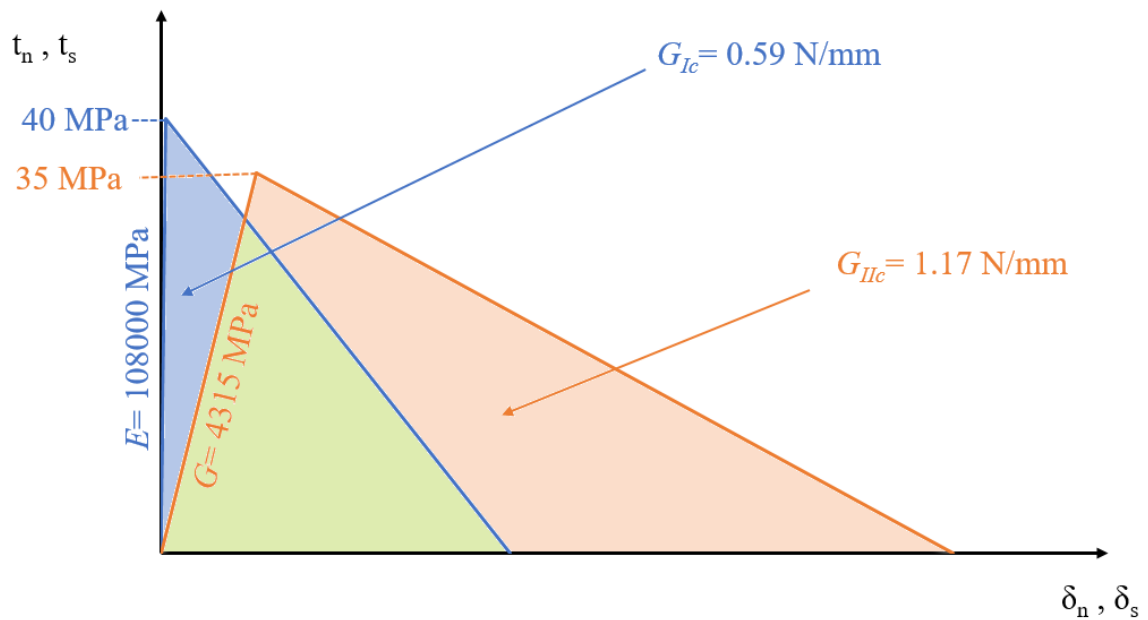

Figure 50 - Triangular law for CFRP at quasi-static conditions.

The boundary conditions were defined as indicated in Figure 51. In one end a clamped condition was added to simulate the static grip of tensile machine while in the other end a

longitudinal displacement was applied, restrained in the perpendicular direction of the displacement, simulating the grip that applies the force during the test.

Figure 51 - Boundary conditions applied for the quasi-static model.

The model also considered thermally induced stresses, introduced during the cooling from the curing stage (from 150ºC to RT). For this purpose, all models include an initial step where the temperature differential is applied, and the resultant stresses are calculated considering the elasticity of the materials and the respective coefficients of thermal expansion.

The mesh design was constructed with elements of different sizes, resorting to biasing techniques (Figure 52). The mesh was based on that employed for prior works and optimized to improve convergence. While joints containing only elastic and cohesive elements are significantly less prone to convergence problems, the models where the substrates include more computationally intensive plastic formulations were found to require more attention. The same optimized mesh was used for all the model under study using cohesive elements, for CFRP substrates and for adhesive, with 0.15 mm and 0.2 mm length was used, respectively. The density of elements was decreased as they move away from the ends of the overlap zone.
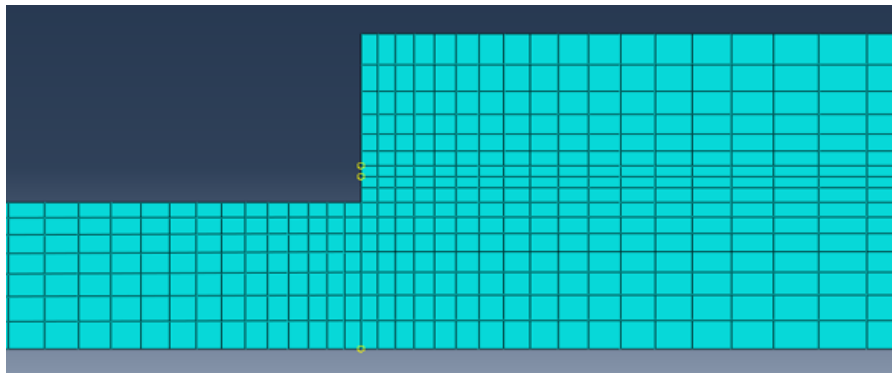

Figure 52 - Representative mesh in the overlap area.

For the visualization of the level of CZM degradation, scalar stiffness degradation (SDEG) was requested in the field outputs. This also enables the monitoring of the crack propagation.

Regarding to the element types, the bondline area was defined as a 4-node-two-dimensional cohesive element (COH2D4) and substrates were defined as a 4-node bilinear plane stress quadrilateral, reduced integration, hourglass control (CPS4R).

4.3 Dynamical model

To recreate the impact conditions of the drop weight test, a two-dimensional model was created resorting to Abaqus/Explicit. Most crash simulations are based on explicit FE-codes since these can simulate fast events within a reasonable execution time. Geometrically wise, the model was similar to the one used for quasi-static simulations with one modification, the addition of a mass to the non-clamped edge that represents the impact block in the experimental tests.

The boundary conditions were like those used in the static model with the difference being instead of a longitudinal displacement in the non-clamped end of the joint, a velocity field of 3000 mm/s was applied to mass that was added to the model (Figure 53). To simulate the 117 Joules of impact energy with a 3m/s velocity of the mass, the density was defined to guarantee that the mass was 26 kg. The mesh geometry used was the same as the static model and SDEG field output was also requested.
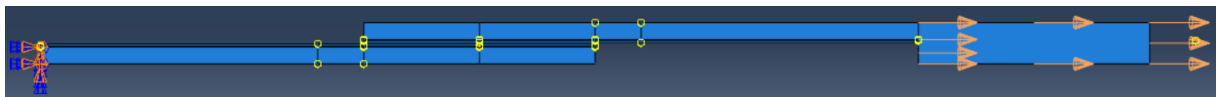

Figure 53 - Boundary conditions applied for the impact model.

Following the same procedure described for the quasi-static model, the dynamical model also included thermally induced stresses during cooling.

For adhesive properties, Young's modulus (E), normal cohesive stress (t_{n0}) and fracture toughness in pure mode I (G_{n0}) were extrapolated from experimental results resorting to a logarithmic trend line as described in the results chapter. Shear modulus (G), shear cohesive stress (t_{s0}) and fracture toughness in pure mode II (G_{s0}) was obtained from a previous work [40, 41, 74]. Again, a new triangular cohesive law was made for the adhesive at impact (Figure 54)
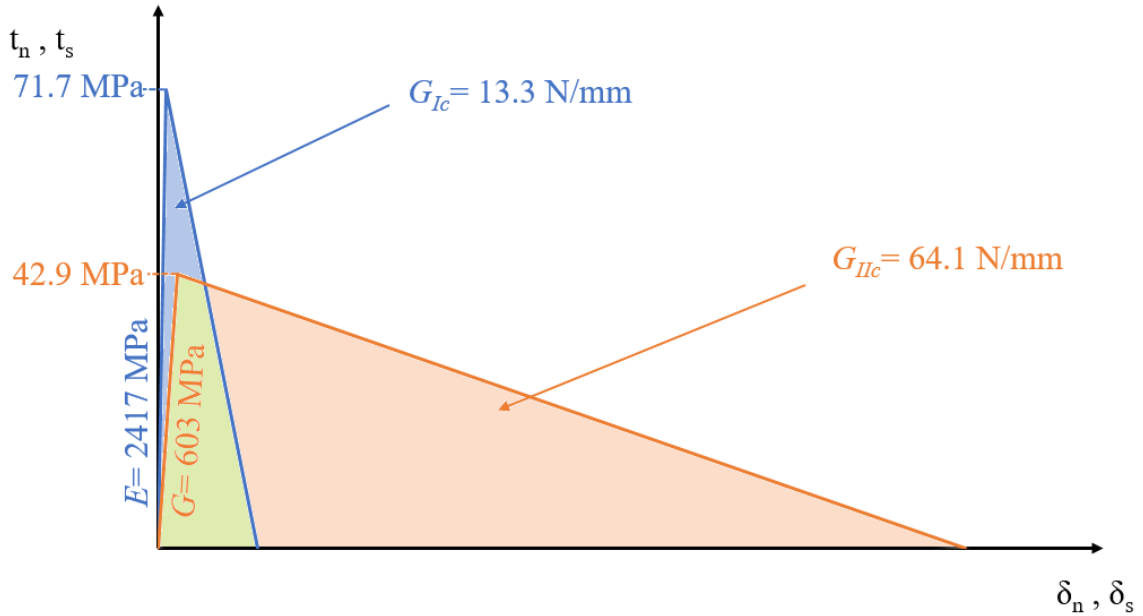

Figure 54 - Triangular law for adhesive XNR6852 E-3 in impact conditions.

As stated in the literature review chapter, the aluminium alloys are insensitive to the strain rate (AA6060 T6), or slightly sensitive (AA5754 H22) and the properties used for the static model could be used for the dynamic as well. The CFRP behaves in a different manner, while strain rate insensitive in the tensile direction (due to the fibres) the same does not occur in the other modes of loading (those governed by the matrix properties). Given the available data, determined in previous works, the CFRP properties from the elastic domain were kept constants and only the fracture energies were considered to vary as a function of the strain rate. A new triangular cohesive law was made for CFRP at impact, shown in Figure 55.
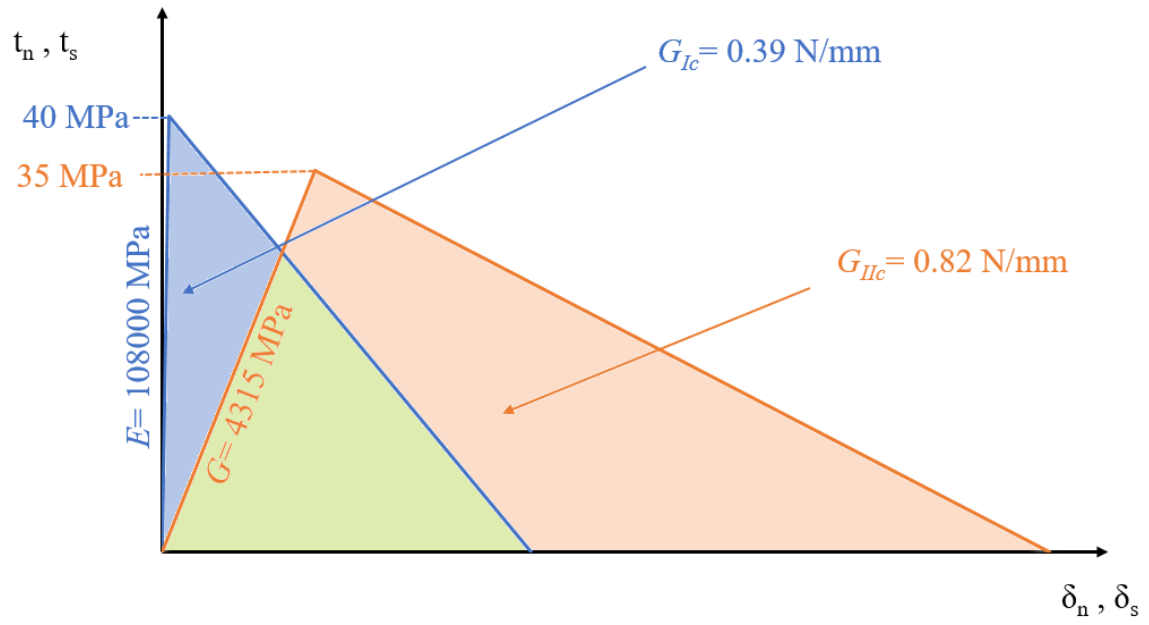
Figure 55 - Triangular law for CFRP in impact conditions.

5 Results and discussion

5.1 Experimental results

5.1.1 Quasi-static tests

For quasi-static tests of SLJs, although four specimens were tested for each combination of substrates and for three different temperatures, only three tests were considered as valid results for most configurations. This was due to surface contamination of some specimens, which failed with almost negligible load even after careful degreasing. The tests were performed with a displacement rate of 1 mm/min. The load, displacement and energy were recorded by the universal testing machine.

5.1.1.1 *Joints with similar substrates*

Figure 56 shows the representative P-δ curves for SLJs with similar substrates at RT for quasi-static conditions. SLJs with aluminium substrates exhibits a significantly large deformation in the plastic domain while SLJs with CFRP substrates, despite the larger failure load, presents a brittle behaviour.
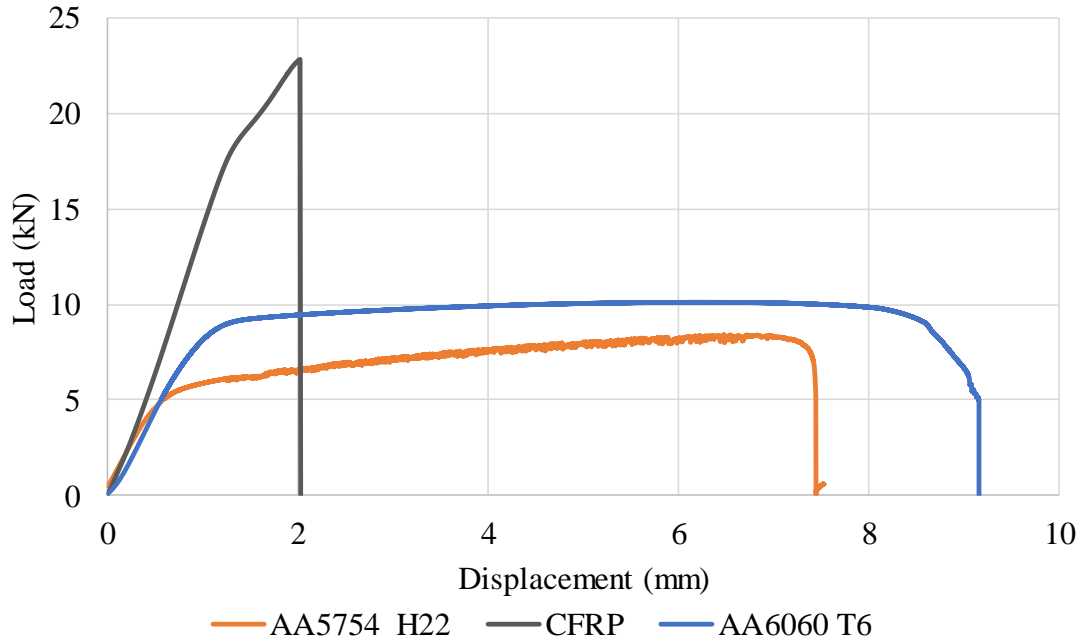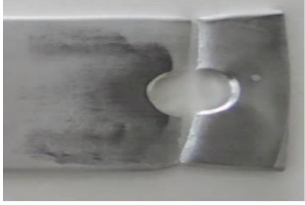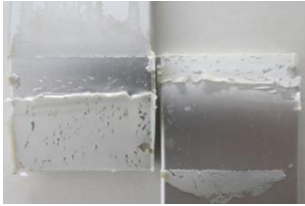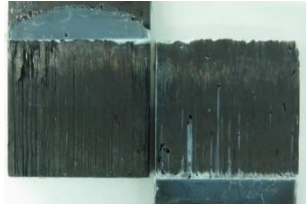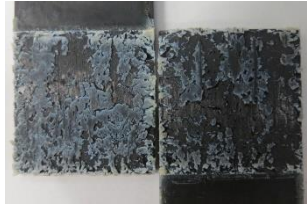
Figure 56 - *P-δ* curves of SLJs using similar substrates tested at quasi-static conditions and RT.

Figure 56 also exhibits two phenomena related to the failure process of aluminium and CFRP. The load-displacement curves of AA5754 H22 alloy exhibit instability during plastic deformation, caused by the Portevin Le Chatellier effect [31-33], which occurs for AA5xxx series alloys. Also noticeable is the decrease in stiffness of the CFRP SLJ as it approaches the failure point. This can be attributed to the gradual breakage of fibres that occurs during the test. In fact, the failure of the fibre can be heard in moments preceding complete delamination failure.

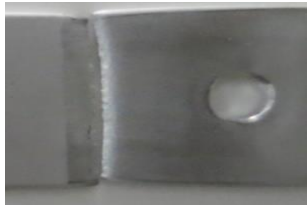The type of failure surface is a critical parameter to study and better understand the mechanical behaviour of adhesive joints. Table 8 shows the typical quasi-static failure surface of all joint similar configurations under study.

Table 8 - Failure surfaces of SLJs using similar substrates (CFRP and aluminium alloys) tested at quasi-static conditions as a function of temperature.

	-30°C (LT)	24°C (RT)	80°C (HT)
AA5754 H22			
AA6060 T6			
CFRP			

By analysing Table 8, it becomes clear that the aluminium joints either fail by cohesive failure in the adhesive, or cohesive failure in the substrate. When cohesive failure in the adhesive occurs, it is possible to notice that, prior to failure, a large deformation in the aluminium substrates happens, thus the aluminium controls the failure. In the case of alloy AA6060 T6 at RT the failure mode is unstable, since half the samples failed by the adhesive and the other half by the substrates, but the failure loads remain constant. Having all that in account it can be concluded that the aluminium joints fail because the onset of plastic deformation of aluminium, again introducing high peel stresses in the end of the overlap for those who fail by the adhesive. In the cases where CFRP joint delamination occurs, this happens

because the adhesive can withstand the high load transmission and the epoxy from the composite is more brittle than the adhesive ergo it delaminates.

From now on and to simplify the reading process, in the figures the aluminium alloys will be referred as Al 1.5 for AA5754 H22 alloy and Al 2.0 for AA6060 T6 alloy. The results of failure load of the similar joints are presented in Figure 57.
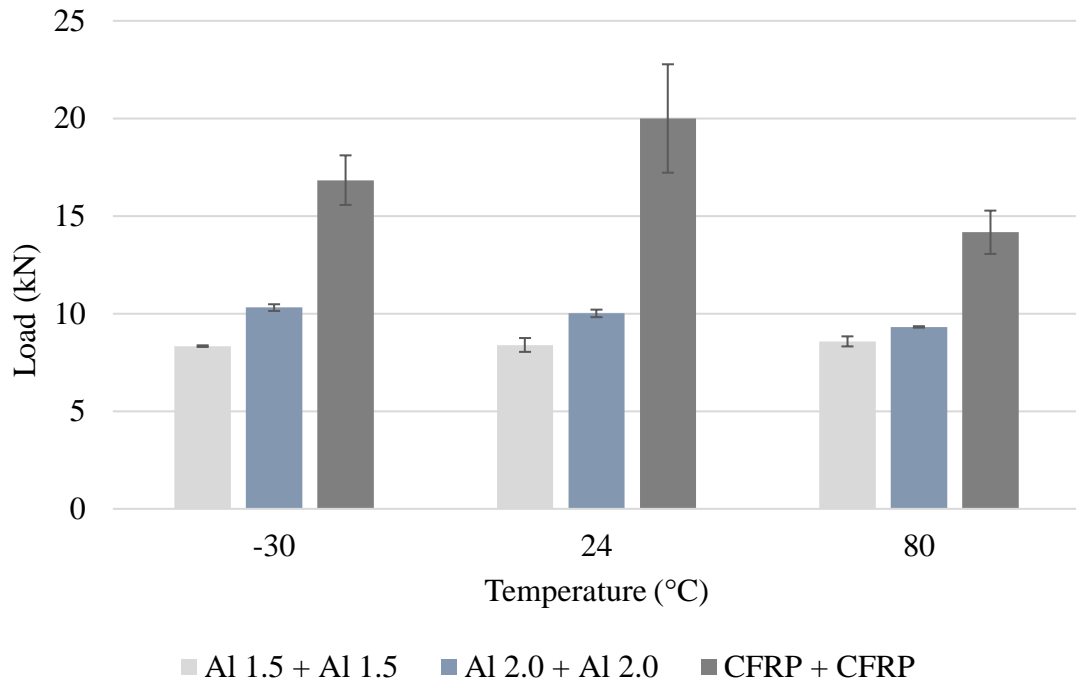

Figure 57 - Failure load of SLJs using similar substrates (CFRP and aluminium alloys) tested at quasi-static conditions as a function of temperature.

From Figure 57 it is possible to observe that the aluminium SLJs are not sensitive to different temperatures. However, the failure load of CFRP joints appears to slightly decline with the increasing temperature. This can be justified with the changing properties of the epoxy resin, not just from the adhesive, but also from the composite substrate. Although ductility increases with temperature, the tensile strength decreases, and this balance promotes lower failure load at high temperature. The adhesive is ductile enough through the temperature range to avoid large stress concentrations and early failure, ergo the decrease of tensile strength is more noticed. It is also possible to perceive that the failure load of the CFRP joints is well

higher than those of the aluminium joints, which leads to the conclusion that failure occurs with major influence of the substrates properties.

The behaviour of the SLJs can also be studied in terms of absorbed energy, shown in Figure 58.
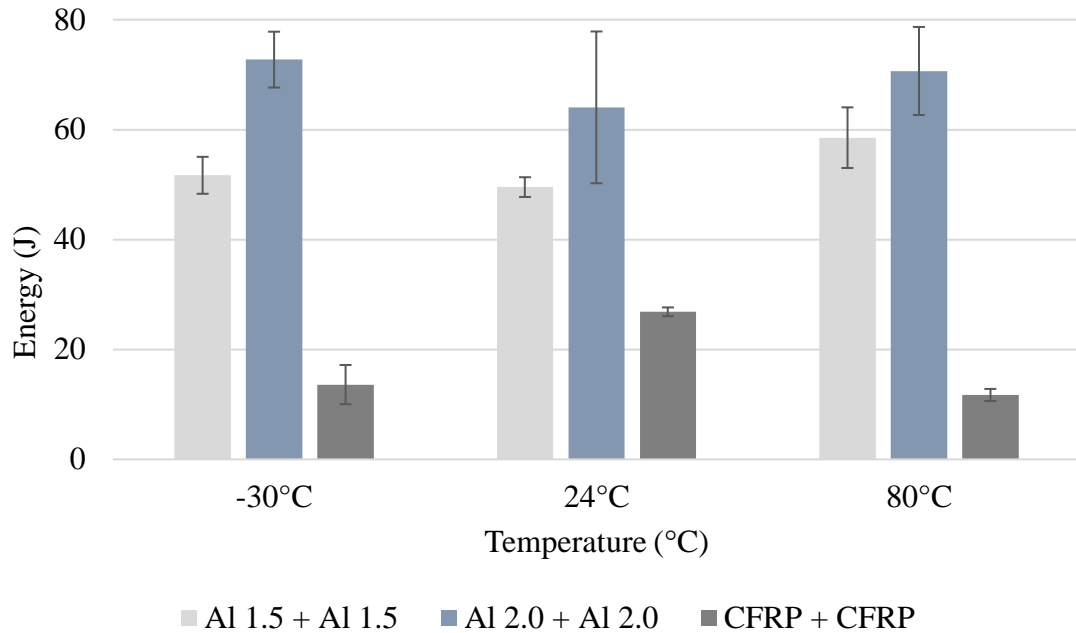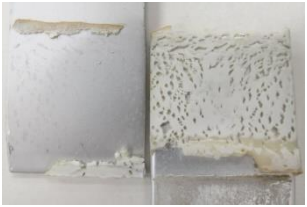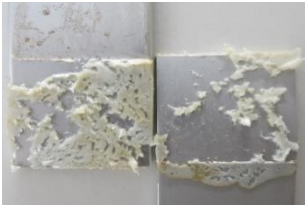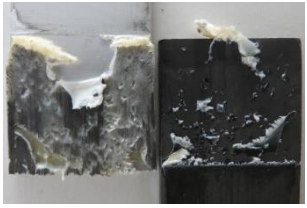

Figure 58 - Energy absorbed by SLJs using similar substrates (CFRP and aluminium alloys) tested at quasi-static conditions as a function of temperature.

The main information gathered from Figure 58 is that SLJs from aluminium substrates absorb significantly more energy than those with CFRP substrates, despite the higher failure load exhibited by CFRP SLJs. As Figure 56 shows, aluminium alloys undergo significantly more plastic deformation before failure. AA6060 T6 alloy absorbs more energy than the AA5754 H22, since the thickness of the substrates of AA6060 T6 is higher and therefore they can withstand higher deformation before failure. There is no temperature dependence on the absorbed energy regarding the aluminium SLJs. However, the CFRP SLJs are temperature sensitive being able to absorb more energy at RT. Since no difference was noticed with the aluminium joints this disparity of energy absorbed in the CFRP joints must be caused by the epoxy from the composite material, being too brittle at low temperature, therefore unable to absorb energy, and losing properties as it approaches T_g.

5.1.1.2   Joints with dissimilar substrates

In terms of failure mode (Table 9), the AA5754 H22 + AA6060 T6 combination fails cohesively by the adhesive, again this can be explained by the onset of plastic deformation of the aluminium, introducing high peel stresses in the adhesive. For AA5754 H22 + CFRP combination, a mixed failure of delamination and cohesive failure occurs for all temperatures except for -30°C, where two distinct types of failure, either by delamination or failure by the aluminium substrate, can be observed. For AA6060 T6 + CFRP combination, cohesive failure in the aluminium substrate is perceived since the aluminium is weaker than the CFRP. The difference in the failure mode between the two different aluminium alloys when combined with the CFRP can be explained by the difference amongst the thickness of the substrates. AA6060 T6 substrates have 2 mm of thickness, in contrast to 1.5 mm for the AA5754 H22 substrates, which is closer to the 2.1 mm of the CFRP substrates. The inferior difference between thicknesses   promotes lower peel stress distribution along the overlap which means that failure changes from delamination (AA5754 H22 + CFRP) to cohesive failure in the aluminium substrate (AA6060 T6 + CFRP).
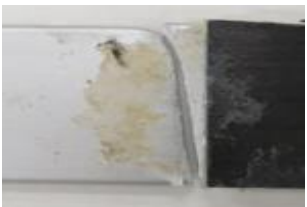
Table 9 - Failure surfaces of SLJs using dissimilar substrates (CFRP and aluminium alloys) tested at quasi-static conditions as a function of temperature.

	-30°C (LT)	24°C (RT)	80°C (HT)
AA5754 H22 + AA6060 T6			
AA5754 H22 + CFRP			
AA6060 T6 + CFRP			

The results of failure loads of the dissimilar joints are presented in Figure 59.

Figure 59 - Failure load of SLJs using dissimilar substrates (CFRP and aluminium alloys) tested at quasi-static conditions as a function of temperature.

The maximum failure load for each situation is defined by the weakest substrate, failing by the AA5754 H22 alloy in the first two combinations (AA5754 H22 + AA6060 T6 and AA5754 H22 + CFRP) and by the AA6060 T6 in the third one (AA6060 T6 + CFRP). No temperature dependence is noticed since the only substrate sensitive to temperature at the range in study is the CFRP.

From Figure 60 it is possible to conclude that the energy values for dissimilar substrates joints are between those of aluminium and CFRP joints with similar substrates. This can be explained by the fact that just one substrate deforms (the aluminium one) in contrast with the similar joints of aluminium where the deformation is symmetric until the peel stress disrupts the adhesive.
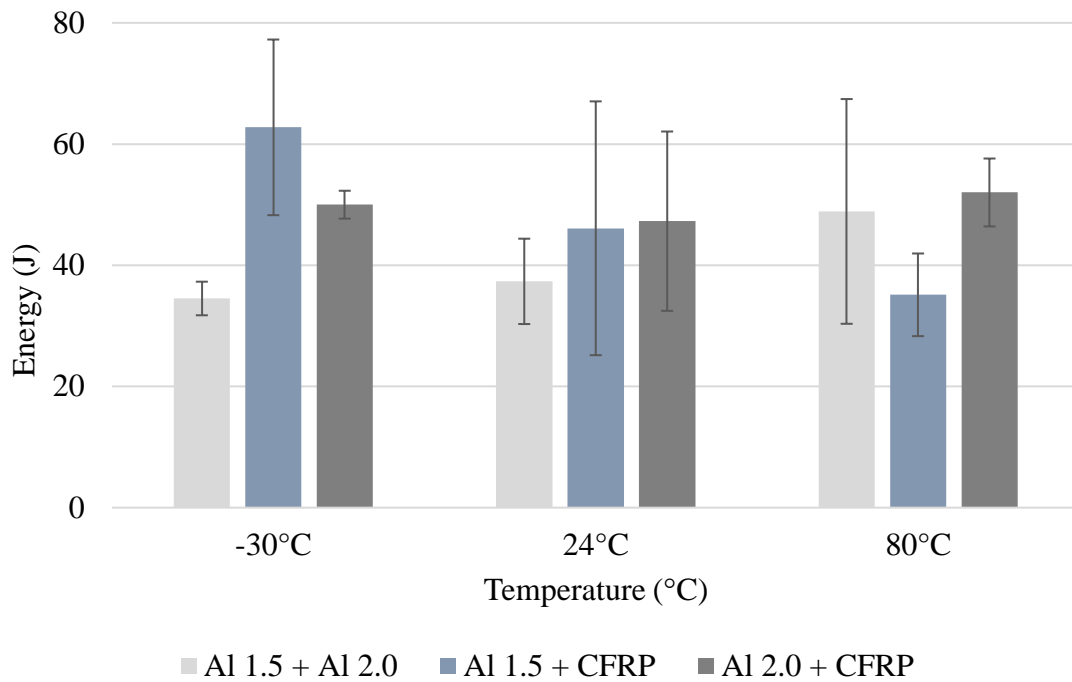
Figure 60 - Energy absorbed by SLJs using dissimilar substrates (CFRP and aluminium alloys) tested at quasi-static conditions as a function of temperature.

5.1.2 Impact tests

For impact tests of SLJs, four specimens were tested for each combination of substrates and for three different temperature, using adhesive Nagase-ChemteX XNR6852 E-3. The specimens were tested with a speed of 3 m/s. A mass of 26 kg was used for the impactor, corresponding to an impact energy of 117 J, sufficient to break all specimen configurations. The load, displacement and energy were recorded by the machine.

5.1.2.1 Joints with similar substrates

Table 10 presents representative images of the failure section and thus the failure mode for all combinations with similar substrates at impact conditions for all testing temperatures.

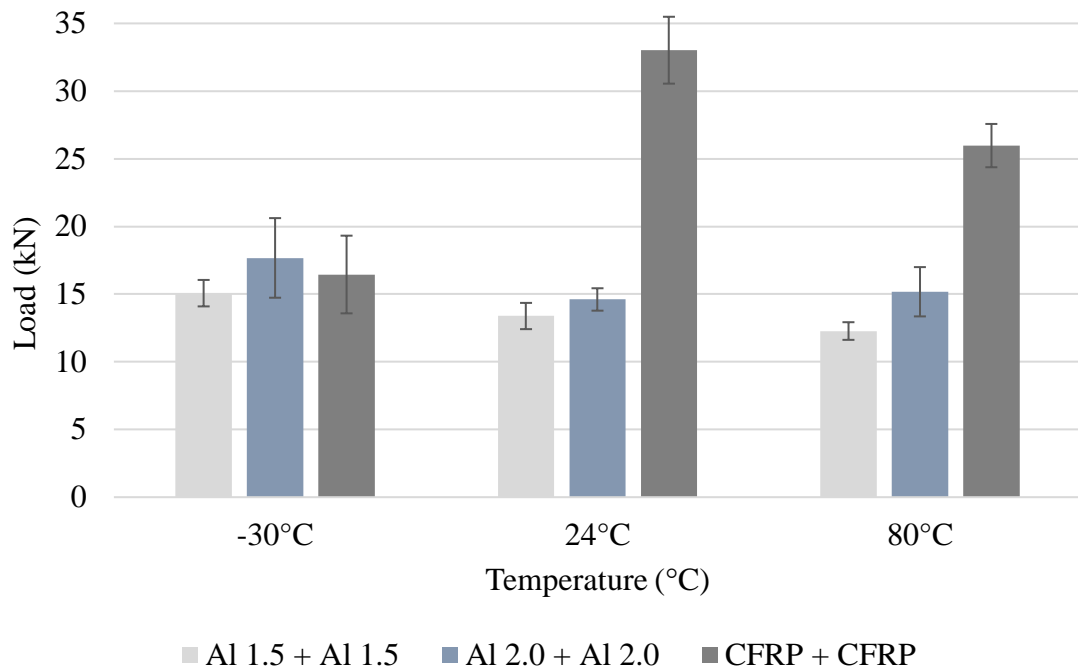Table 10 - Failure surfaces of SLJs using similar substrates (CFRP and aluminium alloys) tested at impact conditions as a function of temperature.

	-30°C (LT)	24°C (RT)	80°C (HT)
AA5754 H22			
AA6060 T6			
CFRP			

For all temperatures tested, the joints with similar substrates of CFRP failed by delamination. However, there are some changes with variation of temperature. For LT and HT there is presence of cohesive failure in the adhesive since the crash resistant epoxy becomes stiffer at LT and more flexible at HT, as well as the CFRP resin. The presence of such mixed failure mode allows to conclude that the adhesive is being loaded until failure, due to decrease of mechanical properties of both the adhesive and CFRP. Regarding the joints with similar aluminium alloys, these failed in the clamped zone for both alloys and for all testing temperatures. The increase of mechanical properties with strain rate and stress concentrations due to the holes of the substrates in the clamped zone could help to explain the observed behaviour.

From Figure 61 it can be observed that the maximum load is achieved by the joint with CFRP substrates at RT.
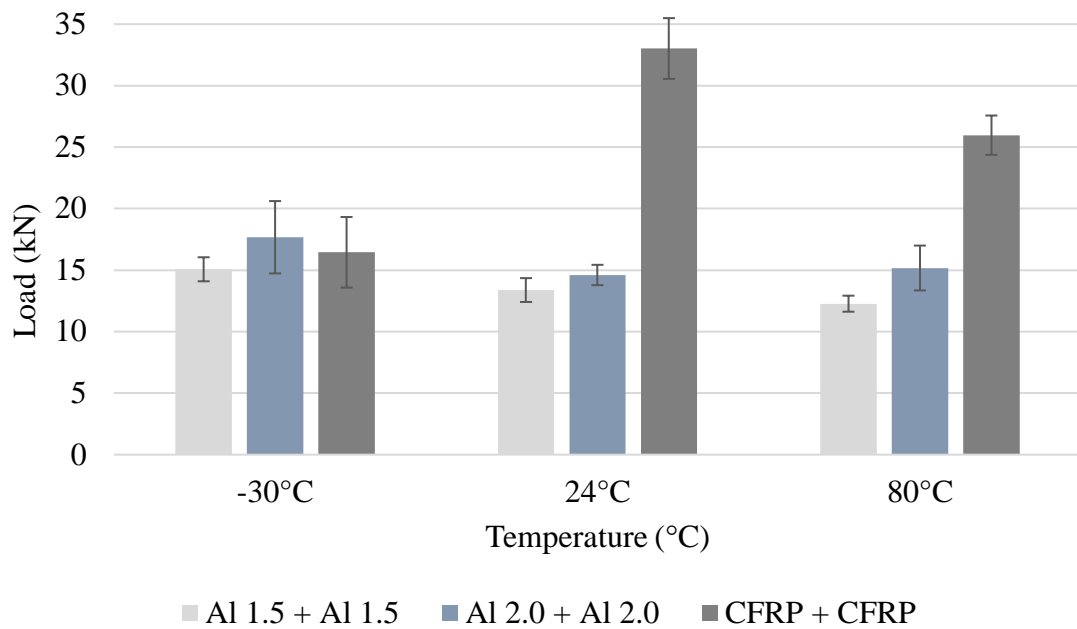
Figure 61 - Failure load of SLJs using similar substrates (CFRP and aluminium alloys) tested at impact conditions as a function of temperature.

Although the adhesive becomes more flexible, reducing the peel loads in SLJs of CFRP substrates for HT, the proximity to the T_g also leads to lower tensile and shear strength, even when considering strain rate dependency. It is the occurrence of a mixed failure mode, with simultaneous delamination and cohesive failure that leads to the lower failure loads. At LT both the adhesive and the CFRP resin become more brittle. Because the joints with AA6060T6 substrates display a higher failure load than the ones with CFRP substrates it is safe to say that LT affects the CFRP resin more significantly.

For SLJs with AA6060 T6 substrates, despite a noticeable decrease from LT to RT in the average value of maximum load, no tendency can be considered since these values fall under the respective standard deviations. The same behaviour can be observed in SLJs with substrates made from AA5754 H22 aluminium alloy.

Figure 62 presents the value of energy absorbed for all combinations with similar substrates at impact conditions for all testing temperatures.

Figure 62 - Energy absorbed by SLJs using similar substrates (CFRP and aluminium alloys) tested at impact conditions as a function of temperature.

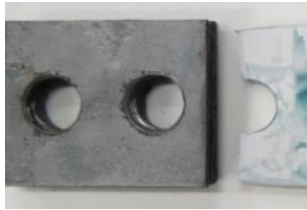No clear tendency can be found for joints with similar substrates of aluminium, for both alloys under study, as function of temperature regarding the energy absorbed at impact conditions. However, as can be perceived in Figure 63, an increase in energy absorbed at impact is observed for joints with similar CFRP substrates as temperature increases. That tendency can be explained by a combination of factors. As stated previously, the literature describes cases where composite structures are able to sustain higher loads and absorb more energy under impact [48, 49]. Some authors [75, 76] have presented work demonstrating that through the failure process of composite materials, the frictional sliding of the fibre within the matrix might be responsible for a large fraction of energy absorption. Figure 64 shows this effect schematically. This type of frictional sliding has been shown to be a complex phenomenon [77] involving both the Van der Walls forces and the mobility of macromolecules at the interface, which results in larger energy absorption for higher impact strain rates [78]. However, increased energy absorption under impact conditions cannot be totally due to the process of delamination and fibre pull-out. The energy absorption and toughness of bulk polymeric materials (which include both the adhesive and the matrix of the composite under study) has been described to increase with the strain rate [79]. Such effect may be due to secondary connections between the

polymeric chains, which are affected by both the temperature and the strain rate and result in higher energy absorption [80]. The secondary connections have been previously identified as responsible for a significant level of rate sensitivity of material properties, which occurs close to strain rate and temperature conditions related to the β-transition viscoelastic behaviour [81].
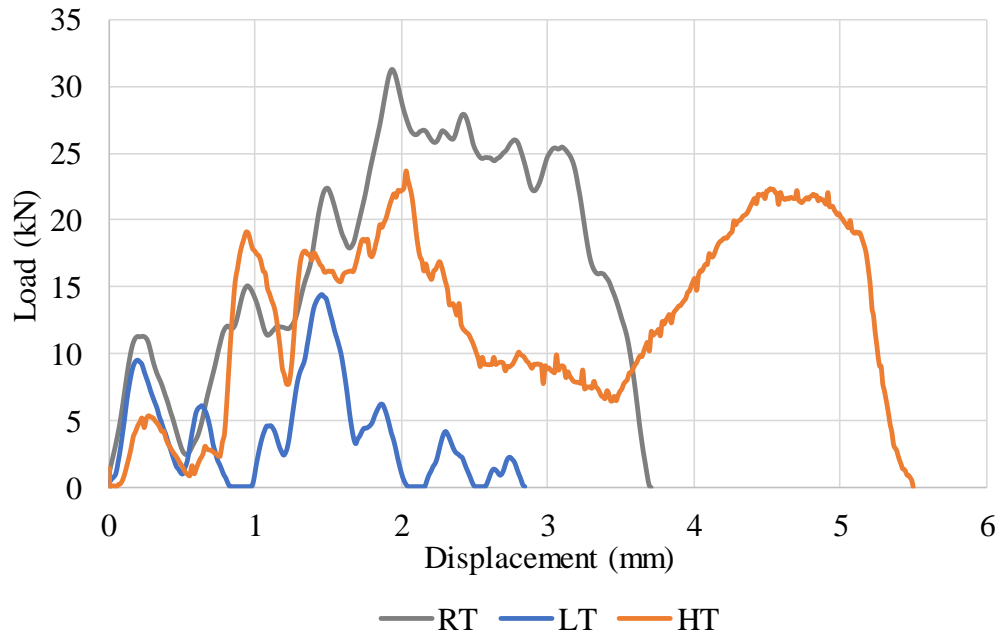
Figure 63 - *P-δ* of SLJs using CFRP similar substrates tested at impact conditions as a function of temperature.
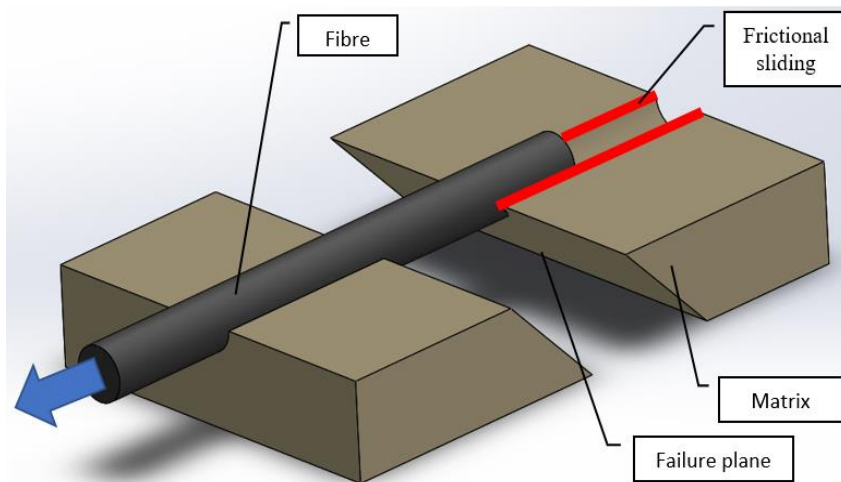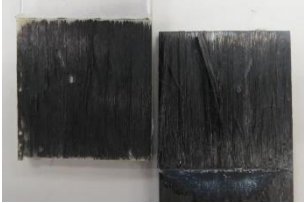
Figure 64 - Representative scheme of frictional sliding phenomenon.

5.1.2.2 Joints with dissimilar substrates

Table 11 presents representative images regarding the failure mode for each dissimilar combination tested at impact conditions for all testing temperatures. Again, all the joints failed in the clamped zone except for AA6060 T6 + CFRP combination at LT, where severe delamination occurred. This can be explained by the viscoelastic and viscoplastic properties of both the adhesive and CFRP resin becoming more brittle for LT. Since delamination is presented we can affirm that the LT effect was more significant for CRFP resin.

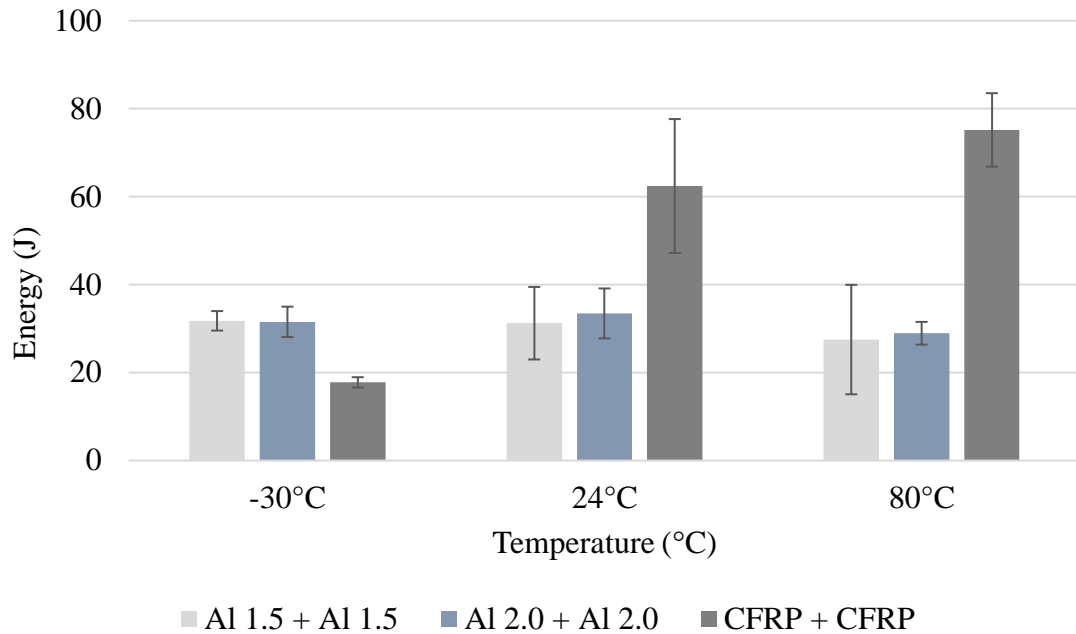Table 11 - Failure surfaces of SLJs using dissimilar substrates (CFRP and aluminium alloys) tested at impact conditions as a function of temperature.

	-30°C (LT)	24°C (RT)	80°C (HT)
AA5754 H22 + AA6060 T6			
AA5754 H22 + CFRP			
AA6060 T6 + CFRP			

The results of failure load of joints with dissimilar substrates at impact conditions for all testing temperatures are presented in Figure 65.
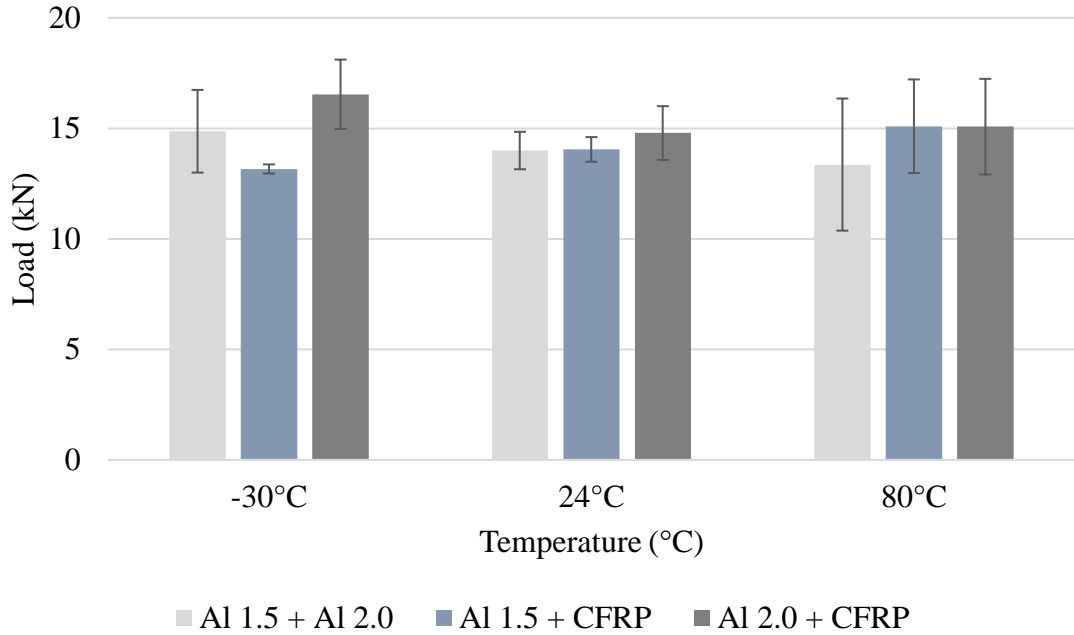
Figure 65 - Failure load of SLJs using dissimilar substrates (CFRP and aluminium alloys) tested at impact conditions as a function of temperature.

Regarding the maximum failure load, no clear tendency was found with the variation of temperature. Again, the maximum failure load is defined by the weakest substrate, the aluminium alloy AA5754 H22 for the first two combinations (AA5754 H22 + AA6060 T6 and AA5754 H22 + CFRP) and by the AA6060 T6 in the third one (AA6060 T6 + CFRP).

The values of absorbed energy are presented in Figure 66. For all dissimilar combinations, a higher value of energy absorbed was measured for RT. This phenomenon could be explained by the fact that the crash resistant epoxy, due to its behaviour as a function of temperature, becomes stiffer at LT and more flexible at HT, as it becomes closer to T_g. A balance between ductility and strength at RT could promote which is also the case for the CFRP resin.
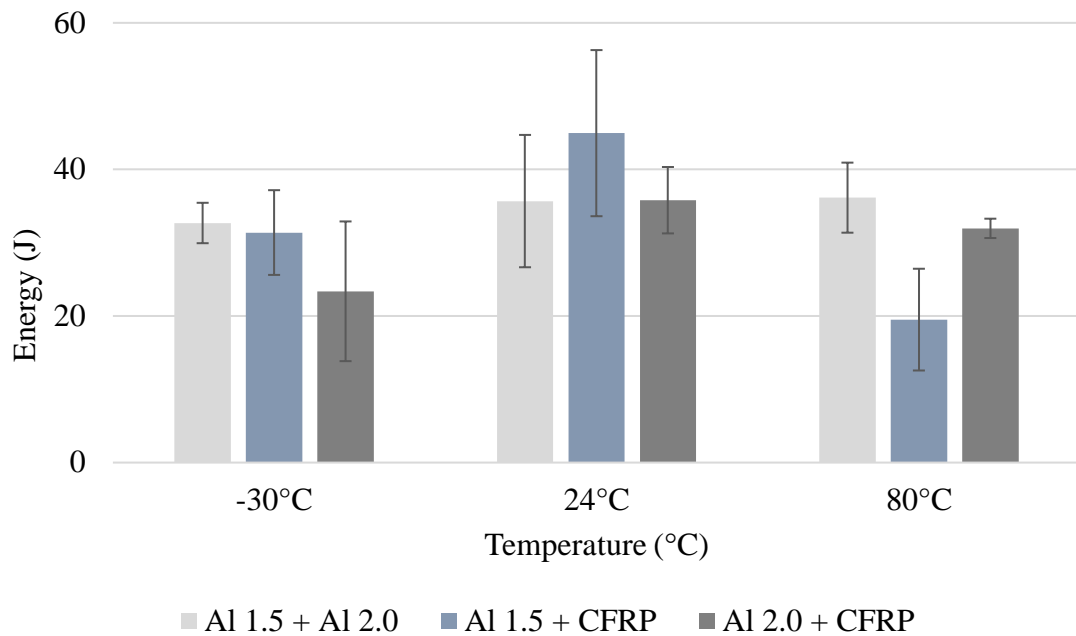
Figure 66 - Energy absorbed by SLJs using dissimilar substrates (CFRP and aluminium alloys) tested at impact conditions as a function of temperature.

5.1.3 Combined temperature-strain rate analysis

To aid in the proper evaluation of the combined effect of temperature and strain rate on the mechanical behaviour of the joints, this section includes three-dimensional plots of the failure load and absorbed energy as a function of the parameters under study.

5.1.3.1 Joints with similar substrates

From Figure 67 to Figure 69 it is shown the failure load of SLJs with similar substrates as function of temperature and strain rate.

Figure 67 - Failure load of SLJs with AA5754 H22 similar substrates as function of temperature and strain rate.

Figure 68 - Failure load of SLJs with AA6060 T6 similar substrates as function of temperature and strain rate.
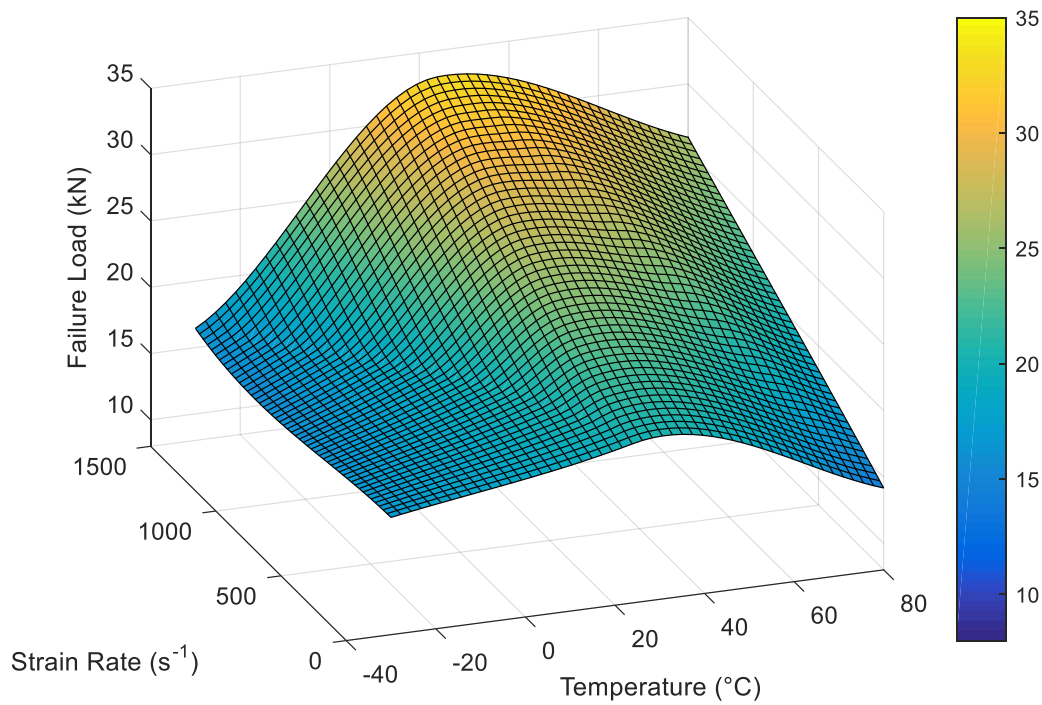
Figure 69 - Failure load of SLJs with CFRP similar substrates as function of temperature and strain rate.

For all types of substrates an increase of failure load with the increase of strain rate was noticed. While, for SLJs with aluminium substrates, the influence of temperature mainly affects the adhesive properties, with the failure load slightly lowering with the increasing of temperature, the SLJs with CFRP substrates demonstrate a peak in the value of failure load for RT independently of the strain rate. The values of failure load are higher for SLJs with CFRP than with aluminium, this behaviour can be explained because CFRP is significantly stiffer than the aluminium alloys.

Overall, increases in strain rate improve the SLJs performance regarding the material used for substrates. However, the influence of temperature has a significant effect in the SLJs with CFRP substrates, while for the aluminium ones there is almost no sensitivity.

From Figure 70 to Figure 72 it is shown the energy absorbed by SLJs with similar substrates as function of temperature and strain rate. It can be noted that, for SLJs with CFRP substrates, the axis orientation is different than the ones with aluminium substrates to improve the visualization of the graphic surface.

Figure 70 - Energy absorbed by SLJs with AA5754 H22 similar substrates as function of temperature and strain rate.

Figure 71 - Energy absorbed by SLJs with AA6060 T6 similar substrates as function of temperature and strain rate.

Figure 72 - Energy absorbed by SLJs with CFRP similar substrates as function of temperature and strain rate.

Notwithstanding the fact that the failure load increases with the strain rate, SLJs with aluminium alloys substrates present higher capacity of energy absorption at quasi-static conditions as can be perceived by Figure 73. This occurrence can be explained by the fact that, when impact conditions are presented, the shock wave passes the overlap, where the adhesive, due to its viscoelastic behaviour, does not allow large deformations, and propagates along the length of the substrate until encounters a weak spot, that is the hole in the clamped zone, where the stress concentration are high. The failure occurs in this weakened section with limited energy absorption. Figure 74 shows the propagation of the stress wave along the joint during an impact test, calculated using the numerical models presented before. Whereas, in a quasi-static situation, all the SLJs is under a uniformly increasing stress state, until, at some point, the onset of plastic deformation occurs in the region of the overlap, and at the same time, the adhesive allows deformation due to the relaxation of the polymeric chains, thus permitting larger deformations in both substrates and absorbing more energy. Figure 75 shows the evolution of stress distribution during a quasi-static test.
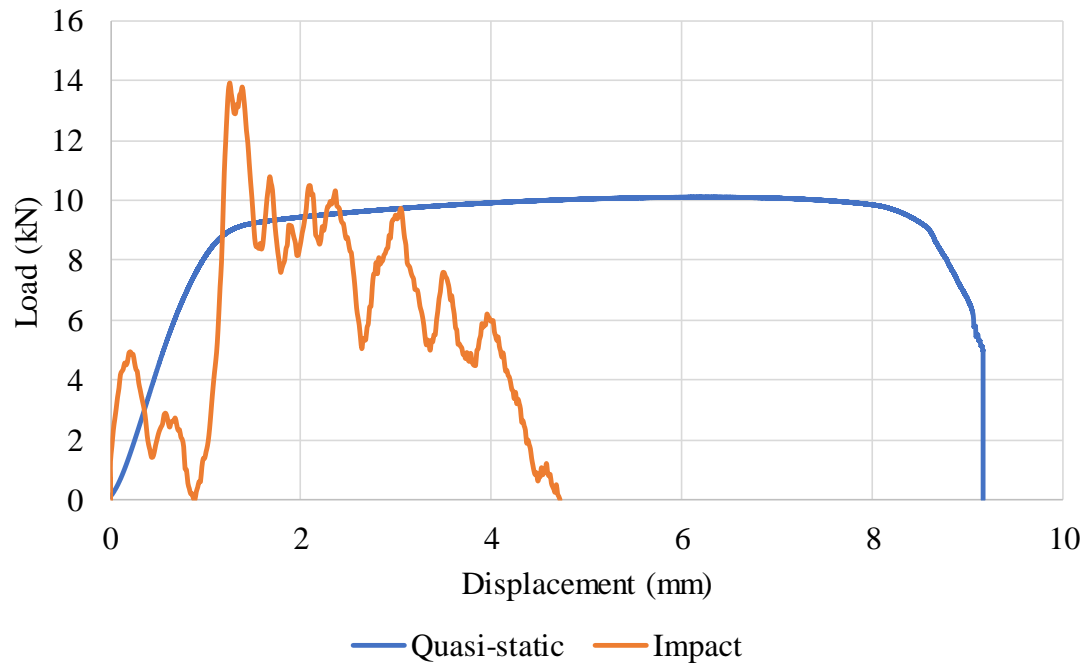
Figure 73 - *P-δ* curves of SLJs with AA6060 T6 similar substrates tested at RT as function of strain rate.
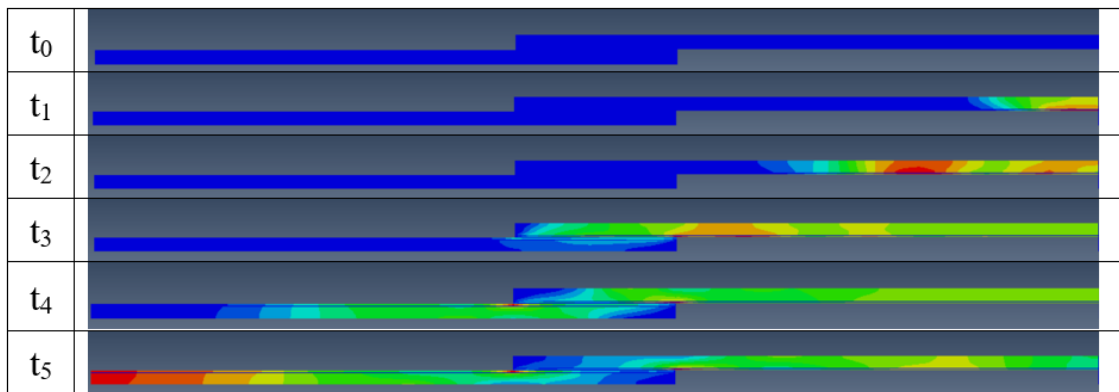
Figure 74 - Stress propagation through the SLJ in impact conditions.
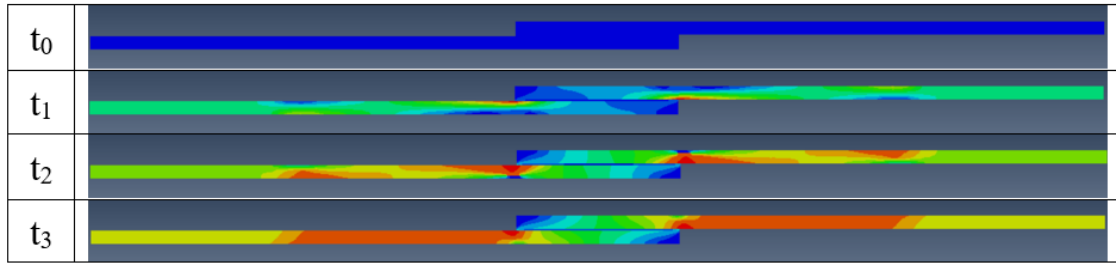
Figure 75 - Stress propagation through the SLJ in quasi-static conditions.

Figure 74 and Figure 75 also clearly demonstrate that the performance of adhesively bonded joints under impact is not only a function of the intrinsic material properties under large strain rates but also of the stress fields present.

Regarding the SLJs with CFRP substrates, there is an increase in the energy absorption level under impact conditions, and it can result from a combination of factors. While both the adhesive and the CFRP matrix become tougher and more flexible with temperature, the frictional sliding of the fibre within the matrix during the delamination process might be responsible for most of the energy absorption.

5.1.3.2   Joints with dissimilar substrates

From Figure 76 to Figure 78 it is shown the failure load of SLJs with dissimilar substrates as function of temperature and strain rate.
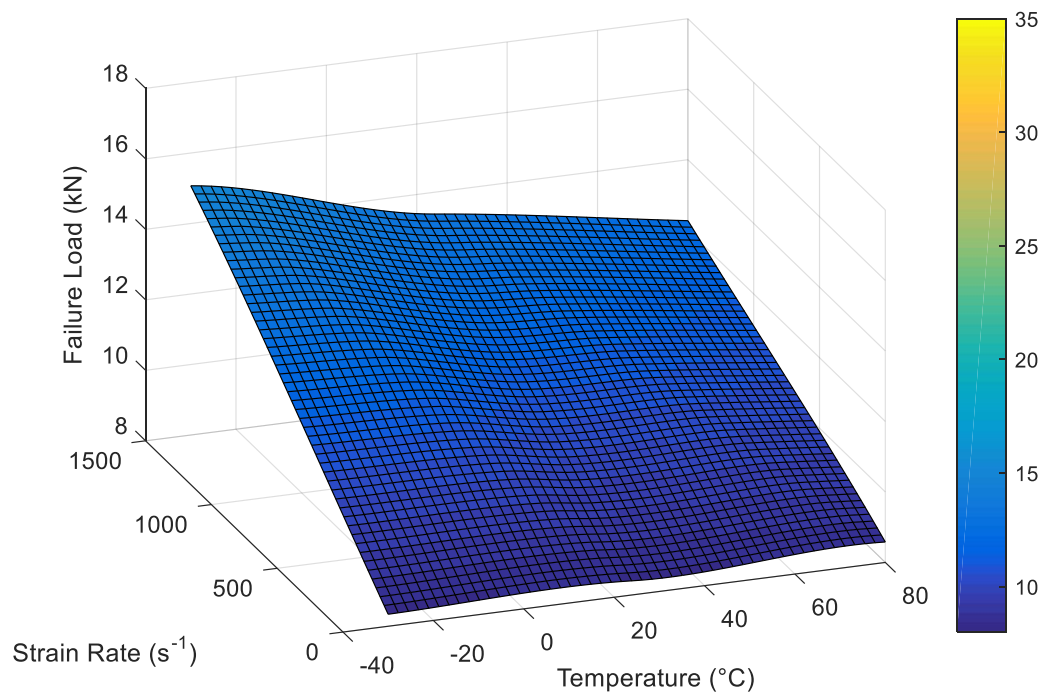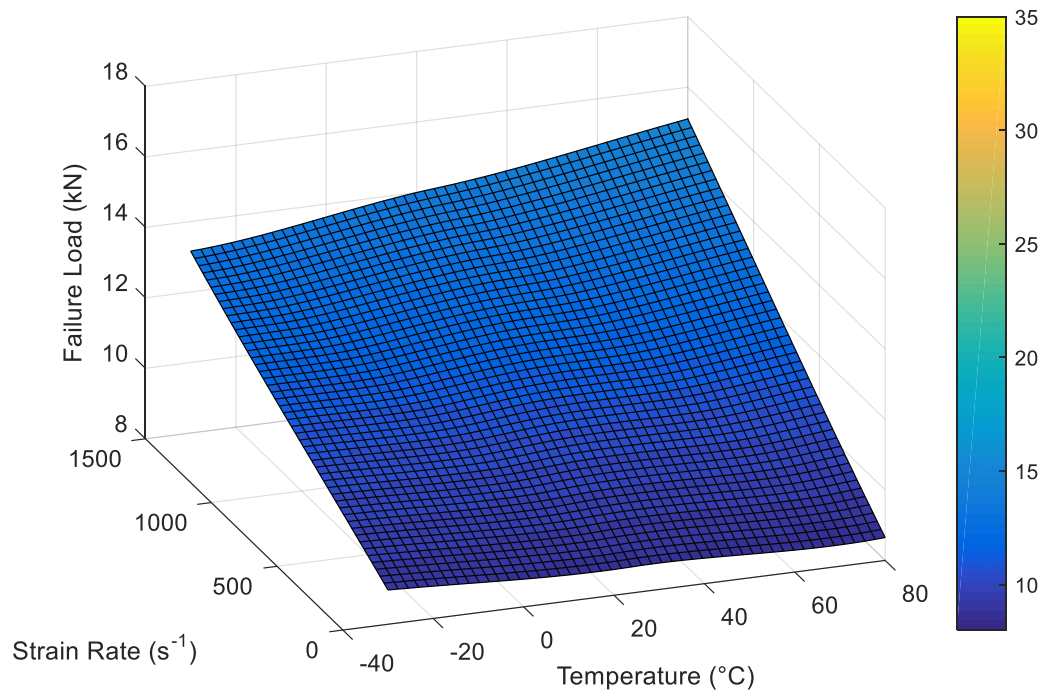
Figure 76 - Failure load of SLJs with AA5754 H22 + CFRP dissimilar substrates as function of temperature and strain rate.
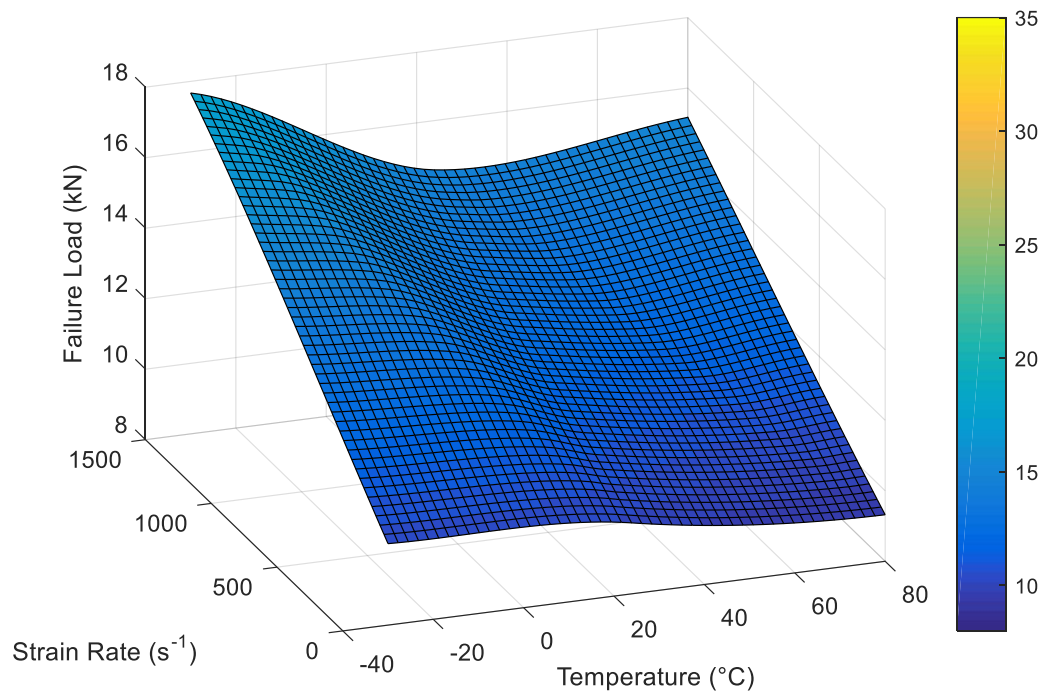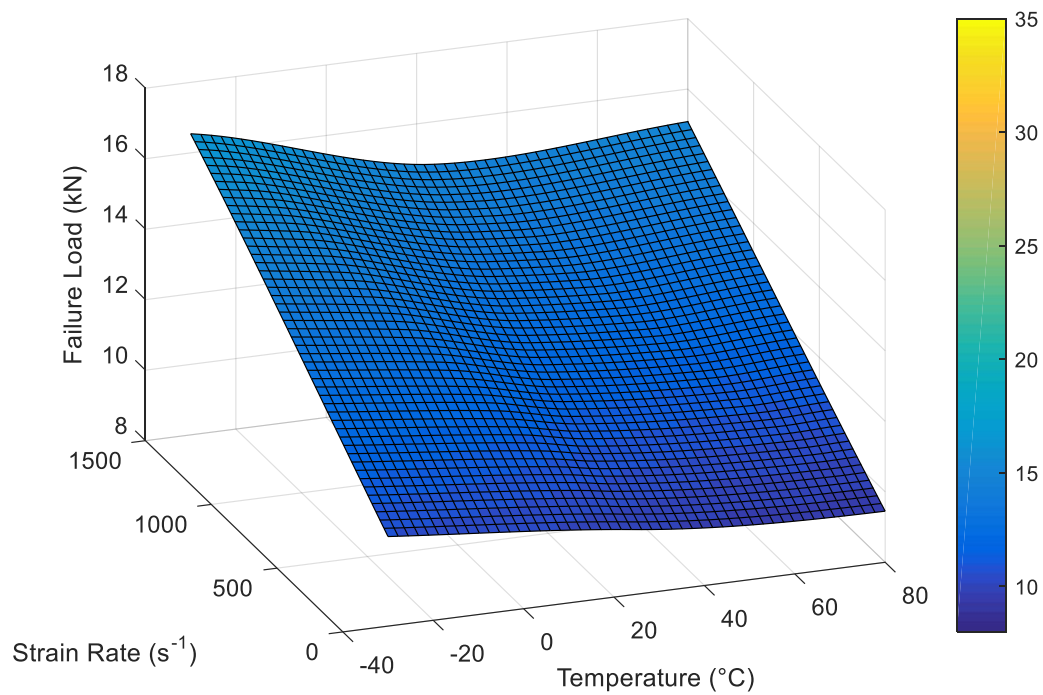

Figure 77 - Failure load of SLJs with AA6060 T6 + CFRP dissimilar substrates as function of temperature and strain rate.
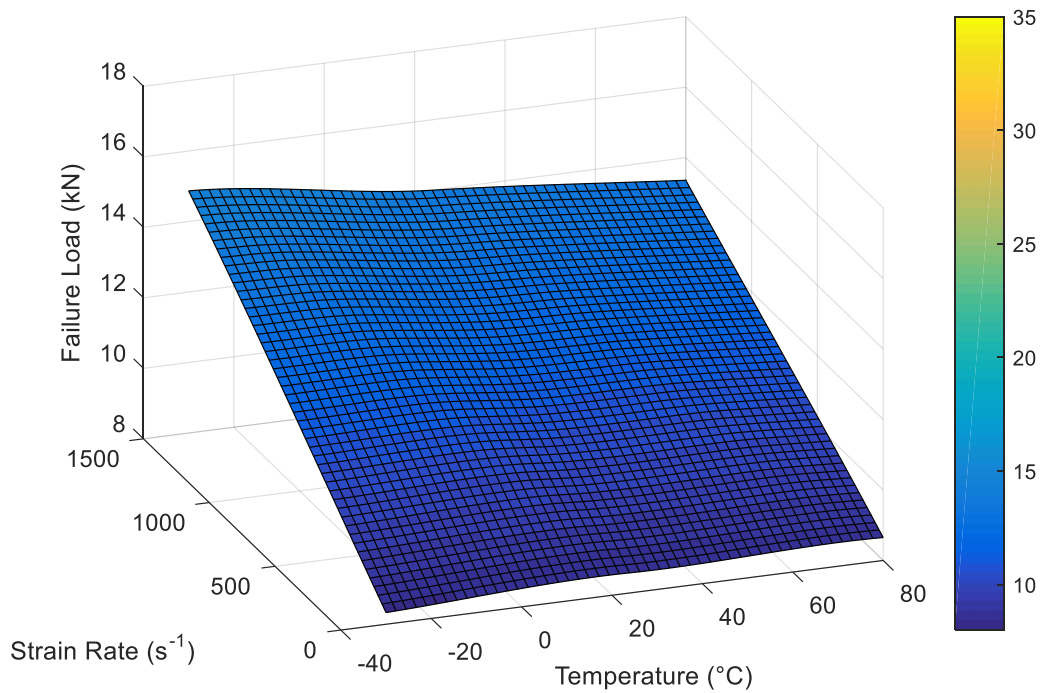
Figure 78 - Failure load of SLJs with AA5754 H22 + AA6060 T6 dissimilar substrates as function of temperature and strain rate.

Although Figure 76 presents a slight increase with temperature at high strain rates, this variation falls under standard deviation, so there is no virtually influence of temperature in the failure load in SLJs with dissimilar substrates of AA5754 H22 + CFRP. The same happens to SLJs with the other two combinations of materials for substrates.

The results of this experimental work demonstrate that, when joining dissimilar materials, the failure load will be imposed by the weakest material, as expected. Again, the strain rate improves the performance of SLJs regarding the combination of materials selected for the substrates. And, because for all the combinations at least one substrate is made from aluminium, the behaviour in terms of failure load tends to mimic the ones observed for SLJs with aluminium substrates, as the failure is controlled mainly by the onset of plastic deformation.

From Figure 79 to Figure 81 it is shown the energy absorbed by SLJs with dissimilar substrates as function of temperature and strain rate.
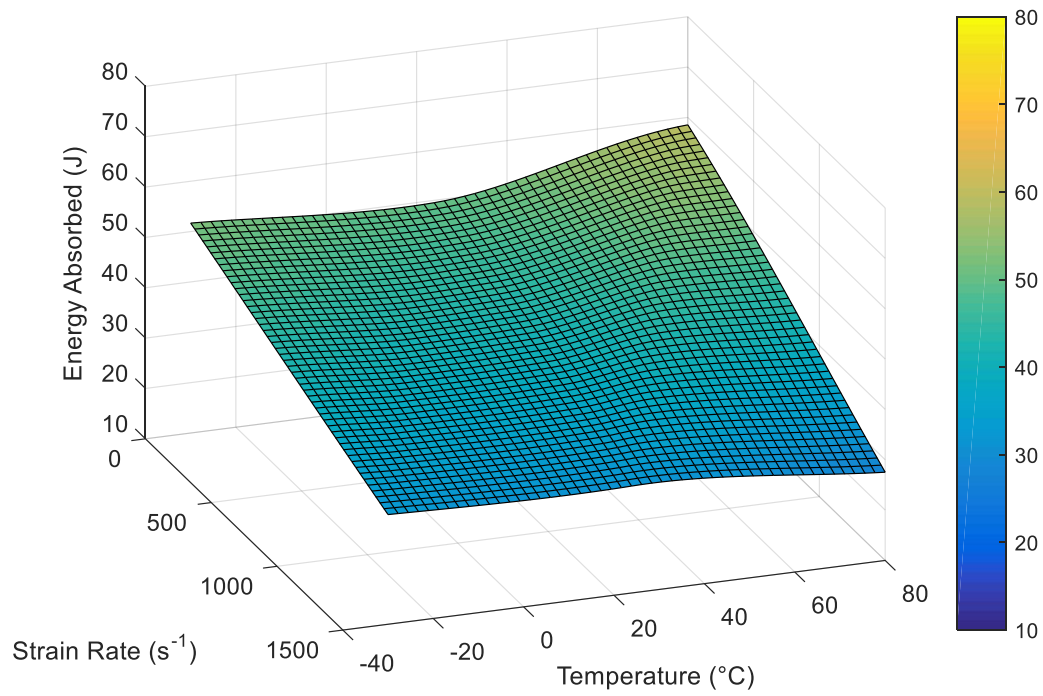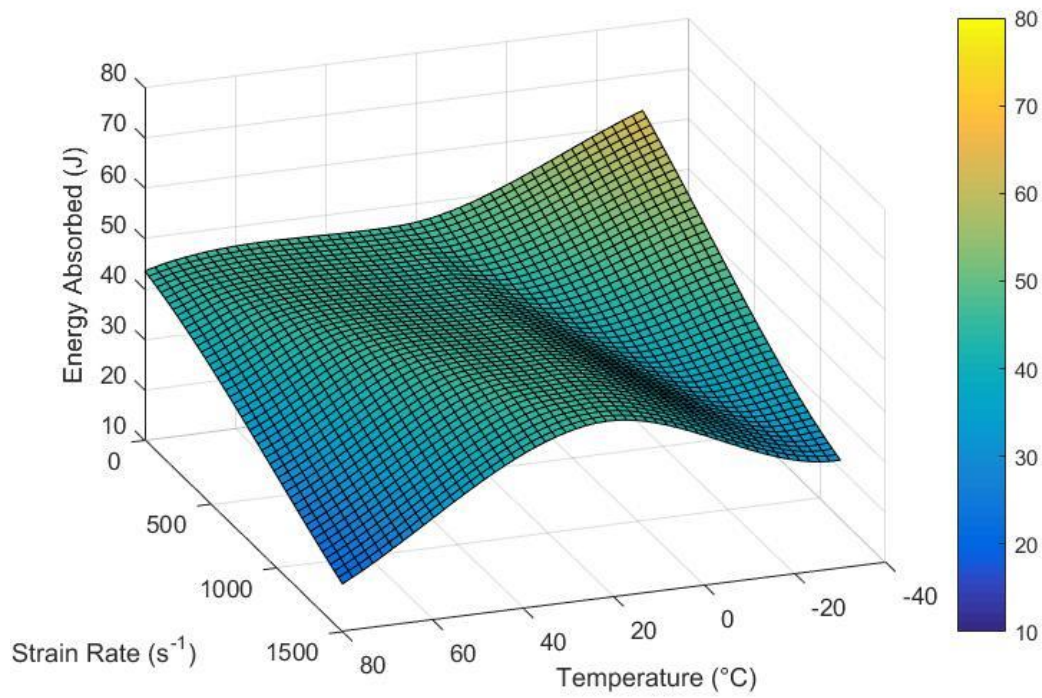
Figure 79 - Energy absorbed by SLJs with AA5754 H22 + CFRP dissimilar substrates as function of temperature and strain rate.
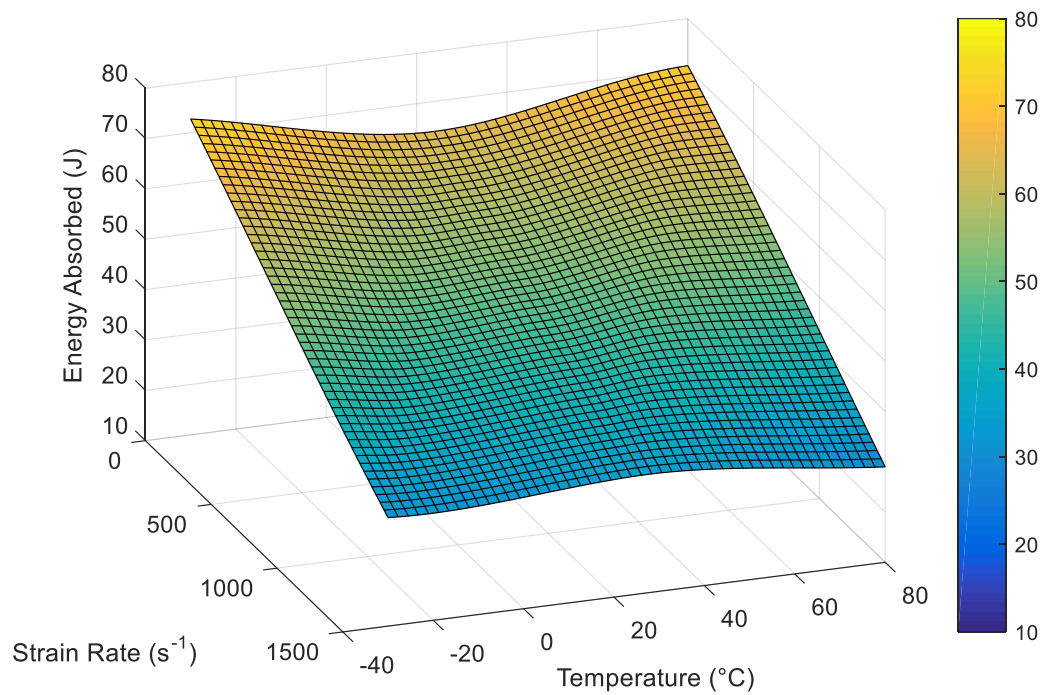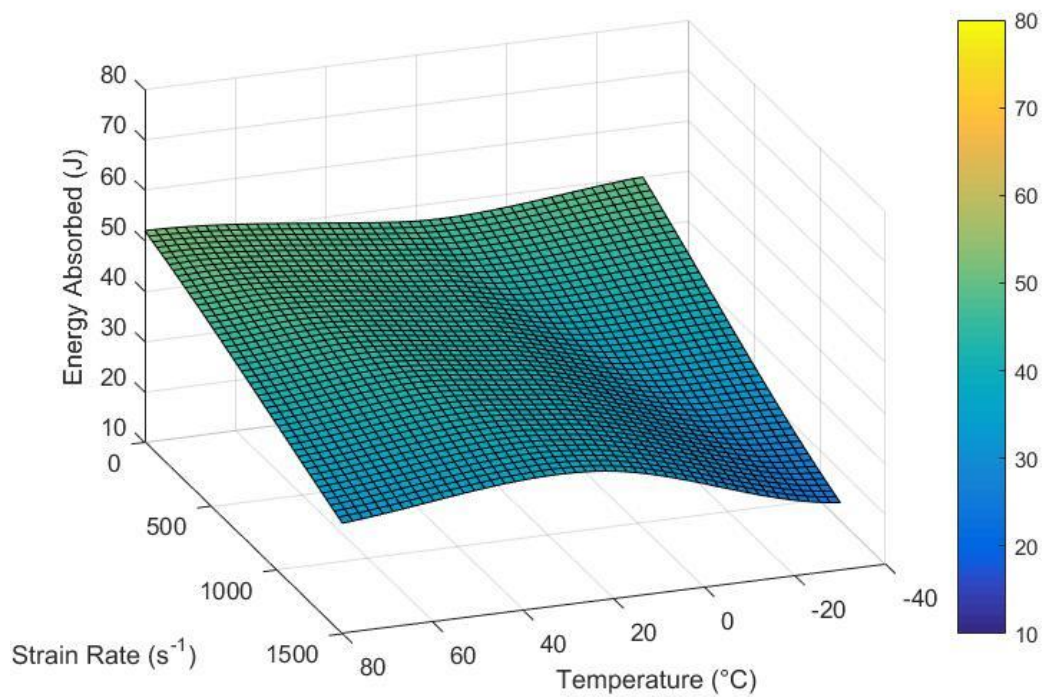

Figure 80 - Energy absorbed by SLJs with AA6060 T6 + CFRP dissimilar substrates as function of temperature and strain rate.
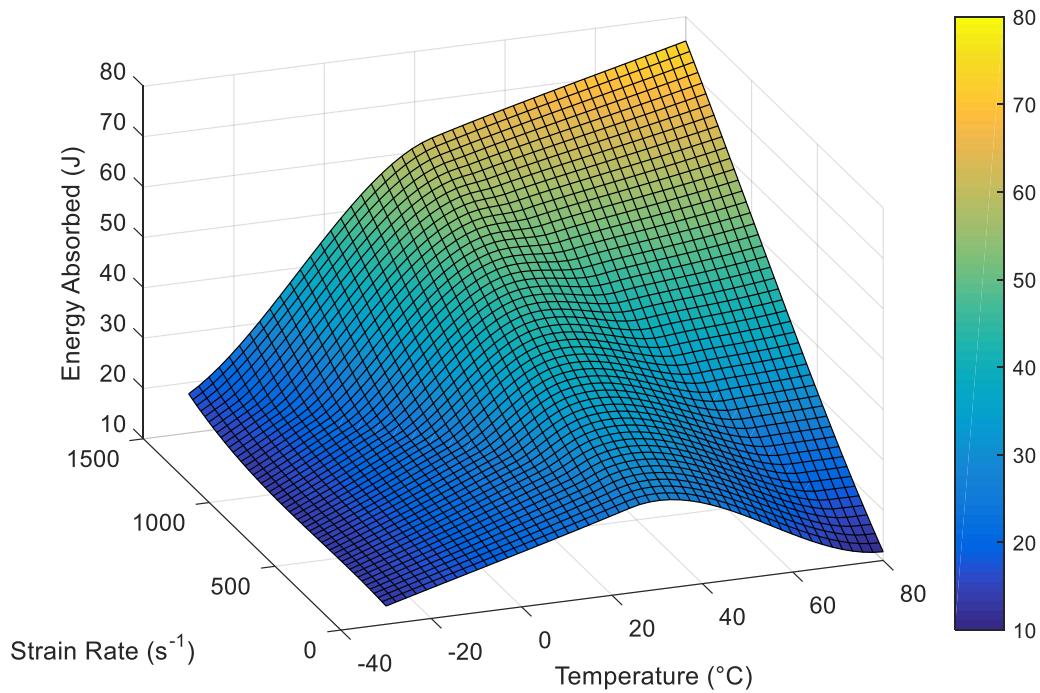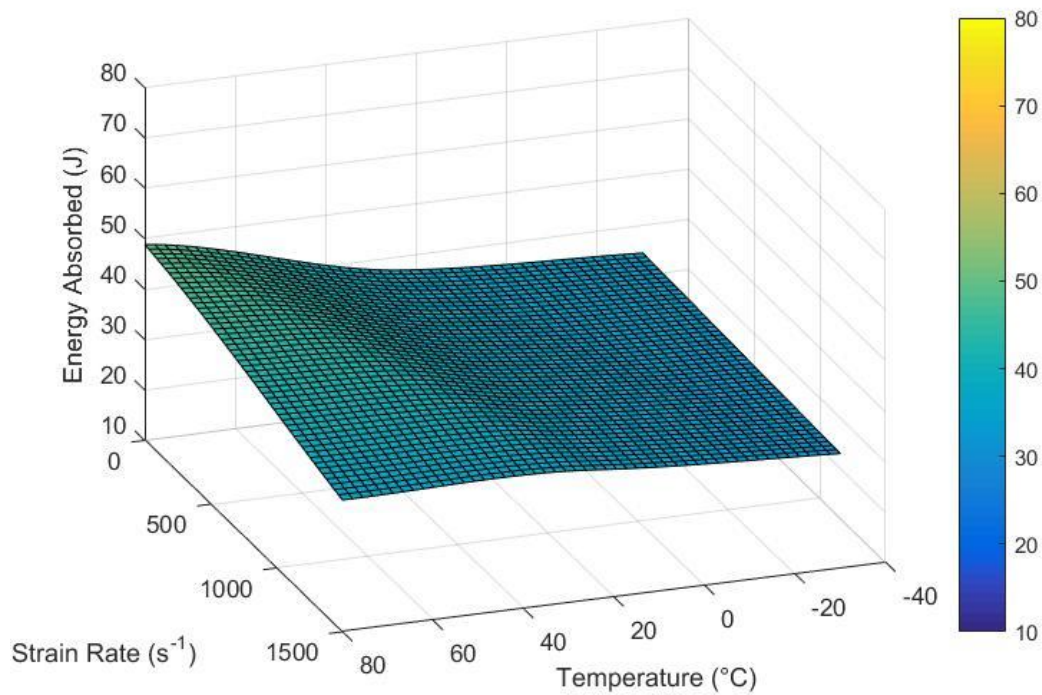
Figure 81 - Energy absorbed by SLJs with AA5754 H22 + AA6060 T6 dissimilar substrates as function of temperature and strain rate.

Regarding the SLJs with dissimilar substrates of aluminium AA6060 T6 and CFRP, a behaviour similar to the one presented on SLJs with similar AA6060 T6 substrates is noticed, with lower energy absorbed for quasi-static conditions, since just the thinner substrate deforms. The lower peak of energy absorbed for impact at LT is due to the failure mode occurred was delamination. The aluminium-aluminium dissimilar joints offer very low temperature dependence with regards to absorbed energy. The dissimilar joints with composite are slightly more sensitive to temperature, although the effect is much less pronounced than that of composite-composite SLJs

5.2 Numerical results of SLJs

As mentioned in the numerical detail chapter, numerical simulations were only made for RT once there was no information available regarding shear properties for the adhesive at

low and high temperature. Representative numerical P-δ curves are presented and compared to experimental data. No simulations are presented for configurations using the aluminium alloy AA5754 H22 due to the insufficient information regarding ductile damage modelling.

5.2.1 Quasi-static

5.2.1.1 Substrates with similar materials

Figure 82 shows the P-δ curves for the experimental results and the numerical simulations of SLJs with similar substrates of AA6060 T6 under quasi-static conditions.

Figure 82 - Comparison between experimental and numerical P-δ curves of SLJs with similar substrates of AA6060 T6 under quasi-static conditions.

The shape of the curve is similar, although, the transition from elastic to plastic behaviour is more abrupt in the numerical simulation. The failure load and the displacement are higher in numerical simulation than the experimental results. Closer results were expected; therefore, the difference could be explained by the limited information regarding materials properties. In addition, the ductile parameters are derived from those of a slightly different

aluminium alloy, which might also explain this difference. Analysing Figure 82, it is possible to notice that, in the numerical simulation, the increase in maximum load in the plastic domain is higher than that observed for experimental results.

Figure 83 shows the P-δ curves for the experimental results and the numerical simulations of SLJs with similar substrates of CFRP under quasi-static conditions.
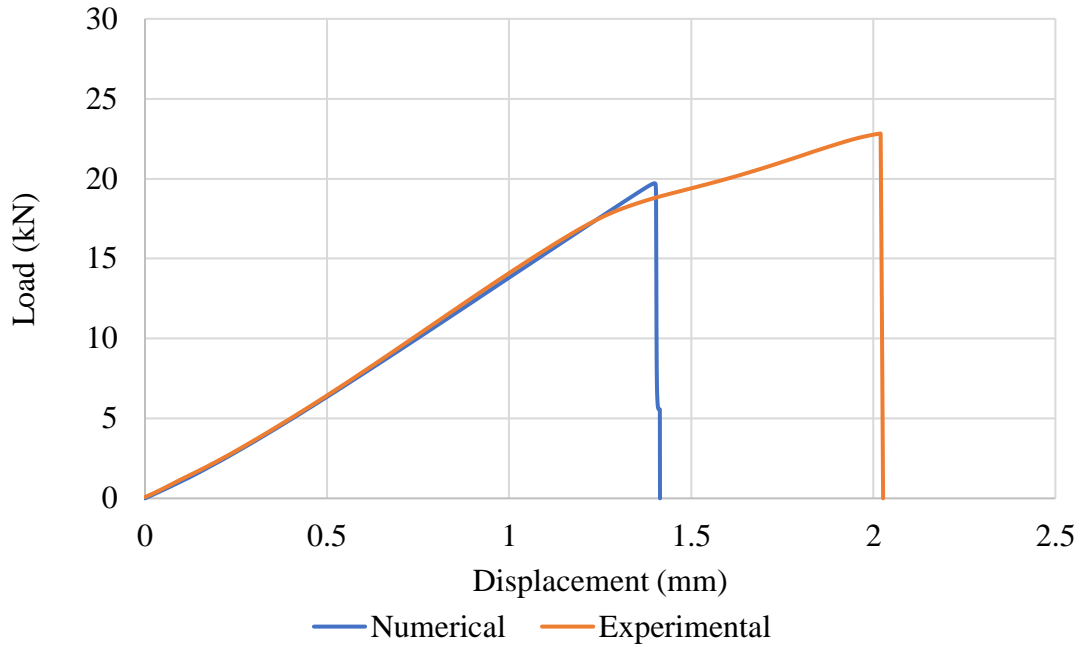
Figure 83 - Comparison between experimental and numerical P-δ curves of SLJs with similar substrates of CFRP under quasi-static conditions.

In this case, the shape of the plots is quite similar, as well as the maximum load values. However, the value for the numerical failure load should be higher than the experimental load, since in numerical simulations perfect conditions exist which cannot be recreated experimentally. That might have occurred because the mechanical properties of the adhesive measured in bulk might differ slightly from those exhibited when present in an adhesive joint.

5.2.1.2   Substrates with dissimilar materials

Figure 84 shows the *P-δ* curves for the experimental results and the numerical simulations of SLJs with dissimilar substrates of AA6060 T6 + CFRP under quasi-static conditions.
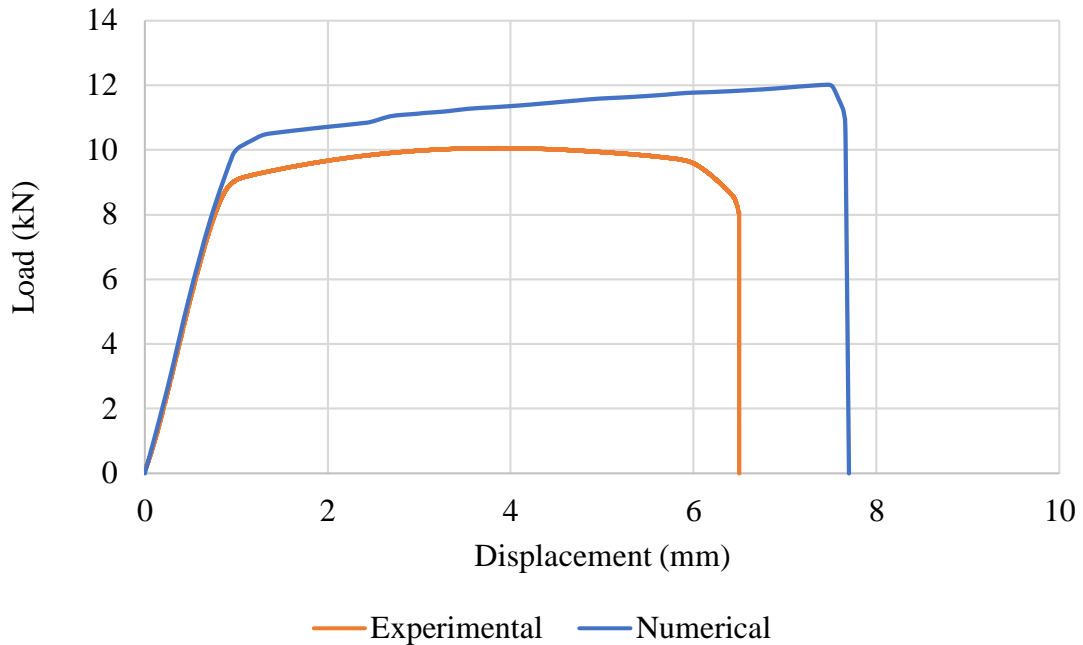
Figure 84 - Comparison between experimental and numerical *P-δ* curves of SLJs with dissimilar substrates of AA6060 T6 + CFRP under quasi-static conditions.

As previously observed using other configurations, the shape of the plots is similar between experimental and numerical results. The maximum load and the displacement are higher in the numerical simulation. The reason of such behaviour is the same that was presented in the case of SLJs with similar substrates of aluminium AA6060 T6.

Overall, the quasi-static models here presented were able to simulate reasonably well the mechanical behaviour of most of the configurations under study. This is especially true when the failure is controlled by delamination of CFRP substrates, which depends on previously validated mechanical properties. However, this is not the case for the failure of aluminium substrates which lack detailed plastic and damage properties for accurate modelling

5.2.2 Impact

5.2.2.1 Substrates with similar materials

Figure 85 shows the P-δ curves for the experimental results and the numerical simulations of SLJs with similar substrates of AA6060 T6 under impact conditions.
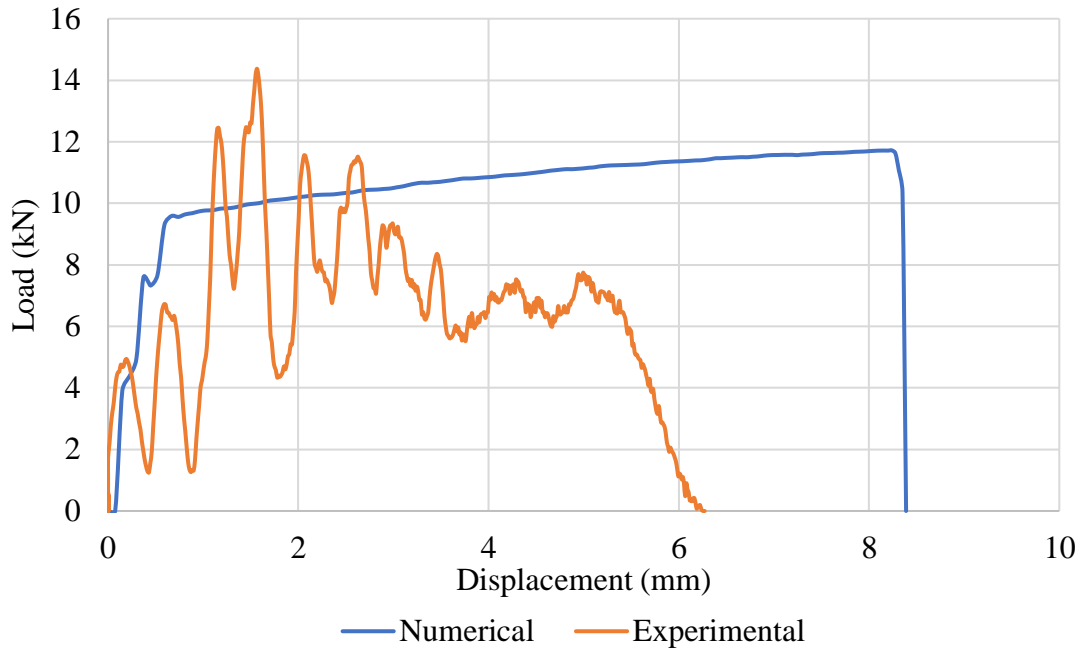
Figure 85 - Comparison between experimental and numerical P-δ curves of SLJs with similar substrates of AA6060 T6 under impact conditions.

For this case, the numerical P-δ curve is not in accordance with the experimental data. This is mostly due the lack of property data related with damage initiation and propagation regarding the aluminium alloy in study.

Figure 86 shows the P-δ curves for the experimental results and the numerical simulations of SLJs with similar substrates of CFRP under impact conditions.
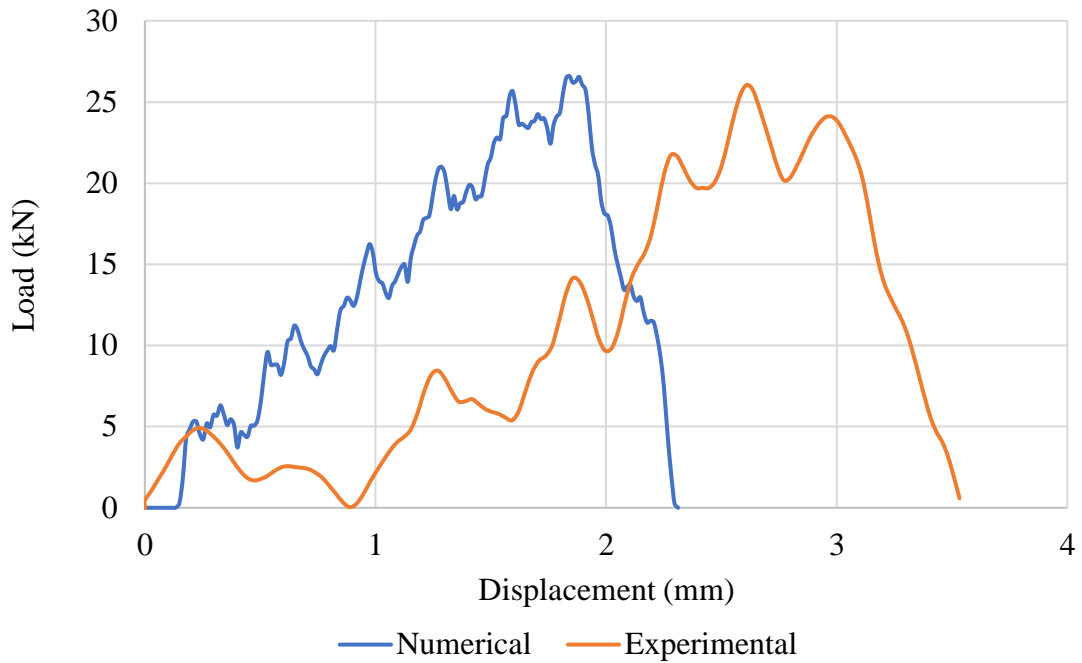
Figure 86 - Comparison between experimental and numerical *P-δ* curves of SLJs with similar substrates of CFRP under impact conditions.

The shape of the *P-δ* curves are very similar. The results are very close except for a difference in the displacement with the numerical simulation presenting a lower value that the experimental results.

5.2.2.2 Substrates with dissimilar materials

Figure 87 shows the *P-δ* curves for the experimental results and the numerical simulations of SLJs with dissimilar substrates of AA6060 T6 + CFRP under impact conditions.
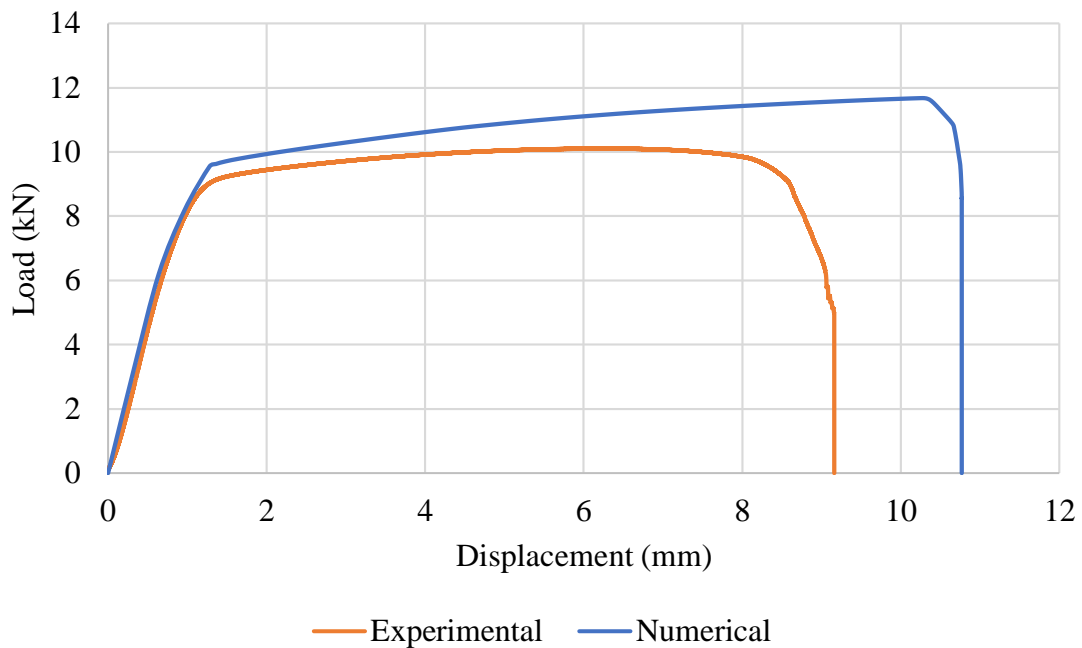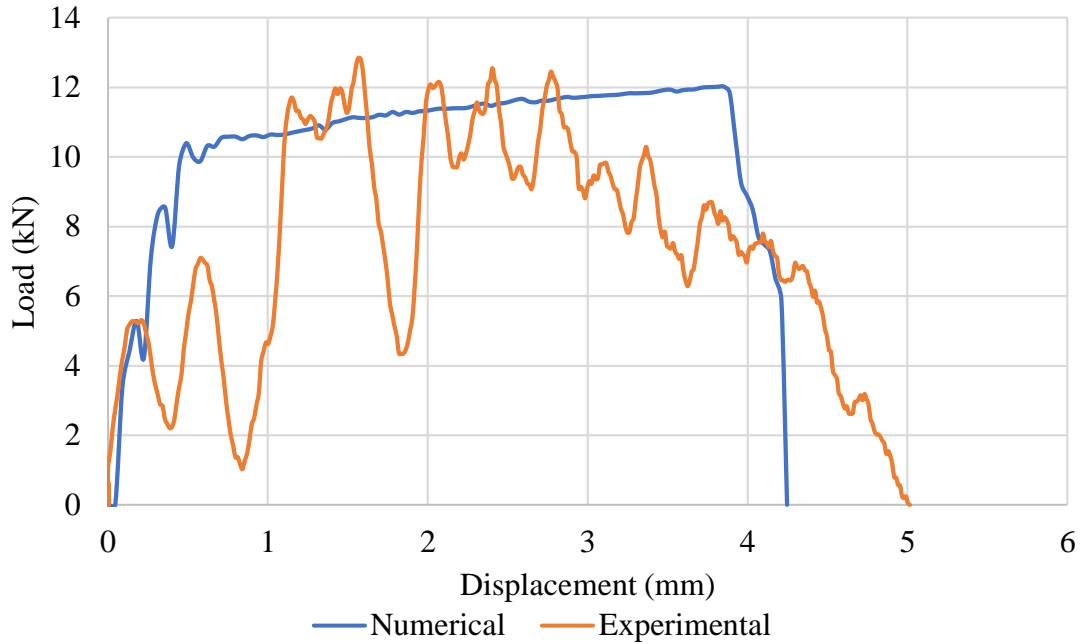
Figure 87 - Comparison between experimental and numerical P-δ curves of SLJs with dissimilar substrates of AA6060 T6 + CFRP under impact conditions.

The behaviour found is similar to that identified for SLJs containing substrates with AA6060 T6. However, for this case the maximum load and the displacement between experimental and simulated data are somewhat close.

The presented impact models were also able to simulate well the mechanical behaviour of most of the configurations under study. Again, modelling the failure process of aluminium was found to be less accurate than simulating cohesive delamination. However, the results still demonstrate that this type models can be successfully used for predicting the behaviour of complex adhesive joints under impact.

6 Conclusions

An in-depth analysis of the quasi-static and impact behaviour of dissimilar adhesive joints subjected to a wide range of temperatures was performed in this work. A list of the conclusions drawn from this work follows:

- The Young´s modulus and tensile stress of the studied crash-resistant adhesive both increase with the increase of strain rate and decrease of temperature;

- The fracture energy in mode I (G_{IC}) of the studied crash-resistant adhesive was found to increase with the increase of strain rate and increase of temperature;

- The CFFR-CFRP joint configuration exhibited the highest failure load for all conditions except for the impact test at -30°C, where the performance of all joints under study was similar. The aluminium joints with similar substrates exhibited low temperature sensitivity and failure loads significantly lower than those exhibited by the CFRP-CFRP joints.

- The performance of the dissimilar joints (maximum load) was found to be limited by the aluminium deformation in all conditions tested;

- In quasi-static conditions the aluminium-aluminium similar joints absorbed the most energy for all temperatures tested due to large level of plastic deformation present. In impact conditions, the CFRP-CFRP joints were those that absorbed more energy due to frictional sliding during delamination. At low temperatures this effect is less pronounced, and the aluminium alloys absorb more energy;

- A significant difference in absorbed energy from static to impact was found when testing the joints with aluminium substrates. This is due to the fact that failure occurred in the clamped section during impact testing;

- This work suggests that quasi-static testing and modelling can be used for the impact strength prediction of joints bonded with crash resistant adhesives. It was verified experimentally that under impact these joints offer failure loads consistently above

those encountered at low strain rates. If the joint is able to sustain a given quasi-static load, under impact it will always perform better. However, this work does not allow to extract the same conclusions with regards to energy absorption due to incomplete data, as under impact the aluminium substrates failed near the clamps with low energy absorption.

- The effect of temperature on joint performance is only pronounced for the CFRP-CFRP SLJs, due to the large temperature dependence of these materials as they approach T_g. As expected, in joints bonded with a crash resistant adhesive and containing aluminium substrates the effect of temperature is very limited, as the substrate is temperature insensitive and the adhesive, although losing strength, becomes tougher.

- The quasi-static models using cohesive zone modelling were able to simulate reasonably well the mechanical behaviour of most of the configurations under study, especially when predicting the failure of CFRP substrates. However, given the limited property data, proper modelling of the aluminium failure process was not possible.

- The impact models developed during this work were also able to simulate reasonably well the mechanical behaviour of most of the configurations under study. Again, the failure process of CFRP materials was found to be more accurately modelled that then the failure process of aluminium.

As a final remark, it is possible to conclude that dissimilar adhesive joints, if used in conjunction with modern crash resistant adhesives, can effectively be used for the construction of automotive structures, without significant sacrifices in joint performance, including energy absorption under impact. Moreover, their performance can also be simulated using advanced cohesive zone models minimizing the need to perform extensive experimental testing.

7 Future works

Due to the complexity of the impact phenomena, there are many experimental procedures that can be performed to further explore the behaviour of the adhesive joints when subjected to high strain rates. A few ideas are listed in this section:

- Due to the difficulties found in modelling the mechanical behaviour of the SLJs with aluminium substrates, an important complementary work could consist in a detailed characterisation of the aluminium substrates, especially their plastic behaviour and ductile damage mechanisms. This would allow to more accurately predict the joint failure loads and the displacement at failure.

- As the failure of the joints was mostly by delamination, the use of techniques that mitigate this type of failure should also be explored. Usage of fibre metal laminates or geometrical modifications that reduce the peel stresses in the composite are of special interest.

- Experiments with alternative substrates geometries and mechanical properties to balance the stiffness of the joint. By adjusting the substrates, it might be possible to improve significantly the performance of the joints, especially under impact conditions.

- The use of mixed adhesives could be explored also in attempt to improve the stress distribution of the joint, reducing peel loads both on the composite and the aluminium substrates.

- To further validate the results and procedures described in this thesis, it would be interesting to perform testing on component scale specimens, with geometries closely resembling that of a finished automotive component.

References

[1] L. F. M. da Silva, A. Öchsner, and R. D. Adams, *Handbook of Adhesion Technology*. Springer Berlin Heidelberg, 2011.

[2] R. D. Adams and W. C. Wake, *Structural Adhesive Joints in Engineering*. Elsevier Applied Science Publishers, 1984.

[3] E. Petrie, *Handbook of Adhesives and Sealants*. McGraw-Hill Education, 2007.

[4] R. D. Adams, *Adhesive Bonding: Science, Technology, and Applications*. Taylor & Francis, 2005.

[5] A. J. Kinloch, *Adhesion and Adhesives: Science and Technology*. Springer, 1987.

[6] W. Lees, *Adhesives in engineering design*. Springer, 1984.

[7] M. D. Banea and L. F. M. d. Silva, "Adhesively bonded joints in composite materials: An overview," *Proceedings of the Institution of Mechanical Engineers, Part L: Journal of Materials: Design and Applications,* vol. 223, no. 1, pp. 1-18, 2009.

[8] R. Adams and J. Harris, "A critical assessment of the block impact test for measuring the impact strength of adhesive bonds," *International Journal of Adhesion and Adhesives,* vol. 16, no. 2, pp. 61-71, 1996.

[9] A. B. Strong, *Fundamentals of composites manufacturing: materials, methods and applications*. Society of Manufacturing Engineers, 2008.

[10] K. Sears, "Automotive engineering: strategic overview," *Steel World,* vol. 2, no. 1, pp. 55-68, 1997.

[11] W. Miller, L. Zhuang, J. Bottema, A. J. Wittebrood, P. De Smet, A. Haszler, and A. Vieregge, "Recent development in aluminium alloys for the automotive industry," *Materials Science and Engineering: A,* vol. 280, no. 1, pp. 37-49, 2000.

[12] U. Lindholm, "Some experiments with the split hopkinson pressure bar∗," *Journal of the Mechanics and Physics of Solids,* vol. 12, no. 5, pp. 317-335, 1964.

[13] J. Bouchet, E. Jacquelin, and P. Hamelin, "Static and dynamic behavior of combined composite aluminium tube for automotive applications," *Composites science and technology,* vol. 60, no. 10, pp. 1891-1900, 2000.

[14] J. Harding and L. M. Welsh, "A tensile testing technique for fibre-reinforced composites at impact rates of strain," *Journal of Materials Science,* vol. 18, no. 6, pp. 1810-1826, 1983.

[15] L. F. Da Silva and R. Adams, "Techniques to reduce the peel stresses in adhesive joints with composites," *International Journal of Adhesion and Adhesives,* vol. 27, no. 3, pp. 227-235, 2007.

[16] A. Kelly, *Concise encyclopedia of composite materials*. Elsevier, 2012.

[17] F. L. Matthews and R. D. Rawlings, *Composite materials: engineering and science*. Elsevier, 1999.

[18] U. Meier, "Carbon fiber-reinforced polymers: modern materials in bridge engineering," *Structural Engineering International,* vol. 2, no. 1, pp. 7-12, 1992.

[19]   R. Mohmmed, A. Ahmed, M. A. Elgalib, and H. Ali, "Low Velocity Impact Properties of Foam Sandwich Composites: A Brief Review," *College of Textiles Engineering, Sudan University of Science and Technology, Sudan,* 2014.

[20]   W. Knauss and L. Gonzalez, "Global Failure Modes in Composite Structures," *NASA Grant NAG 1-1975,* 2001.

[21]   M. Laffan, S. Pinho, P. Robinson, and A. McMillan, "Translaminar fracture toughness testing of composites: a review," *Polymer testing,* vol. 31, no. 3, pp. 481-489, 2012.

[22]   L. F. Da Silva and R. Adams, "Adhesive joints at high and low temperatures using similar and dissimilar adherends and dual adhesives," *International Journal of Adhesion and Adhesives,* vol. 27, no. 3, pp. 216-226, 2007.

[23]   A. Deb, I. Malvade, P. Biswas, and J. Schroeder, "An experimental and analytical study of the mechanical behaviour of adhesively bonded joints for variable extension rates and temperatures," *International journal of adhesion and adhesives,* vol. 28, no. 1, pp. 1-15, 2008.

[24]   J. J. M. Machado, E. A. S. Marques, and L. F. M. da Silva, "Adhesives and adhesive joints under impact loadings: An overview," *The Journal of Adhesion,* pp. 1-32, 2017.

[25]   J. Harris and R. Adams, "An assessment of the impact performance of bonded joints for use in high energy absorbing structures," *Proceedings of the Institution of Mechanical Engineers, Part C: Journal of Mechanical Engineering Science,* vol. 199, no. 2, pp. 121-131, 1985.

[26]   G. Sharon, H. Dodiuk, and S. Kenig, "Effects of loading rate and temperature on the mechanical properties of structural adhesives containing a carrier," *The Journal of Adhesion,* vol. 31, no. 1, pp. 21-31, 1989.

[27]   M. Banea, F. De Sousa, L. Da Silva, R. Campilho, and A. B. de Pereira, "Effects of temperature and loading rate on the mechanical properties of a high temperature epoxy adhesive," *Journal of Adhesion Science and Technology,* vol. 25, no. 18, pp. 2461-2474, 2011.

[28]   D. Holt, "The strain-rate dependence of the flow stress in some aluminum alloys," *Trans. ASM,* vol. 60, pp. 152-159, 1967.

[29]   K. Tanaka and T. Nojima, "Strain rate change tests of aluminium alloys under high strain rate," in *Proceedings of the 19th Japan congress on materials research*, 1975, pp. 48-51.

[30]   U. Lindholm, R. Bessey, and G. Smith, "Effect of strain rate on yield strength, tensile strength and elongation of three aluminum alloys," *J MATER,* vol. 6, no. 1, pp. 119-133, 1971.

[31]   A. H. Clausen, T. Børvik, O. S. Hopperstad, and A. Benallal, "Flow and fracture characteristics of aluminium alloy AA5083–H116 as function of strain rate, temperature and triaxiality," *Materials Science and Engineering: A,* vol. 364, no. 1, pp. 260-272, 2004.

[32]   M. Abbadi, P. Hähner, and A. Zeghloul, "On the characteristics of Portevin–Le Chatelier bands in aluminum alloy 5182 under stress-controlled and strain-controlled tensile testing," *Materials Science and Engineering: A,* vol. 337, no. 1, pp. 194-201, 2002.

[33] T. Naka and F. Yoshida, "Deep drawability of type 5083 aluminium–magnesium alloy sheet under various conditions of temperature and forming speed," *Journal of Materials Processing Technology,* vol. 89, pp. 19-23, 1999.

[34] L. D. Oosterkamp, A. Ivankovic, and G. Venizelos, "High strain rate properties of selected aluminium alloys," *Materials Science and Engineering: A,* vol. 278, no. 1, pp. 225-235, 2000.

[35] R. Smerd, S. Winkler, C. Salisbury, M. Worswick, D. Lloyd, and M. Finn, "High strain rate tensile testing of automotive aluminum alloy sheet," *International Journal of Impact Engineering,* vol. 32, no. 1, pp. 541-560, 2005.

[36] Y. Chen, A. Clausen, O. Hopperstad, and M. Langseth, "Stress–strain behaviour of aluminium alloys at a wide range of strain rates," *International Journal of Solids and Structures,* vol. 46, no. 21, pp. 3825-3835, 2009.

[37] N. Taniguchi, T. Nishiwaki, and H. Kawada, "Tensile strength of unidirectional CFRP laminate under high strain rate," *Advanced Composite Materials,* vol. 16, no. 2, pp. 167-180, 2007.

[38] J. Hou and C. Ruiz, "Measurement of the properties of woven CFRP T300/914 at different strain rates," *Composites Science and Technology,* vol. 60, no. 15, pp. 2829-2834, 2000.

[39] T. Gomez-del Rio, E. Barbero, R. Zaera, and C. Navarro, "Dynamic tensile behaviour at low temperature of CFRP using a split Hopkinson pressure bar," *Composites Science and Technology,* vol. 65, no. 1, pp. 61-71, 2005.

[40] J. Machado, E. Marques, R. Campilho, and L. F. da Silva, "Mode I fracture toughness of CFRP as a function of temperature and strain rate," *Journal of Composite Materials,* vol. 51, no. 23, pp. 3315-3326, 2017.

[41] J. Machado, E. Marques, R. Campilho, and L. F. da Silva, "Mode II fracture toughness of CFRP as a function of temperature and strain rate," *Composites Part B: Engineering,* vol. 114, pp. 311-318, 2017.

[42] G. C. Jacob, J. F. Fellers, S. Simunovic, and J. M. Starbuck, "Energy absorption in polymer composites for automotive crashworthiness," *Journal of composite materials,* vol. 36, no. 7, pp. 813-850, 2002.

[43] S. Ramakrishna, "Energy absorption characteristics of knitted fabric reinforced epoxy composite tubes," *Journal of reinforced plastics and composites,* vol. 14, no. 10, pp. 1121-1141, 1995.

[44] A. G. Mamalis, Y. B. Yuan, and G. Viegelahn, "Collapse of thin–wall composite sections subjected to high speed axial loading," *International journal of vehicle design,* vol. 13, no. 5-6, pp. 564-579, 1992.

[45] D. Schmueser and L. Wickliffe, "Impact energy absorption of continuous fiber composite tubes," *Journal of engineering materials and technology,* vol. 109, no. 1, pp. 72-77, 1987.

[46] G. L. Farley, "Energy absorption of composite materials," *Journal of composite Materials,* vol. 17, no. 3, pp. 267-279, 1983.

[47] P. Thornton, "Energy absorption in composite structures," *Journal of Composite Materials,* vol. 13, no. 3, pp. 247-262, 1979.

[48] P. Thornton, "The crush behavior of pultruded tubes at high strain rates," *Journal of Composite Materials,* vol. 24, no. 6, pp. 594-615, 1990.

[49] G. L. Farley, "The effects of crushing speed on the energy-absorption capability of composite tubes," *Journal of Composite Materials,* vol. 25, no. 10, pp. 1314-1329, 1991.

[50] G. R. Wooley and D. R. Carver, *Stress concentration factors for bonded lap joints*. Louisiana State University and Agricultural and Mechanical College. Division of Engineering Research, 1971.

[51] R. Adams and N. Peppiatt, "Stress analysis of adhesive-bonded lap joints," *Journal of strain analysis,* vol. 9, no. 3, pp. 185-196, 1974.

[52] A. A. Griffith and M. Eng, "VI. The phenomena of rupture and flow in solids," *Phil. Trans. R. Soc. Lond. A,* vol. 221, no. 582-593, pp. 163-198, 1921.

[53] G. Barenblatt, "Equilibrium cracks formed on a brittle fracture," *Doklady Akademii Nauk Sssr,* vol. 127, no. 1, pp. 47-50, 1959.

[54] A. Hillerborg, M. Modéer, and P.-E. Petersson, "Analysis of crack formation and crack growth in concrete by means of fracture mechanics and finite elements," *Cement and concrete research,* vol. 6, no. 6, pp. 773-781, 1976.

[55] H. Khoramishad, A. Crocombe, K. Katnam, and I. Ashcroft, "Predicting fatigue damage in adhesively bonded joints using a cohesive zone model," *International Journal of fatigue,* vol. 32, no. 7, pp. 1146-1158, 2010.

[56] J. Gonçalves, M. De Moura, P. De Castro, and A. Marques, "Interface element including point-to-surface constraints for three-dimensional problems with damage propagation," *Engineering Computations,* vol. 17, no. 1, pp. 28-47, 2000.

[57] M. De Moura, J. Gonçalves, A. Marques, and P. De Castro, "Prediction of compressive strength of carbon–epoxy laminates containing delamination by using a mixed-mode damage model," *Composite Structures,* vol. 50, no. 2, pp. 151-157, 2000.

[58] L. F. Da Silva and R. D. Campilho, "Advances in numerical modelling of adhesive joints," in *Advances in Numerical Modeling of Adhesive Joints*: Springer, 2012, pp. 1-93.

[59] J. Machado, P.-R. Gamarra, E. Marques, and L. F. da Silva, "Numerical study of the behaviour of composite mixed adhesive joints under impact strength for the automotive industry," *Composite Structures,* vol. 185, pp. 373-380, 2018.

[60] L. F. M. da Silva, A. G. de Magalhaes, and M. F. S. de Moura, *Juntas adesivas estruturais*. Publindustria, 2007.

[61] L. F. M. Da Silva and A. Öchsner, *Modeling of adhesively bonded joints*. Springer, 2008.

[62] D. Saldanha, C. Canto, L. Da Silva, R. Carbas, F. Chaves, K. Nomura, and T. Ueda, "Mechanical characterization of a high elongation and high toughness epoxy adhesive," *International journal of adhesion and adhesives,* vol. 47, pp. 91-98, 2013.

[63] Y. Wang and J. Williams, "Corrections for mode II fracture toughness specimens of composites materials," *Composites Science and Technology,* vol. 43, no. 3, pp. 251-256, 1992.

[64]   H. Yoshihara and T. Kawamura, "Mode I fracture toughness estimation of wood by DCB test," *Composites Part A: applied science and manufacturing,* vol. 37, no. 11, pp. 2105-2113, 2006.

[65]   R. D. S. G. Campilho, "Repair of composite and wood structures," Universidade do Porto (Portugal), 2009.

[66]   M. De Moura, J. Gonçalves, J. Chousal, and R. Campilho, "Cohesive and continuum mixed-mode damage models applied to the simulation of the mechanical behaviour of bonded joints," *International Journal of adhesion and Adhesives,* vol. 28, no. 8, pp. 419-426, 2008.

[67]   M. De Moura, R. Campilho, and J. Gonçalves, "Crack equivalent concept applied to the fracture characterization of bonded joints under pure mode I loading," *Composites Science and Technology,* vol. 68, no. 10, pp. 2224-2230, 2008.

[68]   M. De Moura, J. Gonçalves, and A. Magalhães, "A straightforward method to obtain the cohesive laws of bonded joints under mode I loading," *International Journal of Adhesion and Adhesives,* vol. 39, pp. 54-59, 2012.

[69]   G. Dias, M. de Moura, J. Chousal, and J. Xavier, "Cohesive laws of composite bonded joints under mode I loading," *Composite Structures,* vol. 106, pp. 646-652, 2013.

[70]   A. Biel, "Constitutive behaviour and fracture toughness of an adhesive layer," Chalmers tekniska högskola, 2005.

[71]   T. Carlberger, A. Biel, and U. Stigh, "Influence of temperature and strain rate on cohesive properties of a structural epoxy adhesive," *International Journal of Fracture,* vol. 155, no. 2, pp. 155-166, 2009.

[72]   A. Kinloch, G. Kodokian, and M. Jamarani, "Impact properties of epoxy polymers," *Journal of materials science,* vol. 22, no. 11, pp. 4111-4120, 1987.

[73]   X. Chen, Y. Peng, S. Peng, S. Yao, C. Chen, and P. Xu, "Flow and fracture behavior of aluminum alloy 6082-T6 at different tensile strain rates and triaxialities," *PloS one,* vol. 12, no. 7, p. e0181983, 2017.

[74]   H. A. M. Araújo, "Impact and Damping Behaviour of Composite Adhesive Joints," *Master Thesis, Faculdade de Engenharia da Universidade do Porto,* 2016.

[75]   B. Lauke, B. Schultrich, and R. Barthel, "Contribution to the micromechanical interpretation of fracture work of short-fibre-reinforced thermoplastics," *Composites Science and Technology,* vol. 23, no. 1, pp. 21-35, 1985.

[76]   V. Gupta, R. Mittal, and M. Goel, "Energy absorbing mechanisms in short-glass-fibre-reinforced polypropylene," *Composites science and technology,* vol. 37, no. 4, pp. 353-369, 1990.

[77]   L. Lavielle and S. Lamouri, "Polymer-polymer friction: Adhesion dependence," *Lubrication Science,* vol. 12, no. 2, pp. 125-131, 1995.

[78]   M. Tanoglu, S. H. McKnight, G. R. Palmese, and J. Gillespie Jr, "The effects of glass-fiber sizings on the strength and energy absorption of the fiber/matrix interphase under high loading rates," *Composites science and technology,* vol. 61, no. 2, pp. 205-220, 2001.

[79]   W. G. Perkins, "Polymer toughness and impact resistance," *Polymer Engineering & Science,* vol. 39, no. 12, pp. 2445-2460, 1999.

[80] S. Turley and H. Keskkula, "A survey of multiple transitions by dynamic mechanical methods," in *Journal of Polymer Science: Polymer Symposia*, 1966, vol. 14, no. 1, pp. 69-87: Wiley Online Library.

[81] A. Mulliken and M. Boyce, "Mechanics of the rate-dependent elastic–plastic deformation of glassy polymers from low to high strain rates," *International journal of solids and structures,* vol. 43, no. 5, pp. 1331-1356, 2006.